Timing and Frequency Synchronization for OFDM based Systems: Preambles and Timing Metrics

By
Eric Mario Silva Cruz

A Dissertation
Submitted to the Department of Electronic Engineer
In partial fulfillment of the requirements for the degree of:

Ph. D. in ELECTRONIC ENGINEERING

At
National Institute of Astrophysics, Optics and Electronics

November 2013
Tonantzintla, Puebla

Advisors:
Dr. Gordana J. Dolecek
INAOE

Dr. Fredric J. Harris
San Diego State University, SDSU

ABSTRACT

The orthogonal frequency division multiplexing (OFDM) modulation is a multicarrier transmission, which has received considerable attention due to its robustness against inter-symbol interference (ISI) and multipath distortion, low implementation complexity and high spectral efficiency. However, one of the main disadvantages of OFDM based systems is the sensitivity to synchronization errors, characterized mainly by frequency and timing offsets. Frequency offset causes a reduction of desired signal amplitude and introduces inter-carrier interference (ICI). The timing offset originates the rotation of the OFDM subcarrier signal constellation.

This thesis presents a contribution in timing and frequency synchronization for OFDM based systems. The contribution consist on propose modified timing metrics based on preamble sequences in configurations of short and long preamble. The proposed timing metrics are the result of a review of the state of the art of methods, and the corresponding analysis by simulation of timing and frequency synchronization errors. The new proposed timing and frequency synchronization methods are based on weighted preambles; these preambles are designed applying Golay-Rudin-Shapiro (GRS) sequences. GRS sequence exhibits good autocorrelation properties and reduced peak to average power ratio (PAPR), being useful characteristics to obtain algorithms with reduced mean square error (MSE) and improved response of the bit error rate (BER) in OFDM based systems.

RESUMEN

La multiplexación por división de frecuencia ortogonal (OFDM) es una transmisión multiportadora, la cual ha recibido considerable atención debido a su robustez frente a interferencias entre símbolos (ISI) y la distorsión por múltiples trayectorias, baja complejidad de implementación y alta eficiencia espectral. Sin embargo, una de las principales desventajas de los sistemas basados en OFDM es la sensibilidad a los errores de sincronización, que se caracteriza principalmente por desplazamientos de frecuencia y tiempo. El desplazamiento de frecuencia causa una reducción de la amplitud de la señal deseada y a su vez introduce interferencia entre portadoras (ICI). El desplazamiento del tiempo de los símbolos origina la rotación de la constelación de la señal portadora OFDM.

Esta tesis presenta una aportación a la sincronización del tiempo y la frecuencia para sistemas basados en OFDM. La contribución consiste en proponer métricas temporales modificadas, las cuales se basan en preámbulos, con secuencias especiales configuradas en preámbulo corto ó largo. Las métricas de tiempo propuestas son el resultado de una revisión del estado del arte de dichas métricas, y el correspondiente análisis por simulación de errores de temporización y sincronización de frecuencia. Los nuevos métodos de sincronización del tiempo y la frecuencia propuestos se basan en preámbulos ponderados, estos preámbulos se diseñan aplicando secuencias Golay-Rudin-Shapiro (GRS). La secuencia GRS presenta buenas propiedades de auto-correlación y reducida amplitud pico de potencia media (PAPR), siendo características útiles para obtener algoritmos con menor error cuadrático medio (MSE) y una mejora de la tasa de error de bit (BER) en los sistemas basados en OFDM.

ACKNOWLEDGMENTS

First, I would like to express my deep appreciation to my advisor, Professor Gordana J. Dolecek for introducing me to the fascinating world of digital communications and the digital signal processing. I am also very grateful for her patience in correcting and commenting on my thesis.

I would like to thank my co-advisor, Professor Fredric J. Harris, for giving me the opportunity as a scholar visitor researcher at the department of electrical and computer engineering, San Diego State University (SDSU). He is a fascinating teacher and always ready to share his expertise with the students. I benefited greatly from working under his guidance and I have expanded my signal processing skills.

My sincere thanks to my doctoral committee members, Dr. Alfonso Fernández V., Dr. Celso Gutiérrez M., Dr. Esteban Tlelo C., Dr. Javier Díaz C., Dr. Roberto Rosas R.

I would like to thank to the National Institute of Astrophysics Optics and Electronics (INAOE) and the Consejo Nacional de Ciencia y Tecnología (CONACYT) who had faith in me and gave me the opportunity of pursuit my doctoral studies.

I want to thank my friends and their support during all the difficult way, they have changing my life asking the good questions and providing the best answers.

To my parents Aurelia y Mario, my
dear wife Yasmin and my son Joshua,
who is the joy of my life

INDEX

PREFACE

A successful method to get high-speed data transmission over a wired or wireless channel uses a channel partitioning method, which consist on divide the transmission into a number of orthogonal sub channels (subcarriers). The channel partitioning method is often referred to as multicarrier modulation (MCM), also called multichannel modulation. The main advantages of multicarrier transmission are its robustness in frequency selective fading channels and, in particular, the reduced signal processing complexity by equalization in the frequency domain.

The popularity of OFDM systems lies on its ability to transform a wideband *frequency selective* channel to a set of parallel flat *fading* narrowband channels, where a block of information symbols is transmitted in parallel subcarriers (tones), denoted as frames or packets. All subcarriers are orthogonal to each other over all the symbol duration and can be separated by *correlators* in the receiver. The mentioned operation simplifies the channel equalization problem, and makes it robust against inter-symbol interference (ISI) originated by *multipath* propagation. The OFDM system is efficiently implemented by the use of discrete Fourier transform (DFT), which was proposed by Weinstein and Ebert. The DFT implementation avoids the use of a bank of subcarrier oscillators at the transmitter/receiver.

One disadvantage of the OFDM system is its high sensitivity to synchronization errors. In the presence of synchronization errors, the orthogonality between the carriers is lost and inter-carrier interference (ICI) is introduced. Furthermore, interference between adjacent transmitted OFDM blocks occurs, resulting in inter-symbol interference (ISI). Other disadvantage of the OFDM signal is the high peak-to-average power ratio (PAPR), which consists of the superposition of many low rate streams modulated at different frequencies, when high PAPR occurs, the digital-to-analog (D/A) converter and power amplifier of the transmitter would require a large dynamic range.

Multiple synchronization errors of the OFDM signal during its transmission are caused by affectations as the following: the multipath channels, Doppler effects, and the components of the analog and digital front end.

The main synchronization issues in OFDM are:

- Carrier frequency offset
- Carrier phase error
- Symbol timing offset
- Sampling clock offset

Two of the most important synchronization issues are, first, the timing synchronization, where it is necessary to estimate the correct starting point of the symbol, and second, the frequency synchronization, which recover the correct clock frequency.

The principal methods to solve timing and frequency offset are the data-aided synchronizers. In particular, varieties of timing metrics have been developed during the last decades, and it is based on autocorrelation of well-designed sequences. The applied sequences have good correlation properties, where each sequence is transmitted in a designed pattern (preamble), prior to the OFDM data symbol, and are detected in the receiver by means of the timing metric.

In this thesis is provided a general background of preamble sequences with good autocorrelation properties and low peak to average power ratio (PAPR). They are applied in diverse preamble configurations, with the finality of synchronize the signal within the timing metric. The designed preambles allow the design of algorithms with a low mean square error (MSE).

The performance of the OFDM system is measured by the bit error rate (BER); it is defined as the ratio of the average number of erroneous detected bits to the total number of transmitted bits. BER is originated because of the additive white Gaussian noise (AWGN), time and frequency offsets, erroneous equalization, or an incorrect detection obtained by the receiver.

Chapter 1

INTRODUCTION

1.1 Objective of the Thesis

The main objective of this thesis is to develop more accurate timing metrics for OFDM based systems, this in comparison with the existing methods in the literature.

The timing and frequency synchronization errors of OFDM based systems are analyzed, and in order to reduce these two drawbacks the modified timing metrics will be applied. The functionality of the proposed methods requires considering sequences with good correlation properties, low peak to average power ration (PAPR), and structured in configurations of short and long preambles.

The performance of the proposed algorithms will be evaluated by means of the mean square error (MSE). A complete evaluation of the whole OFDM system will be made by means of corroborating the transmitted and received symbols, with the evaluation of the Bit Error Rate (BER) of the signal.

1.2 Outline of the Thesis

To accomplish the objective of this thesis, the doctoral document is organized as follows:

First, the characterization of the OFDM transceiver based on the discrete Fourier transform (DFT) is provided in chapter two. Subsequently, it is explained the application of a cyclic prefix (CP), and the diverse effects that modify the transmitted signal. Additionally, the Physical layer of systems based on OFDM is explained at the end of chapter two.

Chapter three presents the timing and frequency synchronization errors of OFDM systems. These two types of errors affect the received signal, and their effects produce inter-symbol and/or inter-carrier interference. The correct timing of the symbol is related to define the correct beginning of each data block. In the same way, if the frequency offset of the received signal is good estimated, then it is possible demodulate correctly the received data symbols.

Fourth chapter is focused on the description of different data-aided synchronization methods. The data-aided methods are based on well-designed sequences, applied sequences are configured in a pattern called preamble. Depending on the characteristic pattern, a preamble is classified into short and long preamble. Usually, the short preamble is used to estimate the coarse carrier frequency offset (CFO) parameter, and the long preamble is used for computing the symbol timing offset, fine frequency offset (FFO) and the channel estimation.

The CAZAC sequences, pseudo noise and Golay, are commonly used to design preambles for OFDM based systems. These sequences need to be well selected and properly arranged in the preambles, to carry on the task of synchronization. An OFDM receiver that uses a data-aided method applies a timing metric to achieve the synchronization. Chapter five presents the state of art of timing metrics algorithms. The review of existing timing methods starts with the Schmidl and Cox method, which is based on the auto-correlation and cross-correlation of a special designed preamble. Additionally, the data-aided methods developed to improve the accuracy of Schmidl and Cox method are detailed in this chapter.

Once the state of art of timing metrics have been reviewed, with the aim of understanding their operation, the simulation and performance of the timing metric are presented in Chapter six. The proposed designs of synchronization algorithms were developed. The proposed algorithms works in configurations of short and long preamble, which are based on a scrambling process defined by a Golay sequence. Each configuration has its appropriate designed timing metric.

The performances of the reviewed and proposed methods are estimated by computing the mean square error (MSE) and the resulting bit error rate (BER) of the data. In Chapter six is detailed the proposed normalized detection of the primary synchronization signal (PSS), which is related to the secondary synchronization signal (SSS) as a part of the process called cell search in the long term evolution (LTE) system. The complete cell search process to acquire access of a mobile user to a base station is explained and simulated.

Finally, conclusions obtained of the thesis and future work are detailed in Chapter seven.

Chapter 2

ORTHOGONAL FREQUENCY DIVISION MULTIPLEXING (OFDM)

In this chapter are explained the required elements to understand the OFDM system. It starts by describing the concept of multichannel modulation and the principle of orthogonality. Then, the difference between baseband and bandpass OFDM signals is explained. Next, the design of OFDM technology based on discrete Fourier transform (DFT) and the functionality of the cyclic prefix is shown. the importance of Peak to Average Ratio of the transmitted symbol, and finally, the spectrum shaping to limit the bandwidth of the transmitted symbol is detailed.

2.1 Multicarrier Modulation

Muticarrier Modulation (MCM) is the principle of transmitting data by dividing input stream into several symbol streams (each one has a lower symbol rate) and using these sub streams to modulate several subcarriers [134-134]. The earliest multicarrier modulation method is the frequency division multiplexing (FDM), consisting of independent data modulated on different subcarriers multiplexed in frequency. Bandpass filters are used in the receiver to separate the subcarriers. The purpose of non-overlap is to eliminate the possible interference among adjacent subcarriers, also known as inter-carrier interference (ICI).

Orthogonal frequency division multiplexing (OFDM) transmission scheme is a multicarrier modulation system. This method avoids the use of individual band limited filters and furthermore, the spectra of subcarriers are overlapped for bandwidth efficiency. The separation of the signals at the receiver is achieved by spacing two adjacent subcarriers by a value of $1/T$, where T is the symbol period, so that all subcarriers are orthogonal to each other and can be separated by correlators in the receiver [134-135].

2.2 Principles of OFDM

The operational principle of the OFDM system consists of dividing the available bandwidth B into a number N_c of subbands (subcarriers or subchannels). Each subband has a width of $\Delta f = B/N_c$, over which the wireless channel can be considered non-dispersive or flat *fading*. The data is transmitted at the rate of R symbols per second (baud rate), with a symbol period $T_s = N_c/R$, and a long compared to the maximum excess delay of the wireless propagation channel $T_s \gg \tau_{\max}$, where $\tau_{\max}$ is the spread delay of the channel . If the delay is larger than about 10% of the symbol duration, then the received signal suffer inter-symbol interference (ISI), which can drastically increase the bit error rate (BER). At the same time, the bandwidth of the sub-bands can be small compared to the coherence bandwidth of the channel $B_{coh} \gg B / N_c$, [134-134].

2.2.1 Orthogonality

A general form of the *baseband* OFDM signal in the first symbol period is described as,

$$s(t) = \sum_{k=0}^{N_c-1} d\left(k\right) e^{j2\pi f_k t} = \sum_{k=0}^{N_c-1} d\left(k\right) \varphi_k(t), \text{ for } 0 \le t \le T_{sym} \tag{2.1}$$

where $\left\{d\left(k\right)\right\}_{k=0}^{N-1}$ are the complex symbols for being transmitted by the N_c subcarriers of the OFDM signal, which can be selected of a sequence of *m*-ary phase shift keying (M-PSK) or *m*-ary Quadrature amplitude modulation (QAM) symbols, [12-15], and will be converted into N_c parallel streams with a serial-to-parallel (S/P) conversion. Due to the S/P conversion, the duration of the transmitted OFDM symbol is extended to $T_{sym} = N_c T_s$, where T_s is the symbol period of the data. We have,

$$\varphi_k = \begin{cases} e^{j2\pi f_k t} & \text{if } 0 \le t \le T_{sym} \\ 0 & \text{otherwise} \end{cases}, \tag{2.2}$$

where φ_k is the waveform for the *k-th* subcarrier, and $f_k = f_0 + k\Delta f$ the subcarrier frequency, with f_0 the lowest frequency used $(k = 0)$, and $\Delta f = 1/T_{sym}$ is the spacing between the adjacent subcarriers, [134]. The OFDM symbol is restricted to the time window interval $\left[0, T_{sym}\right]$, where the subcarriers are of finite duration. The spectrum of the OFDM signal can be considered as the sum of the frequency shifted *sinc* functions in the frequency domain, and the overlapped neighboring *sinc* functions are spaced by $1/T_{sym}$, given in (2.3) and is shown in Figure 2.1.

$$T_{sym} \cdot \exp\left(-j\pi f T_{sym}\right) \cdot \frac{\sin\left(\pi f T_{sym}\right)}{\pi f T_{sym}}. \qquad (2.3)$$

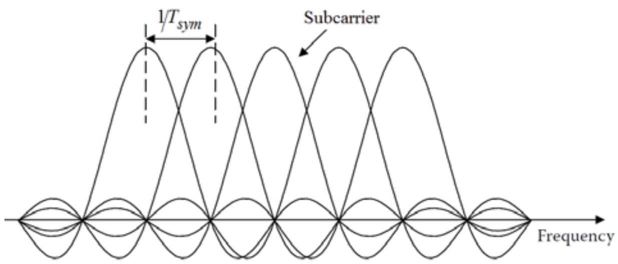

Figure 2.1. *Sinc* functions.

Consequently, the different subbands overlap, although they do not interfere with each other at $f = f_k$, $k = 0,1,\ldots,N_c - 1$. The symbol duration must be long enough such that $T_{sym}\Delta f = 1$, which is called *orthogonality condition* [12, 22], defined by,

$$\frac{1}{T_{sym}}\int_0^{T_{sym}} \varphi_k(t)\varphi_l(t)dt = \frac{1}{T_{sym}}\int_0^{T_{sym}} e^{j2\pi(k-l)\Delta f t}dt = \delta\left[k-l\right] = \begin{cases} 1, & \forall \text{integer } k = l \\ 0, & \text{otherwise} \end{cases}. \qquad (2.4)$$

Using the orthogonal condition the OFDM signal can be demodulated by,

$$\frac{1}{T_{sym}}\int_0^{T_{sym}} s(t)e^{-j2\pi f_k t}dt = \frac{1}{T_{sym}}\int_0^{T_{sym}} \left(\sum_{l=0}^{N_c-1} d(l)\varphi_l(t)\right)\varphi_l^*(t)dt = \sum_{l=0}^{N_c-1} d(l)\delta\left[l-k\right] = d\left(k\right). \qquad (2.5)$$

The orthogonality is the essential condition for avoid the inter-carrier interference.

2.2.2 Baseband and Bandpass

A wireless OFDM signal is generated in *baseband* and then up-converted to the Radio Frequency (RF) band for transmission (*bandpass* signal) [13]. The subcarrier frequencies are symmetrically distributed around a nominal center frequency f_c of the RF band. The *bandpass* OFDM signal in the continuous time domain is defined by,

$$s_l(t) = \mathrm{Re}\left\{\left\{\frac{1}{T_{sym}}\sum_{l=0}^{\infty}\sum_{k=0}^{N_c-1} d(k)_l\, e^{j2\pi f_k(t-lT_{sym})}\right\} e^{j2\pi f_c t}\right\}, \quad 0 \le t \le T_{sym} \tag{2.6}$$

The second exponential in (2.6) corresponds to the carrier frequency f_c, which is a frequency-shifted version of the *baseband* signal, and is defined as,

$$f_k = f_c - \frac{N_c - 1}{2T_{sym}}. \tag{2.7}$$

If a *bandpass* OFDM signal is desired, the up-conversion process needs a reference signal of frequency f_c, and a *bandpass* filter, whose frequency response rejects the lower sideband of the mixer output, as shown in the Figure 2.2.

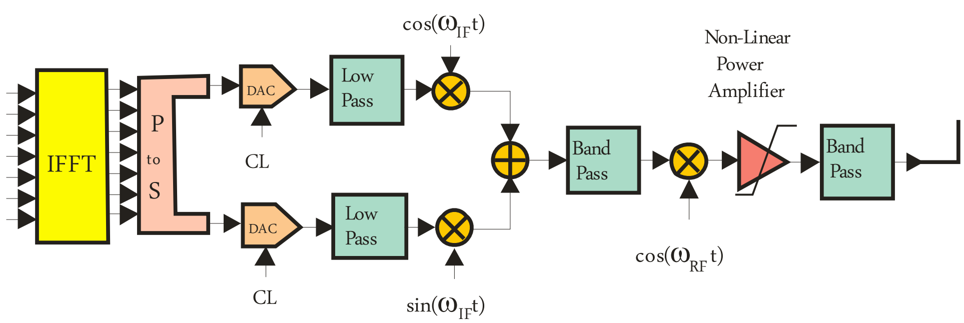

Figure 2.2. Transmitted baseband and bandpass signal.

The real part of the complex envelope of the *bandpass* OFDM signal corresponds to the continuous OFDM *baseband* signal. In the receiver, a down-converter with a reference of $-f_c'$ will be used to translate the signal to *baseband*, (Figure 2.3), which is achieved by multiplying the received signal by $-f_c'$, equation 2.8. Additionally it is required to apply a low-pass filter operation, [13].

$$s_l(t) = \mathrm{Re}\left\{\left\{\frac{1}{T_{sym}}\sum_{l=0}^{\infty}\sum_{k=0}^{N_c-1} d\left(k\right)_l e^{j2\pi f_k\left(t-lT_{sym}\right)}\right\}e^{-j2\pi f_c t}\right\}, \quad 0 \le t \le T_{sym}. \tag{2.8}$$

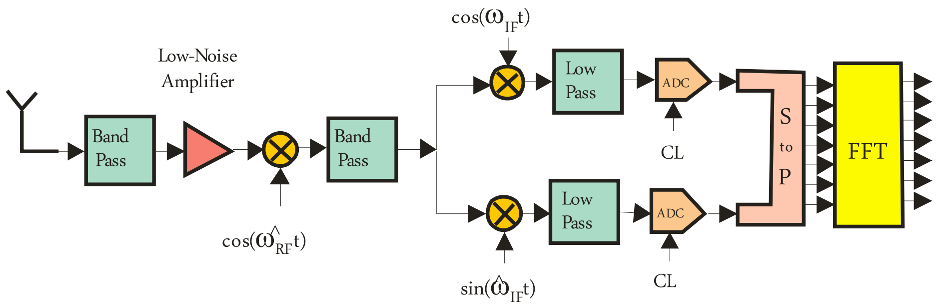

Figure 2.1. OFDM Receiver.

2.2.3 DFT Based OFDM

Discrete Fourier transform (DFT) based digital OFDM system is usually implemented by using a parallel bank of tuned filters, and is characterized by applying the inverse discrete Fourier transform (IDFT) in the modulator and, reciprocally, the discrete Fourier transform (DFT) is applied in the demodulator. The system complexity can be reduced by using the inverse fast Fourier transform and fast Fourier transform (IFFT / FFT) algorithms, [11-15].

The *baseband* OFDM signal $s\left(t\right)$ is sampled at periodic intervals $t = nT_s = nT_{sym} / N_c$, $n = 0,1,2,\dots,N_c - 1$

$$s(t) = \sum_{k=0}^{N_c-1} d\left(k\right)e^{j2\pi f_k t} \triangleq s\left(\frac{nT_{sym}}{N_c}\right) = \sum_{k=0}^{N_c-1} d\left(k\right)e^{j2\pi f_k \frac{nT_{sym}}{N_c}}. \tag{2.9}$$

Without loss of generality, by setting $f_0 = 0$, it follows $f_k T_{sym} = k$. Then we get the N_c-point IDFT taken for the transmitted symbols $\left\{d\left(k\right)\right\}_{k=0}^{N-1}$, to generate $\left\{s\left(n\right)\right\}_{n=0}^{N\text{-}1}$ samples for the sum of N_c orthogonal subcarrier signals, forming the corresponding discrete-time OFDM symbol given by,

$$s(n) = \frac{1}{N_c} \sum_{k=0}^{N_c-1} d(k) e^{j2\pi \frac{kn}{N_c}} = IDFT\{d(k)\}, \tag{2.10}$$

where $1/N_c$ is a normalization factor.

In a reciprocal way, are obtained the transmitted symbols,

$$\frac{1}{N_c} \sum_{n=0}^{N_c-1} s(n) e^{-j2\pi \frac{kn}{N_c}} = DFT\{s(n)\} = d(k). \tag{2.11}$$

In a practical OFDM system, the sampling frequency should be at least $2N_c / T_{sym}$ to avoid aliasing. To overcome that problem, a solution is to increase the number of samples to $2N_c$ [13]. The complex data $d(k)$ can be recovered in the receiver by the DFT block if the samples are received without any distortion, which is expressed in equation 2.12, (Figure 2.4),

$$d(k) = \sum_{n=-N_c/2+1}^{N_c/2} s(n) \mathrm{e}^{j2\pi \frac{kn}{N_c}}, \quad k = -N_g, ..., N_c - 1, \tag{2.12}$$

where $s(n)$ represent the received complex data symbols.

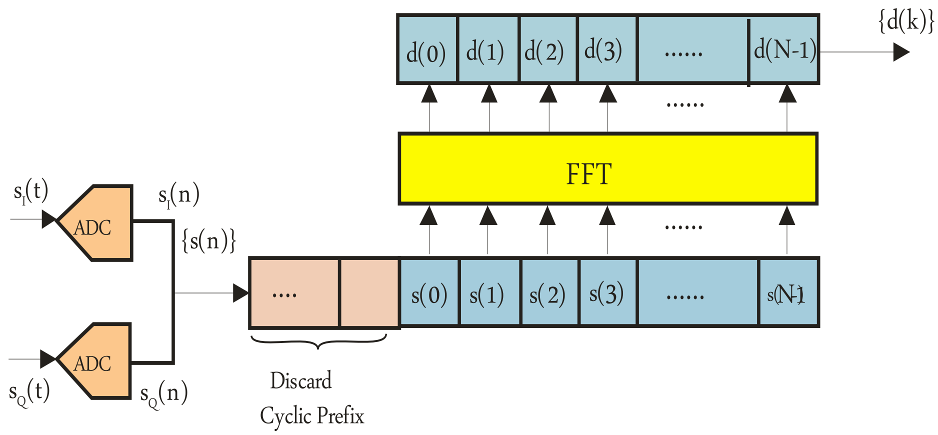

Figure 2.2. Sampled received signal.

The FFT algorithm provides an efficient way to implement the DFT and the IDFT. It reduces the number of complex multiplications from N_c^2 to $\frac{N_c}{2}\log_2 N_c$ for an N_c-point DFT or IDFT, [13].

2.2.4 Cyclic Extension

Passing the transmitted OFDM signal through a time dispersive channel causes inter-symbol interference (ISI), and additionally, the orthogonality between subcarriers is lost, resulting in an inter-carrier interference (ICI). To deal with *delay* dispersion of wireless channels, a cyclic extension of the symbol is used in OFDM systems, which is named *cyclic prefix* (CP), with a length N_g at least equal to the root mean square (RMS) channel length (τ_{RMS}), [13, 14, 22]:

$$s(n) = \frac{1}{N_c} \sum_{k=-N_c/2}^{N_c/2} d(k) \mathrm{e}^{j2\pi \frac{kn}{N_c}}, \quad k = -N_g, \ldots, N_c - 1, \tag{2.13}$$

where the N_g last samples of each symbol are cyclical extended at the beginning of the corresponding symbol, as shown in Figure 2.5. Resulting in a shifted index range $[0, N_c - 1]$ of the N_c-point DFT to $[-N_c/2, N_c/2 - 1]$.

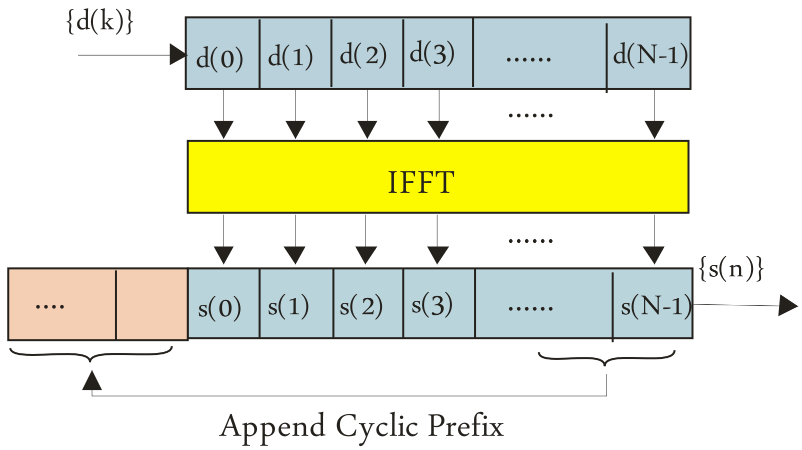

Figure 2.3. Sampled transmitted signal and cyclic prefix.

In continuous time the *cyclic prefix* is represented by,

$$\bar{s}(t) = \begin{cases} s(t+T_{sym}), & \text{if } -T_g \le t \le 0 \\ s(t) & , \text{ if } 0 < t \le T_{sym} \end{cases}, \tag{2.14}$$

where T_g denotes the length of the cyclic extension added at the beginning of the symbol.

The benefits of applying a *cyclic prefix* are; first, it avoids ISI, because it acts as a guard space between successive symbols. Second, it converts the linear convolution with the channel impulse response into a cyclic convolution where the subcarriers remain orthogonal and there is no ICI. However, the use of a *cyclic prefix* increases the occupied bandwidth, which reduces the spectral efficiency [13].

2.2.5 Peak To Average Power Ratio

The peak-to-average power ratio (PAPR), consists of the superposition of many low rate streams modulated at different frequencies. For relatively large values of the number of subcarriers N_c, regardless of the modulated data symbols $d(k)$, both the real and imaginary components of $s(t)$ have Gaussian distribution, [13, 21]. The consequence of that is a Rayleigh distribution on the amplitude of the OFDM transmitted symbol $s(t)$, whereas power is Chi-square distributed with a cumulative distribution function (CDF). Because the Nyquist samples are uncorrelated Gaussian random variables, they are independent. The probability that the PAPRs of all samples are less than some threshold is given by,

$$F_N(\lambda) = \Pr(PAPR \le \lambda) = \left[F_\lambda(\lambda)\right]^N = \left(1 - \mathrm{e}^{-\lambda}\right)^N . \tag{2.15}$$

which is the joint cumulative distribution function (CDF) for the PAPR of N samples. Defining the peak to average power ratio (PAPR) as the ratio of the maximum to the average transmitted signal, defined by the following equation,

$$\mathrm{PAPR} = \frac{\max\left(\left|s_k\right|^2\right)}{\frac{1}{N_c}\sum_{k=0}^{N_c-1}\left|s_k\right|^2}, \quad k = 0,1,...,N_c - 1 , \tag{2.16}$$

where s_k represents the *k*-th sample of the transmitted signal.

When high PAPR occurs, the digital-to-analog (D/A) converter and power amplifier of the transmitter would require a large dynamic range, [13, 21].

2.2.6 Spectrum Shaping

The OFDM symbol is a summation of truncated complex exponential function of different frequencies. The power spectral density (PSD) consists of $\left|\sin(f)/f\right|^2$ shaped spectra, where a spectral mask could be applied to avoid interference between adjacent bands and the out-of-band spectrum decreases according to the *sinc* function. When the number of subcarriers decreases in an OFDM symbol its bandwidth increases. Consequently, it requires the reduction of the OFDM spectrum by applying windowing or pulse shaping, where a typical window is the raise cosine function, where a roll-off factor β represents the percentage of the roll-off segment on both sides of the window function, with a symbol duration T_{sym}, including the *cyclic prefix*. The OFDM symbol is convolved with the window function, where the window position can be adjusted in manner that, the resulting symbol has a period of length βT_{sym}. After the windowing, the transmitted signal is given by equation 2.18,

$$s(t)=\frac{1}{T_{sym}}\sum_{k=-N_c/2}^{(N_c/2)-1} d_k e^{j2\pi\frac{k}{T_{ym}}t}\bullet g\left(t-\frac{T_{sym}}{2}\right),\quad 0\le t\le T_{sym} \tag{2.17}$$

The PSD of the windowed OFDM signal is a sum of PSD of all subcarriers, as shown in Figure 2.6.

$$S_w(f)=\sum_{k=0}^{N_c-1}\left|G(f-f_k)\right|^2. \tag{2.18}$$

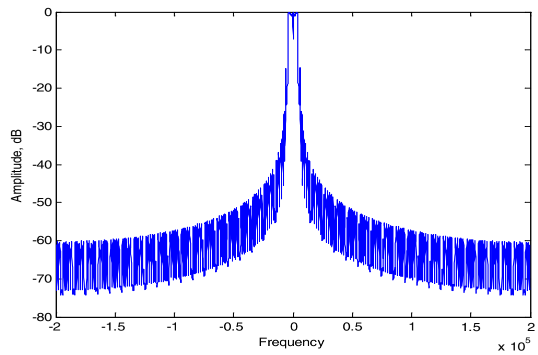

Figure 2.4. Power Spectral Density of a windowed OFDM symbol.

2.3 Physical Layer based on OFDM

Modern wireless digital communication systems have adopted OFDM as modulation mechanism at physical layer (PHY) or air access, such as wireless local area network (WLAN) systems based on the IEEE 802.11a [13, 14, 21], wireless metropolitan area network (WMAN) systems based on the standard IEEE 802.16e (worldwide interoperability for microwave access–WiMAX) and 3GPP based LTE systems,[23-27].

The transmission format of a standard physical layer (PHY) is a frame, which consists of a preamble part and a data or payload part, [13, 26]. The frame has the objective of making acquisition and demodulation possible in the receiver. In addition, the following processes are implemented in the physical (PHY) layer; burst detection, auto gain control (AGC), timing acquisition, CFO acquisition, channel estimation, equalization. A generic OFDM receiver is illustrated in Figure 2.7.

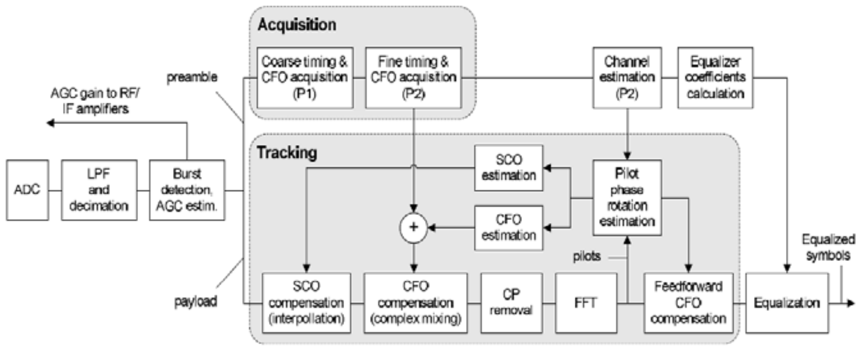

Figure 2.7. Generic OFDM receiver, [26].

2.3.1 WLAN

The institute of electrical and electronic engineers (IEEE) and The European telecommunication standards institute (ETSI) developed the IEEE 802.11a and Hiperlan/2 standards, respectively, to address low-mobility and high bandwidth applications, and are implemented by wireless local area networks (WLAN) [12].

The parameters for a WLAN based on OFDM, are defined in Table I.

Table I. WLAN parameters.

Parameter	**Value**
Sampling rate f_s=1/T_{sym}	20Msamples/s
Duration of useful data symbol T_u	64/20MHz=3.2µs
Duration of cyclic extension T_g	16/20MHz=0.8 µs or 8/20MHz=0.4 µs
Overall symbol duration T_{sym} =T_u + T_g	80/20MHz=4 µs
Number of data subcarriers N_{SD}	48
Number of pilot subcarriers N_{SP}	4
Total number of subcarriers N_{ST}	52 (N_{SD}+ $N_{SP)}$
Subcarrier spacing Δ_t	312.5kHz (1/T_u)
Total Bandwidth	20MHz
Used Bandwidth	312.5kHz*(48+4)=16.25MHz

Hiperlan/2 defines logic channels, which are transmitted through physical bursts (PhyB). Five different types of physical bursts are defined for Hiperlan/2, defined as follows,

- The *broadcast PhyB*, (Figure 2.8A).
- The *downlink PyhB*, (Figure 2.8B).
- The *short uplink PhyB* and the *long uplink PhyB*, (Figures 2.8C and 2.8D).
- The *direct link PhyB*.

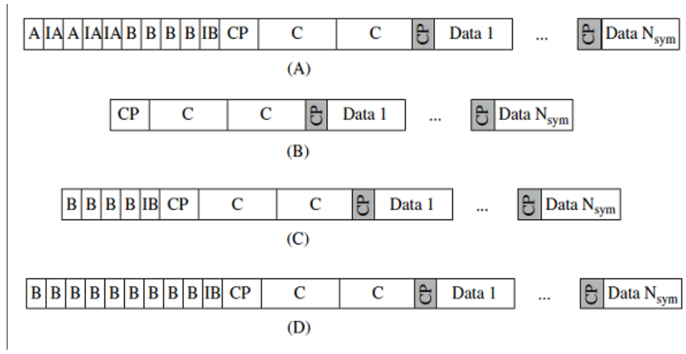

Figure 2.8. Physical burst of Hiperlan/2, [16].

The physical layer defines seven modes of operation, and combines each one with a specific modulation and coding scheme, [16].

The medium access control (MAC) layer controls the access of information to the physical layer and therefore the radio link. In Hiperlan/2, the access point (AP) takes the control of the MAC frame. Each MAC frame starts with a broadcast burst, which will be employed for automatic gain control and channel estimation, as well as frequency and frame timing synchronization [12]. The broadcast burst consists of a preamble part of length equal to $16\mu s$ long and a payload section of length equal to $(N_{sym} \cdot T_s)$. The preamble consists of, two equal length parts, [13, 26]:

- The first part of the preamble (P1), which is $8\mu s$ long and consists of 10 identical short symbols (named 'B', of $800ns$ long), it is designed to enable burst detection and *coarse* acquisition of timing an carrier frequency offset.
- The second part of the preamble (P2) is $8\mu s$ long and consists of two identical long symbols (named 'C' with $3.2\mu s$ long). A double *cyclic prefix* of $1.6\mu s$ is added, in a manner that P2 will be completely continuous in phase and cyclic. This part of the

preamble is designed to enable the fine acquisition of the timing, detect the carrier frequency offset and the channel estimation.

For a WLAN OFDM PHY, 52 subcarriers are used per channel, where 48 sub-carriers carry the data and four sub-carriers are pilots, which facilitate sampling offset tracking, carrier frequency offset tracking and phase noise compensation. These pilot signals are allocated in subcarriers -21, -7, 7 and 21, as shown in Figure 2.9.

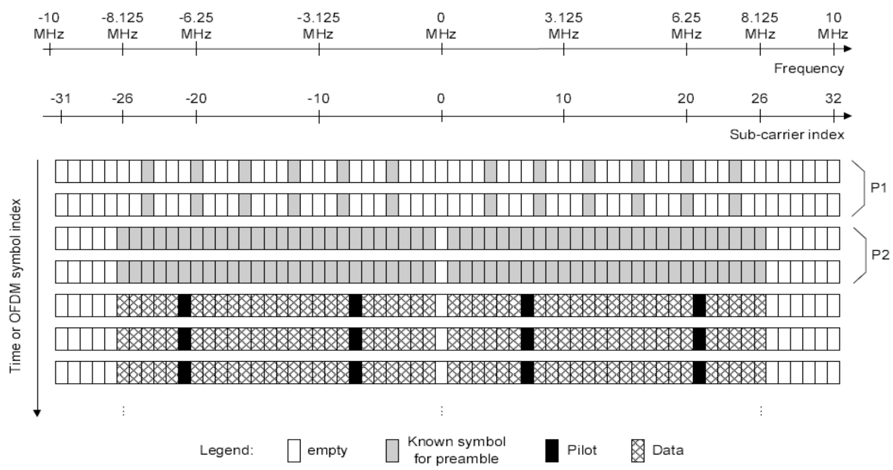

Figure 2.9. WLAN physical layer, [26].

The nominal carrier frequencies for Hiperlan/2 are allocated in two frequency bands. A lower frequency band from 5150 MHz to 5250 MHz and an upper frequency band 5470 MHz and 5725 MHz, [12]. The carrier frequency f_c corresponds to its carrier number, $n_{carrier}$, which is defined as,

$$n_{carrier} = \left(f_c - 5000\text{MHz} \right) / 5\text{MHz}. \tag{2.19}$$

2.3.2 WiMAX

The IEEE 802.16e is a suite of broadband wireless technologies complementary to IEEE 802.11 Wi-Fi. In particular, the IEEE 802.16e standard defines the broadband wireless metropolitan area network (WMAN) air interface specification, which provide broadband data link to pedestrian and mobile terminals, within a radius of 1-3 miles, [24, 27]. The 802.16e comprises a large variety of PHY configurations, capable of supporting both time division duplexing (TDD) and frequency division duplexing (FDD) based networks, with a bandwidth ranging from 1.25MHz to 20MHz, [27].

The fixed and Mobile versions of WiMAX have slightly different implementations of the OFDM physical layer. Fixed WiMAX, is determined by the IEEE 802.16-2004 standard, it employs a 256 FFT-based OFDM physical layer. The distribution of subcarriers is; 192 subcarriers selected for data, eight subcarriers as pilots and the rest of them are used as guard band. Since the FFT size is fixed, the subcarrier spacing only varies with channel bandwidth, (Table II). When larger bandwidths are used, the subcarrier spacing increases and the symbol time decreases. Decreasing the symbol time implies that a larger fraction needs to be allocated as guard time to overcome delay spread. (e.g. for maximum delay spread, a 25 percent guard time can accommodate a delay spread up to $16\mu s$ in a 3.5 MHz channel).

Mobile WiMAX is based on the IEEE 802.16e-2005 standard, it uses a scalable OFDMA-based physical layer, and the FFT size can be from 128 to 2048 bits. The subcarrier spacing is fixed to 10.94 kHz, which keeps the OFDM symbol duration, and the scaling adaptation has a minimal impact on higher layers. The subcarrier spacing of 10.94 kHz has a good balance between satisfying the *delay* spread and Doppler spread requirements for operating in mixed, fixed and mobile environments. This subcarrier spacing can support *delay* spread values up to 20 μs and vehicular mobility up to 125 Km/h when operating in 3.5GHz.

A subcarrier spacing of 10.94 kHz implies that 128, 512, 1024 and 2048 FFT are used when the channel bandwidth is 1.25MHz, 5MHz, 10MHz, 20MHz, respectively. Table II shows in a general form the OFDM-related parameters for the OFDM-PHY and the OFDMA PHY.

Table II. OFDM PHY and OFDMA PHY, [27].

Parameter	**Fixed WiMAX OFDM PHY**	**Mobile WiMAX Scalable OFDMA-PHY**			
FFT size	256	128	512	1024	2048
Number of used data subcarriers	192	72	360	720	1440
Number of pilot subcarriers	8	12	60	120	240
Number of null/guardband subcarriers	56	44	92	184	368
Cyclic prefix	1/3, 1/16,1/8,1/4				

Oversampling rate	Depends on bandwidth: 7/6 for 256 OFDM, 8/7 for multiples of 1.75MHz, and 28/25 for multiples of 1.25MHz, 1.5MHz, 2MHz, or 2.75MHz				
Channel bandwidth (MHz)	3.5	1.25	5	10	20
Subcarrier frequency spacing (kHz)	15.625	10.94			
Useful symbol time (μs)	64	91.4			
Guard time assuming 12.5% (μs)	8	11.4			
OFDM symbol duration (μs)	72	102.9			
Number of OFDM symbols in 5ms frame	69	48.0			

In FDD mode, both base station (BS) or access point (AP) and the mobile station (MS) or mobile terminal (MT) transmit at the same time in different frequencies, one for the *downlink* and one for the *uplink*.

In TDD mode, separate transmission times are allocated for *downlink* and *uplink* along a unique frame. An advantage of TDD systems is that both *uplink* and *downlink* directions share the same RF conditions of the channel (in contrast, FDD systems use distinct frequencies in each direction), which allows measurement data collected in the *uplink* to be used for RF tuning of the *downlink*.

A WiMAX TDD network requires frame level synchronization. *Downlink* frames are synchronized at the base station by global position system (GPS). The BS controls frame timing, where the synchronization signals are extracted at the receiver.

The received *downlink* frame timing is used to synchronize the *uplink* frame transmission, where adjustment information is sent by the BS to the MS to adjust its timing. A representative TDD *downlink* subframe is depicted in Figure 2.10.

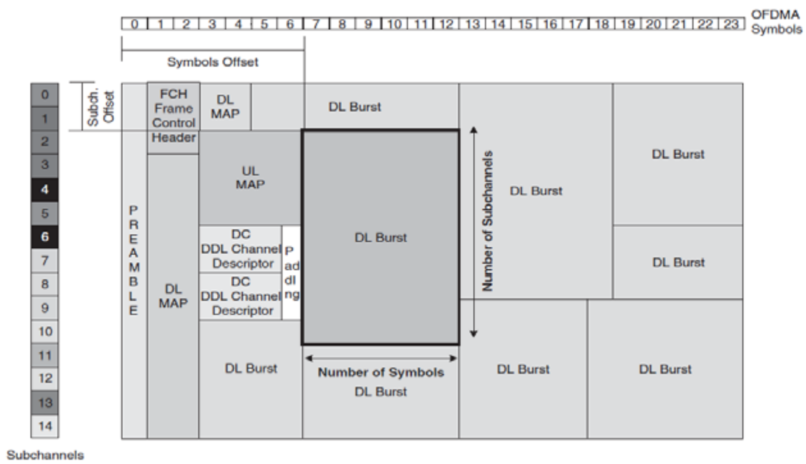

Figure 2.10. Downlink subframe and preamble allocation, [24].

Base stations control the time access by defining the beginning of *downlink* subframes, where the *downlink* subframe begins with a preamble symbol. The preamble is a pre-defined pattern (PN sequence), which allows to determinate the FFT size, channel estimation, time synchronization, frequency synchronization, cell and segment identification.

2.3.3 LTE

The long term evolution (LTE) is a mobile communication standard specified by the 3rd Generation Partnership Project (3GPP) within Release 8, [23]. LTE offers transmission rates up to 50 Mbps on the *uplink* and 100 Mbps on the *downlink*. In this system, a scalable transmission bandwidth from 1.08 to 19.8 MHz is designed, allowing mobility up to 350 Km/h, [23-26].

Long term evolution systems uses a framed structure defined by the eNodeB (eNB) or base station (BS), for the *downlink* and *uplink*. The basic structure is valid for both directions, while channel allocation is different for each. The uplink frame timing is defined at the eNB, so the user equipment (UE) or mobile station (MS) has to adjust its timing signal, and by this way, the data arrive at the right moment at the eNB.

The LTE physical layer uses:

- Orthogonal frequency division multiple access (OFDMA) is used in the *downlink*.

- DFT-S-OFDMA (Discrete Fourier transform spread OFDMA) in the *uplink*, [28, 29]. The spread is done over multiples of 12 subcarriers, [24].

Each channel is divided into frequency band of 15 kHz, each specified by a subcarrier frequency. All the LTE signals derive their timing from a clock operating at $30.72\text{MHz} = 15\text{kHz} \cdot 2048$, which is the timing required for the 2048 point DFT specified for 20MHz channels. In the time domain, the 3GPP choose a base time unit of $T_{sym} = 1/(15\text{kHz} \cdot 2048) = 32.55ns$ per clock period to define the different PHY durations.

Downlink and *Uplink* transmissions are organized into radio frames with a period defined in equation 2.21.

$$T_f = 307200 \cdot T_{sym} = 10ms \text{ per frame} \tag{2.21}$$

As indicated in Figure 2.11 each frame consists of 20 slots, numbered from 0 to 19, each one has a duration of 0.5ms for FDD transmissions, [28].

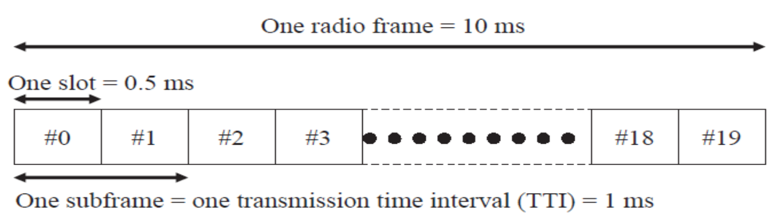

Figure 2.11. FDD Frame, [28].

An even numbered slot and their consecutive slot define a subframe, each sub-frame has a duration of 0.5ms (15360T_s), and represents a transmission time interval (TTI).

One LTE frame structure is configured in FDD or TDD. The FDD structure is called structure Type I, and the TDD frame is named structure type 2. In each frame, the subframes 0 and 5 always carry *downlink* physical channels. Subframes 1 and 6 carry synchronization signals and always contain a guard period (GP). The other frames can be either *uplink* or *downlink* physical channels. Special slots are the UpPTS and DwPTS, which refers to *uplink* and *downlink*, pilot time slots, and their location will depend on the direction of transmission of the physical channels, [23-28].

Each slot in the frame is further divided into N_{symbol}^{UL} DFT-S-OFDMA symbols or N_{symbol}^{DL} OFDM symbols for the *uplink* and *downlink*, respectively. A resource element is defined by the index pair (*k*,*l*) in a slot, where *k* and *l* are the subcarrier and OFDM/DFT-S-OFDMA symbol index, respectively.

A physical resource block (RB) is defined as N_{SC}^{RB} consecutive subcarriers in the frequency domain, and consist of $\left(N_{symbol}^{UL} \times N_{SC}^{RB}\right)$ resource elements in the *uplink* and $\left(N_{symbol}^{DL} \times N_{SC}^{RB}\right)$ resource elements in the *downlink*. The smallest unit than can be scheduled for transmission is a RB, which is 12 subcarriers wide (180 kHz) and has one slot duration (6 or 7 symbols, depending of the *cyclic prefix* used).

Two cyclic prefixes (CP) are possible in LTE, (Figure 2.12):

- Short CP for distances up to 1406km ($4.687\mu s$, $1/16^{\text{th}}$ of symbol duration or $144T_s$).
- Extended CP for distances up to 5km ($16.66\mu s$, $1/4^{\text{th}}$ of symbol duration or $512T_s$).
- An especial extended CP, with a length of $33.33\mu s\left(1024T_{sym}\right)$ for subcarrier spacing of $\Delta_f = 15\text{kHz}$.

The CP could be different for the *downlink* and *uplink*. The CP duration has to accommodate the *multipath* spread and timing deviations in the *uplink*.

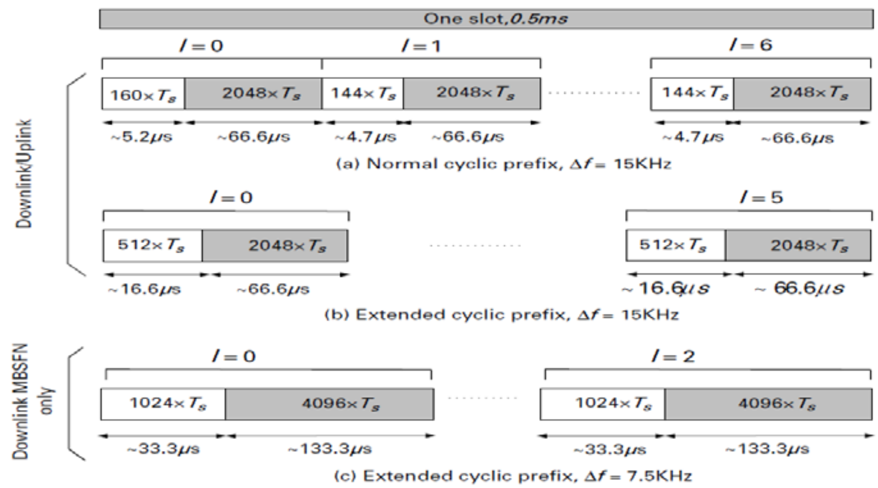

Figure 2.12. Normal and Extended Cyclic prefix, [23].

The synchronization in 3GPP LTE communication system is a particular challenging task in the *uplink* because of the UE are located at different positions. Each UE should acquire and compensate its relative time and frequency offsets before the communication take place. This process is usually achieved in two steps; the cell search procedure and the random access, [23].

The primary goal of the cell search is to enable the acquisition of the received timing (the synchronization signal timing) and frequency of the *downlink* signal. Additionally the terminals must also acquire the transmission bandwidth, the cell identification number, the radio frame timing (more than one synchronization signal is transmitted per radio frame) and the *cyclic prefix* length.

2.3.4 Summary of chapter two

The OFDM system allows the efficient use of the available bandwidth by transmiting orthogonal subcarriers in a symbol period. The orthogonality is achieved by applying the inverse discrete Fourier transform (IDFT) in the transmitter, and the DFT in the receiver. This kind of system makes use of a cyclic prefix (CP) to reduce the affectations originated by the multipath propagation channel. The peak-to-average power ratio (PAPR) consists of, the superposition of many low rate streams modulated at different frequencies. For relative large values of subcarriers in an OFDM symbol a high PAPR occurs and the power amplifier of the transmitter would require a large dynamic range. Additionally, the transmitted symbol and adjacent symbols avoids interference between them, by means of apply a windowing function.

The transmission format of a standard physical layer (PHY) is a frame, which consists of a preamble part and a data. The preamble part is implemented to define burst detection, auto gain control (AGC), timing acquisition, CFO acquisition, channel estimation, equalization.

For a WLAN OFDM PHY, a frame starts with a broadcast burst, which will be employed for automatic gain control and channel estimation, as well as frequency and frame timing synchronization. A WiMAX TDD network requires frame level synchronization at the base station (BS), where the synchronization signals are extracted at the receiver. The *downlink* subframe begins with a preamble symbol, this preamble is a pre-defined pattern (PN sequence), which allows to determinate the FFT size, channel estimation, time synchronization, frequency synchronization, cell and segment identification.

The long term evolution (LTE) is specified by the 3rd Generation Partnership Project (3GPP) within Release 8. The LTE physical layer uses Orthogonal frequency division multiple access (OFDMA) in the downlink, and DFT-S-OFDMA (Discrete Fourier transform spread OFDMA) in the uplink. The synchronization in 3GPP LTE communication system is a particular challenging task in the *uplink* because of the UE are located at different positions. Each UE should acquire and compensate its relative time and frequency offsets before the communication take place. This process is usually achieved in two steps; the cell search procedure and the random access. The primary goal of the cell search is to enable the acquisition of the received timing (the synchronization signal timing) and frequency of the *downlink* signal

Chapter 3

SYNCHRONIZATION ERRORS IN OFDM SYSTEMS

One of the principal disadvantages of OFDM is its sensitivity to synchronization errors, characterized mainly by the frequency and timing offsets. Frequency offset causes a reduction of desired signal amplitude and introduces inter-carrier interference (ICI), and is originated by the loss of orthogonality among subcarriers. The timing offset originates the rotation of the OFDM signal constellation, and causes inter-symbol interference (ISI). In this chapter, the impact of timing and frequency synchronization errors will be analyzed.

3.1 Effects of synchronization errors in OFDM

In wireless communication receivers, *coherent demodulation* needs to make use of a local oscillator (LO) at the same frequency and phase as the transmitted carrier signal of the transmitted signal, [31]. The demodulation of the received OFDM signal to *baseband* involves oscillators whose frequency may be unmatched with the transmitted frequencies. This results in a carrier frequency offset (CFO). Additionally, demodulation usually introduces phase noise acting as an unwanted phase modulation of the carrier wave. Frequency offset and phase errors between the transmitted and received frequency cause inter-carrier interference (ICI), which strongly degrade the performance of OFDM systems, [13-15, 26].

The received *baseband* signal is sampled at the analog-to-digital (A/D) converter with a sampled clock offset different to the transmitted, which originates a symbol timing offset (STO). In addition, the STO is increased by the Doppler Effect due to the mobility of the receiver, causing the contraction or expansion in time of the signal waveform. Timing synchronization is necessary to determine accurately where the OFDM symbol begins. As a result, a proper selection of the N_c-point DFT is defined [13-15, 22].

The orthogonality of the OFDM symbol is maintained by adding a *cyclic prefix*, with a length restricted to the channel impulse response length. A small timing error only appears as pure phase rotation of the data symbols and may be compensated by a channel equalizer [11-

22], still preserving the orthogonality. A large timing error results in inter-symbol interference (ISI) between adjacent symbols and inter-carrier interference (ICI).

Communicating data between a transmitter and a receiver requires some form of pathway or medium. For example in wireless communications the channel is often modeled by a random attenuation (known as fading) of the transmitted signal, followed by additive white Gaussian noise (AWGN). The channel impulse response (CIR) of a wireless transmission, affects the orthogonality among subcarriers of the received OFDM signal [31], and is expressed as follows.

$$h(t,\tau) = \sum_{m=1}^{I} \alpha_m \delta(t-\tau_m), \quad (3.1)$$

where τ is the time *delay* variable,

α_m, is the gain of the *m*-th channel path,

τ_m, denotes the *delay* of the *m*-th path.

By convolving the transmitted signal with the CIR, (Figure 3.1), and adding additive white Gaussian noise (AWGN), the received signal is,

$$r(t) = \sum_{m} \alpha_m(t) \cdot s(t-\tau) + z(t), \quad (3.2)$$

where $z(\cdot)$ is the AWGN,

$s(t)$ is the transmitted symbol,

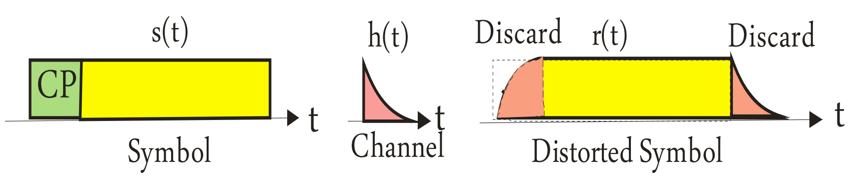

Figure 3.1. Convolution of Symbol and Channel.

Assuming that the discrete channel response is as follows, [13, 31],

$$\mathbf{h} = \{h_0, h_1, ..., h_{M-1}\}, \quad (3.3)$$

where h_k are the taps of a finite impulse response (FIR) of order M that define the power delay profile of the channel impulse response, for $k = 0,...,M-1$. The samples in the $\mathbf{h}$ vector are T_{sym} spaced.

The cyclic extension on the OFDM symbol adds $M-1$ samples [13,14], in front of the original symbol, for example with a channel of length $M = 3$ for an OFDM symbol of $N_c = 6$ samples, we have that, the original symbol is $\mathbf{s} = \{s_0, s_1, s_2, s_3, s_4, s_5\}$ and the symbol with CP is $\mathbf{s}_{CP} = \{s_4, s_5, s_0, s_1, s_2, s_3, s_4, s_5\}$, where the channel is defined by $\mathbf{h} = \{h_0, h_1, h_2\}$. The output $\mathbf{x}$ is the linear convolution of the $\mathbf{s}_{CP}$ and $\mathbf{h}$. However it is possible to determine the output $\mathbf{x}$ only by the current symbol $\mathbf{s}$, by applying the circular convolution of $\mathbf{s}$ and $\mathbf{h}$, and is equivalent to,

$$\mathbf{r} = \mathbf{s}\begin{bmatrix} h_0 & h_1 & h_2 & 0 & 0 & 0 \\ 0 & h_0 & h_1 & h_2 & 0 & 0 \\ 0 & 0 & h_0 & h_1 & h_2 & 0 \\ 0 & 0 & 0 & h_0 & h_1 & h_2 \\ 0 & 0 & 0 & 0 & h_0 & h_1 \\ 0 & 0 & 0 & 0 & 0 & h_0 \end{bmatrix}. \tag{3.4}$$

The received signal with an infinite number of OFDM symbols, (Figure 3.2), is defined by,

$$s_l(t) = \left\{ \frac{1}{\sqrt{N_c}} \sum_{l=-\infty}^{\infty} \sum_{k=0}^{N_c-1} d(k)_l \, e^{j2\pi \frac{k}{T_{sym}}\left(t - T_g - lT_{sym}\right)} \right\} \cdot g\left(t - lT_{sym}\right), \quad 0 \le t \le T_{sym}, \tag{3.5}$$

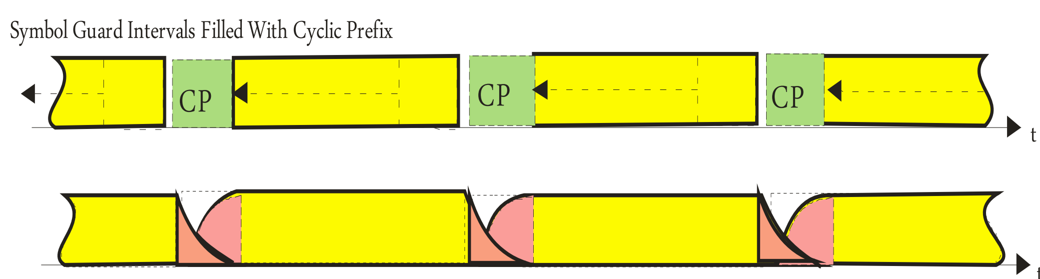

Figure 3.2. Train of OFDM symbols.

3.1.1 Symbol Timing Error

The received sampled complex valued *baseband* signal under the presence of AWGN, timing and frequency offset can be expressed as follows,

$$r(n) = s(n-\delta)e^{\frac{j2\pi\varepsilon\cdot n}{N_c}} + z(n), \tag{3.6}$$

where ε represent the carrier frequency offset,

δ is the timing offset,

z is the additive white Gaussian noise (AWGN).

$n = mT_{sym}$ is the sampling period.

The symbol timing offset δ (time domain) incurs the phase offset $2\pi k\delta/N_c$ (frequency domain), as shown in Table III, [22].

Table III. Timing Offset.

The effect of Timing offset (TO)		
	Received Signal	**TO (δ)**
Time domain	$r(n)$	$s(n+\delta)$
Frequency domain	$R(k)$	$e^{2\pi k\delta/N}S(k)$

Depending on the location of the estimated starting point of OFDM symbol, the effect of symbol timing offset is different and originate multiples cases, [13, 14, 22], as is depicted in Figure 3.3.

Case I: The estimated starting point of the OFDM symbol coincide with the exact timing point where the symbol begins. The transients at the boundaries of an OFDM block disturb the adjacent blocks only during the cyclic prefix, as shown in Figure 3.3. As the receiver selects the samples outside the cyclic prefix, no inter-symbol interference is introduced.

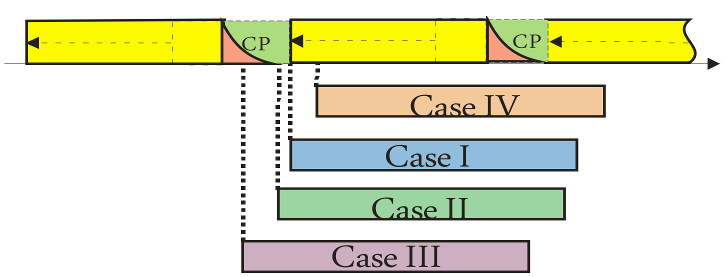

Figure 3.1. Location of the starting point of an OFDM symbol.

Case II: The estimated starting point is located before the exact point and out of the maximum channel *delay* spread. The *l*-th symbol is not overlapped with the previous (*l-1*)-th symbol and ISI is avoided in this case. By taking the FFT of the received samples we observe that,

$$R_l(k)=\frac{1}{N_c}\sum_{n=0}^{N_c-1}s_l(n+\delta)e^{-j2\pi nk/N_c}=\frac{1}{N_c}\sum_{n=0}^{N_c-1}\left\{\sum_{p=0}^{N_c-1}s_l(k)e^{j2\pi(n+\delta)p/N_c}\right\}e^{-j2\pi nk/N_c}$$
$$=\frac{1}{N_c}\sum_{p=0}^{N_c-1}s_l(k)e^{j2\pi k\delta/N_c}\sum_{n=0}^{N_c-1}e^{j2\pi\frac{(p-k)}{N_c}n}=s_l(k)e^{j2\pi k\delta/N_c}\ , \tag{3.7}$$

where,

$$\sum_{n=0}^{N_c-1}e^{j2\pi\frac{(p-k)}{N_c}n}=e^{j\pi(p-k)\frac{N_c-1}{N_c}}\cdot\frac{\sin\left[\pi(k-p)\right]}{\sin\left[\pi(k-p)/N_c\right]}=\begin{cases}N_c & for\ k=p\\ 0 & for\ k\neq p\end{cases}. \tag{3.8}$$

We can observe in equation 3.7 that the orthogonality among subcarrier is preserved, with only a phase offset that is proportional to the timing offset δ and subcarrier index k, which originates a rotation of the original signal constellation.

Case III: The starting point of the symbol is positioned within the interval of the maximum *delay* spread. In this case, the location of the symbol causes ISI and the orthogonality of the subcarriers is lost. Additionally, inter-carrier interference occurs.

Case IV: The symbol is located after the exact starting point. The signal within the FFT interval consists of a part of the current OFDM symbol $s_l(k)$ and a part of the next one $s_{l+1}(k)$, and is defined as follows,

$$r_l(k)=\begin{cases}s_l(n+\delta) & \text{for } 0\leq n\leq N_c-1-\delta\\ s_{l+1}(n+2\delta-N_g) & \text{for } N_c-\delta\leq n\leq N_c-1\end{cases}, \tag{3.9}$$

$$
\begin{aligned}
R_l(k) &= FFT\{r_l(n)\} \\
&= \sum_{n=0}^{N_c-1-\delta} s_l(n+\delta) e^{-j2\pi nk/N_c} + \sum_{n=N_c-\delta}^{N_c-1} s_{l+1}(n+2\delta-N_g) e^{-j2\pi nk/N_c} \\
&= \sum_{n=0}^{N_c-1-\delta}\left(\frac{1}{N_c}\sum_{p=0}^{N_c-1} d_l(p) e^{j2\pi(n+\delta)p/N_c}\right) e^{-j2\pi nk/N_c} + \sum_{n=N_c-g}^{N_c-1}\left(\frac{1}{N_c}\sum_{p=0}^{N_c-1} d_{l+1}(p) e^{j2\pi(n+2\delta-N_g)p/N_c}\right) e^{-j2\pi nk/N_c} \\
&= \frac{1}{N_c}\sum_{p=0}^{N_c-1} d_l(p) e^{j2\pi p\delta/N_c} \sum_{n=0}^{N_c-1-\delta} e^{j2\pi\frac{(p-k)}{N_c}n} + \frac{1}{N_c}\sum_{p=0}^{N_c-1} d_{l+1}(p) e^{j2\pi p(2\delta-N_g)/N_c} \sum_{n=N_c-\delta}^{N_c-1} e^{j2\pi\frac{(p-k)}{N_c}n} \\
&= \frac{N_c-\delta}{N_c} d_l(p) e^{j2\pi p\delta/N_c} + \mathrm{ICI} + \mathrm{ISI},
\end{aligned}
\tag{3.10}
$$

where,

$$
\mathrm{ICI} = \sum_{p=0,\, p\neq k}^{N_c-1} d_l(p) e^{j2\pi p\delta/N_c} \sum_{n=0}^{N_c-1-\delta} e^{j2\pi\frac{(p-k)}{N_c}n}, \tag{3.11}
$$

$$
\mathrm{ISI} = \frac{1}{N_c}\sum_{p=0}^{N_c-1} d_{l+1}(p) e^{j2\pi(2\delta-N_g)/N_c} \sum_{n=N_c-\delta}^{N_c-1} e^{j2\pi\frac{(p-k)}{N_c}n}, \tag{3.12}
$$

$$
\sum_{n=0}^{N_c-1-\delta} e^{j2\pi\frac{(p-k)}{N_c}n} = e^{j\pi(p-k)\frac{N_c-1-\delta}{N_c}} \cdot \frac{\sin\left(\left(N_c-\delta\right)\pi\left(k-p\right)/N_c\right)}{\sin\left(\pi\left(k-p\right)/N_c\right)} = \begin{cases} N_c-\delta & for \quad p=k \\ Nonzero & for \quad p\neq k \end{cases}. \tag{3.13}
$$

The ICI implies that the orthogonality has been destroyed, and ISI term exists.

In order to take the N_c-point FFT symbol, a symbol timing synchronization must be performed to detect the exact starting point of each symbol (with the CP removed) [22]. Timing offset introduces a phase rotation as shown in Figure 3.4. When the orthogonality of the symbols is preserved a slightly phase rotation can be compensated after FFT.

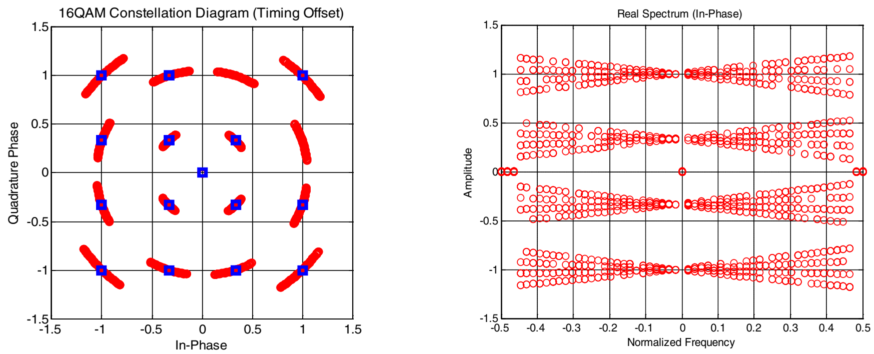

Figure 3.2. Timing Offset.

3.1.2 Carrier Frequency Offset

The carrier frequency applied to the *baseband* signal at the transmitter and the *passband* in the receiver must be equal. In general, there are two main types of distortion associated with the carrier signal. One is the phase noise due to the instability of carrier signal generators used at the transmitter and receiver. The other is the carrier frequency offset (CFO) caused by Doppler frequency shift f_D (i.e. Table IV), [13-15, 20].

Being f_c the carrier frequency in the transmitter and f_c' the carrier frequency generated in the receiver. The frequency f_{offset} is the difference between the reference frequencies f_c and f_c': $f_{offset} = f_c - f_c'$.

Table IV. Doppler frequency offset.

System	Carrier Frequency, f_c	Subcarrier Spacing, Δ_f	Velocity, v	Doppler Frequency, f_D	Normalized CFO, ε
Mobile WiMAX	2.3 GHz	9.765kHz	120km/h	255.55Hz	0.0263
3GPP LTE	2 GHz	15kHz	120km/h	222.22Hz	0.0148

The normalized carrier frequency offset (CFO), ε, can be written as a ratio of the f_{offset} to subcarrier spacing Δf, defined by,

$$\varepsilon = \frac{f_{offset}}{\Delta f}. \tag{3.14}$$

The normalized frequency offset is shown in Figure 3.5, where is possible to observe the misalignment of the subcarrier with respect to the correct frequency, and the ICI results of selecting components in frequency of adjacent subcarriers.

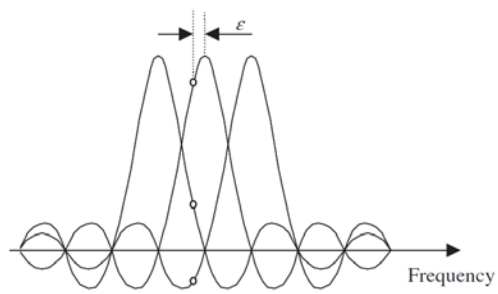

Figure 3.3. Normalized CFO, [22].

Analyzing the constellation of the received symbols, the phase and amplitude distortion is evident in Figure 3.6a and 3.6b, respectively. These distortions increase with a higher value of carrier frequency offset.

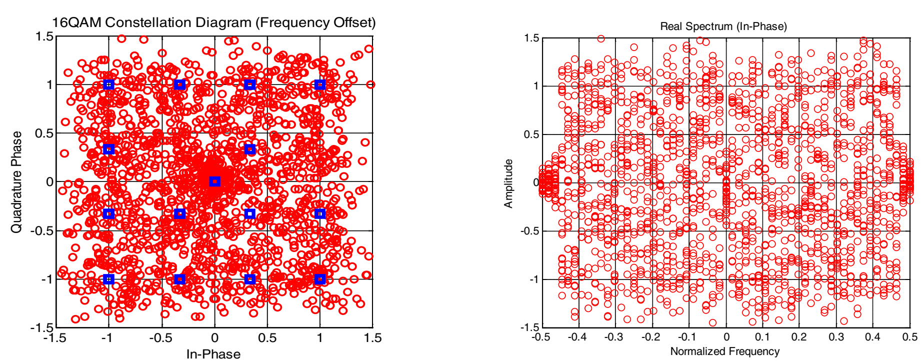

(a) (b)

Figure 3.4. Frequency offset.

It is possible to separate the value ε into two terms, $\varepsilon = \varepsilon_i + \varepsilon_f$, where ε_i represent the integer part of the complete frequency offset, and ε_f denote the fractional part of ε with a range delimited by $|\varepsilon_i| < \frac{1}{2}$. The integer offset rotates the signal by the factor $e^{j2\pi\varepsilon_i n/N_c}$, which originates a cyclic shift of the signal $d(k-\varepsilon_i)$ of each subcarrier. The orthogonality of the subcarriers is not affected (no inter-carrier interference occurs), [13-15, 20-22]. The affectation of the signal in the time and frequency domain is determined in Table V.

Table V. Carrier frequency offset.

The effect of carrier frequency offset (CFO)		
	Received signal	**Effect of CFO ε**
Time-domain	$y[n]$	$e^{j2\pi n\varepsilon/N}x[n]$
Frequency-domain	$Y[k]$	$X[k-\varepsilon]$

The affectation originated by the fractional offset ε_f is as follows:

$$
\begin{aligned}
R_l(k) &= FFT\{s_l(n)\} = \sum_{n=0}^{N-1} s_l(n)e^{-j2\pi kn/N} \\
&= \sum_{n=0}^{N-1}\frac{1}{N}\sum_{m=0}^{N-1}H(m)d_l(m)e^{j2\pi(m+\varepsilon_f)n/N}e^{-j2\pi kn/N} + \sum_{n=0}^{N-1}z_l(n)e^{-j2\pi kn/N} \\
&= \frac{1}{N}\sum_{m=0}^{N-1}H(m)d_l(m)\sum_{n=0}^{N-1}e^{j2\pi(m-k+\varepsilon_f)n/N} + Z_l(k) \\
&= \frac{1}{N}H(k)d_l(k)\sum_{n=0}^{N-1}e^{j2\pi\varepsilon_f n/N} + \frac{1}{N}\sum_{m=0,m\neq k}^{N-1}H(m)d_l(m)\sum_{n=0}^{N-1}e^{j2\pi(m-k+\varepsilon_f)n/N} + Z_l(k) \\
&= \frac{1}{N}\frac{1-e^{j2\pi\varepsilon_f}}{1-e^{j2\pi\varepsilon_f/N}}H(k)d_l(k) + \frac{1}{N}\sum_{m=0,m\neq k}^{N-1}H(m)d_l(m)\frac{1-e^{j2\pi(m-k+\varepsilon_f)}}{1-e^{j2\pi(m-k+\varepsilon_f)/N}} + Z_l(k) \\
&= \frac{1}{N}\frac{e^{j\pi\varepsilon_f}\left(e^{-j\pi\varepsilon_f}-e^{j\pi\varepsilon_f}\right)}{e^{j\pi\varepsilon_f/N}\left(e^{-j\pi\varepsilon_f/N}-e^{j\pi\varepsilon_f/N}\right)}H(k)d_l(k) \\
&\quad + \frac{1}{N}\sum_{m=0,m\neq k}^{N-1}H(m)d_l(m)\frac{e^{j\pi(m-k+\varepsilon_f)}\left(e^{-j\pi(m-k+\varepsilon_f)}-e^{j\pi(m-k+\varepsilon_f)}\right)}{e^{j\pi(m-k+\varepsilon_f)/N}\left(e^{-j\pi(m-k+\varepsilon_f)/N}-e^{j\pi(m-k+\varepsilon_f)/N}\right)} + Z_l[k] \\
&= e^{j\pi\varepsilon_f(N-1)/N}\left\{\frac{\sin(\pi\varepsilon_f)}{N\sin(\pi\varepsilon_f/N)}\right\}H_l(k)d_l(k) + \mathrm{ICI} + Z_l(k)
\end{aligned}
\tag{3.15}
$$

$$\text{where, ICI} = e^{j\pi\varepsilon_f (N-1)/N} \sum_{m=0}^{N-1} \frac{\sin\left(\pi\left(m-k+\varepsilon_f\right)\right)}{N\sin\left(\pi\left(m-k+\varepsilon_f\right)/N\right)} H(m)\, d_l(m)\, e^{j\pi(m-k)(N-1)/N} \tag{3.16}$$

The first term in equation 3.16 denotes the amplitude and phase distortion of the *k*-th subcarrier frequency component, originated by the fractional frequency offset. Frequency offset influences the orthogonality and it is necessary to be corrected before apply the DFT.

3.1.3 Summary of chapter three

In this chapter, have been reviewed the timing and frequency synchronization error of the OFDM transmitted signal, which results in Inter symbol interference (ISI) and Inter carrier interference (ICI).

Frequency offset and phase errors between the transmitted and received frequency cause inter-carrier interference (ICI), which strongly degrade the performance of OFDM systems. A large timing error results in inter-symbol interference (ISI) between adjacent symbols and inter-carrier interference (ICI).

The channel impulse response (CIR) of a wireless transmission, affects the orthogonality among subcarriers of the received OFDM signal, where the multipath propagation originates the most considerable affectations over the transmitted signal.

The effects of symbol timing offset depends on the location of the estimated starting point of OFDM symbol and originates multiples cases, where the timing offset estimation allows to define correctly the beginning of the OFDM symbol avoiding the ISI and ICI.

The estimation of the frequency offset requires determine the integer and fractional frequency offset, directly related to the subcarrier spacing of the transmitted symbol.

Chapter 4

PREAMBLES

The present chapter is focused to explain the diversity of methods to achieve the goal of synchronization, in specific the data aided methods based on preamble sequences. The preamble sequences are configured in a short or long preamble, which are characterized to synchronize the coarse and fine frequency offset. The preamble-based systems are specially applied to synchronize the OFDM systems, such as, IEEE 802.11a, WiMAX and LTE. The synchronization preambles are designed with pseudo noise, Gold, CAZAC and Golay sequences.

4.1 Synchronization Schemes

Timing and frequency synchronization schemes uses some form of repetition in the transmitted OFDM signal and can be divided into the following categories:

- Data- aided method
- Non-data-aided method

The Non-data-aided often uses the *cyclic prefix* inserted in the guard interval, [13,15].

Synchronization based on data-aided methods uses a training sequence or pilot symbol for estimation. This kind of method detects the start of the frame, define the symbol timing, and perform the estimation of the carrier frequency offset, [13-16, 22].

Synchronization is usually implemented in two phases:

- Acquisition phase or coarse synchronization
- Tracking phase or fine synchronization

Synchronization of the OFDM systems can be performed in the following steps, [11-22]:

- Coarse timing frame synchronization
- Coarse frequency offset correction
- Fine frequency correction, (after FFT)

- Fine timing correction, (after FFT)

Acquisition estimation schemes generally have a wide frequency range, but low accuracy. Tracking algorithms have a narrow frequency range and finer accuracy.

Coarse synchronization and *fine synchronization* can be carried out by utilizing either the OFDM inherent *cyclic prefix* or a specially designed pilot tone or training sequence (preamble). For both schemes exist the following methods, [13-16]:

- The maximum likelihood (ML) method
- Minimum mean squared error (MMSE) method
- Maximum correlation (MC) method

In a timing synchronization scheme, the initial estimation is evaluated over a wide range of samples depending on the estimation method. The receiver may need to search over $N_c + N_g$ samples to approximate the starting time. Once the initial timing start $\hat{\theta}$ has been found, the phase tracking may involve searching over a narrower range.

In the case of frequency synchronization, coarse frequency synchronization acquisition finds the correct tone numbering and fine frequency acquisition the fractional offset, from the available receiver subcarriers. In practice, the fine frequency offset is estimated in first place, and the coarse frequency offset in the second place.

4.2 Preamble Sequences

The design of the preamble sequence is classified in the following categories, [13-16, 22],

- Short training symbol or short preamble
- Long training symbol or long preamble

The short training symbols are applied to make coarse carrier frequency offset estimation with a large unambiguous range, and the long training symbols can be used for estimation of timing, fine frequency offset, and channel estimation, [13]. Both training symbols can do the same. However, the short training symbols provide quicker measurements and adjustments.

The period of repetitive structures defines a long preamble, with a symmetric sequence defined by a half of OFDM symbol and period $L_L = N_c/2$, as shown in Figure 4.1.

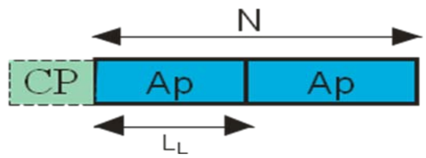

Figure 4.1. Long preamble.

A short preamble is a repetitive period sequence A_p of length $L_S = N_c/4$, (Figure 4.2).

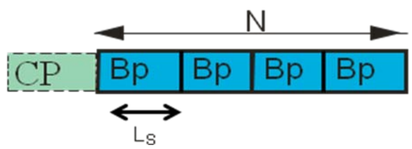

Figure 4.2. Short preamble.

The functionality of these preambles depends on well-designed sequences. The design and selection of the sequences for the diverse applications are based on their properties of autocorrelation and cross-correlation. An important criterion of design is the reduced PAPR in order to avoid nonlinearity degradation during synchronization. The most important sequences used are *m*-sequences, Gold, CAZAC and Golay sequences, [32-38]. On the following section are detailed the design of sequences used for synchronization in OFDM based systems.

4.2.1 Preamble for IEEE 802.11a

The OFDM symbol of IEEE 802.11a is implemented by a 64-point FFT, where only 52 subcarriers are used. The other 12 subcarriers are just null carriers. The nonzero subcarrier indexes range from -26 to 26; with the 0^{th} subcarrier unused and 4 subcarriers are used for pilot symbols. The total of data subcarriers is 48.

The OFDM synchronizer for the IEEE 802.11a WLAN standard uses two $8\mu s$ symbols for the detection of the start of the packet, timing, and frequency offset. Figure 4.3 shows the OFDM training structure (preamble), where t_1 to t_{10} denote repetitions of a short training symbol, where T_1 and T_2 are identical parts of a long training symbol with $GI-2$ as its *cyclic prefix*, [12, 13],

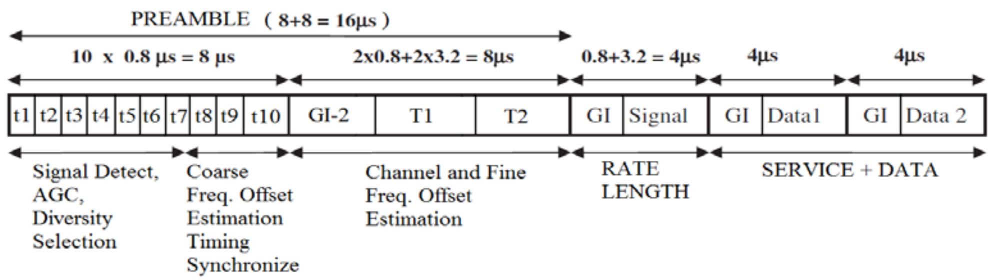

Figure 4.3. IEEE 802.11a preamble, [12].

The short training symbols are located on nonzero subcarriers whose indexes are multiple of 4, i.e., $\{\pm4,\pm8,\pm12,\pm16\pm20,\pm24\}$, as shown in Figure 4.4.

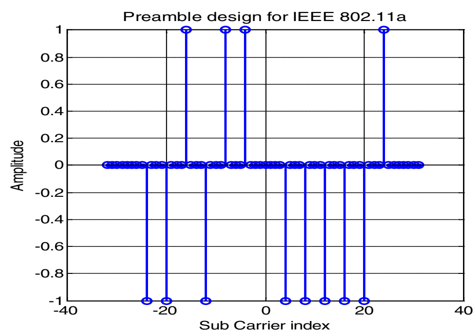

Figure 4.4. Short training symbol.

A short OFDM training symbol consists of 12 subcarriers, which are modulated by the elements of the sequence S:

$$\begin{aligned} S_{-26,26} = \sqrt{13/6}\times\{&0,0,1+j,0,0,0,-1-j,0,0,0,1+j,\\ &0,0,0,-1-j,0,0,0,-1-j,0,0,0,1+j,0,0,0\\ &0,0,0,-1-j,0,0,0,-1-j,0,0,0,1+j,\\ &0,0,0,1+j,0,0,0,1+j,0,0,0,1+j,0,0\} \end{aligned} \tag{4.1}$$

The multiplication by a factor of $\sqrt{13/6}$ is used to normalize the average power of the resulting OFDM symbol, which utilizes 12 out of 52 subcarriers.

The spectral lines of $S_{-26,26}$, with indices that are a multiple of 4 and non zero amplitude, results in a periodicity of $T_{FFT}/4 = 0.8\mu s$. The output samples of the 64-point IFFT actually have a period of 16 samples. Consequently, we can obtain four short training symbols from the output of the 64-point IFFT. The remaining six short training symbols are obtained by periodic extension. Note that the magnitude of time domain samples of a short symbol is not constant [12], as shown in Figure 4.5.

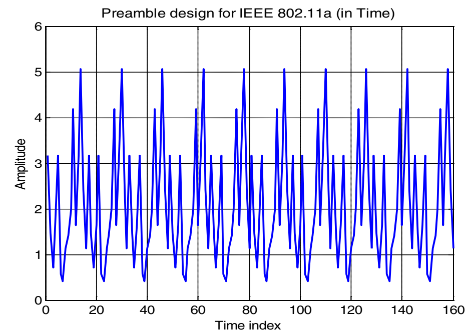

Figure 4.5. Preamble with ten short training symbols.

The long training symbol is represented on each non-zero subcarrier. A long OFDM training symbol consists of 52 subcarriers (excluding the DC component), which are modulated by the elements of a sequence *L* given by equation 4.2, (Figure 4.6). The pilots are *M*-PSK symbols modulated by a pseudo binary sequence to prevent the generation of spectral lines.

$$\begin{aligned} L_{-26,26} = \{&1,1,-1,-1,1,1,-1,1,-1,1,1,1,1,1,1,-1,-1,1,\\ &1,-1,1,-1,1,1,1,1,0,1,-1,-1,1,1,-1,1,-1,1,\\ &-1,-1,-1,-1,-1,1,1,-1,-1,1,-1,1,-1,1,1,1,1\} \end{aligned} \tag{4.2}$$

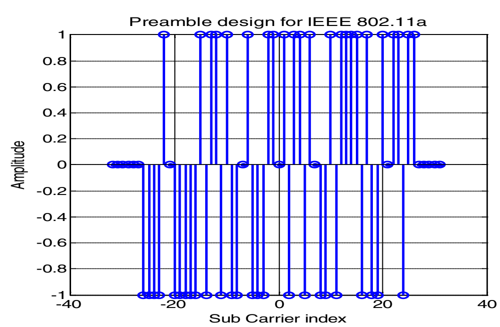

Figure 4.6. Long training symbol.

After the preamble, in each OFDM symbol, four of the subcarriers are dedicated to pilot signals in order to make the coherent detection robust against frequency offsets and phase noise. These pilot signals are located in subcarriers -21,-7, 7 and 21. The time-domain samples are obtained by 64 point IFFT, with extended two periods plus a cyclic extension, (Figure 4.7).

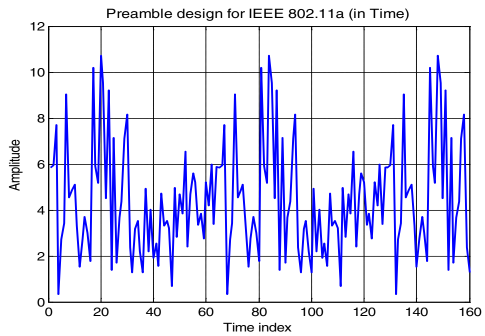

Figure 4.7. Preamble with three long training symbols.

The IEEE 802.11a standard requires the maximum offset per user to be 20 parts per million (ppm), which means that the offset seen by the receiver could be as high as 40 ppm. Thus, the maximum offset is 232 kHz for carrier frequency of 5.8 GHz, which is within the 625 kHz range that can be estimated. The IEEE 802.11a wireless local area network (WLAN) standard does not specify particular synchronization techniques to be used, other than the structure and distribution of the training symbols. However, the long training symbol structure is similar to Schmidl and Cox [39] method, and the short training symbol structure consists of multiple repetitions of a basic pattern, [12].

4.2.2 Preamble for WiMAX

The preamble designed for OFDMA (WiMAX) is an extended version of the preamble applied for OFDM (WLAN) systems, given in Figure 4.8. The main difference between the preamble for WLAN and WiMAX is in the frame designed for multiple accesses. The WiMAX frame is split into two subframes separated by guard periods, where the first subframe contains the *downlink* symbols and the continuous subframe contains the *uplink* symbols. The allocation of the synchronization preamble is located in the *downlink* subframe.

The main objective of the preamble is carry out when a mobile station is turn on, or enters a new cell area, scanning for a valid WiMAX base station. The first step on synchronization process is to detect the preamble and estimate the coarse symbol timing, and secondly is estimated the carrier frequency offset (CFO). The symbol timing and CFO can be estimated jointly or individually, [13-16].

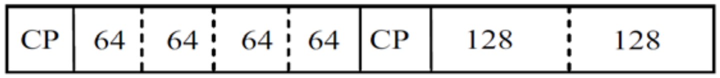

Figure 4.8. Preamble for IEEE 802.16 OFDM *downlink* access.

The functionality of the pilot–assisted synchronization methods depend on well-designed pilot tones or preambles. The basic principles behind this kind of methods are the auto–correlation, cross–correlation and hybrid detection of the transmitted preamble, [12, 13]. The big advantage of these methods is that can be implemented on one-bit quantization of the received signal. This allows a reduced complexity of the digital part and hence lowers the power consumption. Taking the advantage of the repetition pattern of a sequence, numerous training preambles have been proposed in the literature, they are designed in particular for OFDM and OFDMA systems, (e.g., Table VI).

Table VI. Preamble Design for Timing and Frequency Synchronization.

Method	Preamble	Designed Sequence
Schmidl and Cox, (1997), [39]	$\mathbf{S}_s = [A\ A]$	A = PN sequence of length L =N/2, (where N is the length of an OFDM symbol).
Minn et al., (2003), [40]	$\mathbf{S}_s = [A\ A\ -A\ -A]$	A = PN sequence of length L=N/4, (where L is a power of 2 lengths, e.g. 16, 32, 64).
B. Park, (2003), [41]	$\mathbf{S}_s = [A\ B\ A^*\ B^*]$	A,B = PN sequence of length L=N/4, * = Complex Conjugated value.
G. Ren, (2005), [42]	$\mathbf{S}_s = [C\ C]\bullet B$	C = CAZAC sequence of length L, B = PN sequence of length N.

4.2.3 Preamble for LTE System

The cell search procedure in LTE begins with a synchronization procedure, which makes use of two specially designed preamble signals, which are broadcast in each cell, [22-25]:

- The primary synchronization signal (PSS)
- The secondary synchronization signal (SSS)

The primary goal of the cell search procedure is to enable the acquisition of the received timing and frequency of the *downlink* signal (e.g., *downlink* synchronization signals are transmitted in the sub frame 1 and 6 for FDD). The detection of PSS and SSS signals not only enables time and frequency synchronization, but also provides the mobile station with the physical layer identity of the cell, the *cyclic prefix* length, and informs to the MS whether the cell uses FDD or TDD.

The PSS and SSS are transmitted on the central 1.08MHz band, consisting of 72 subcarriers (subcarrier spacing of 15 kHz) including guard band, (Figure 4.9), within a scalable transmission bandwidth (from 1.25 to 20MHz).

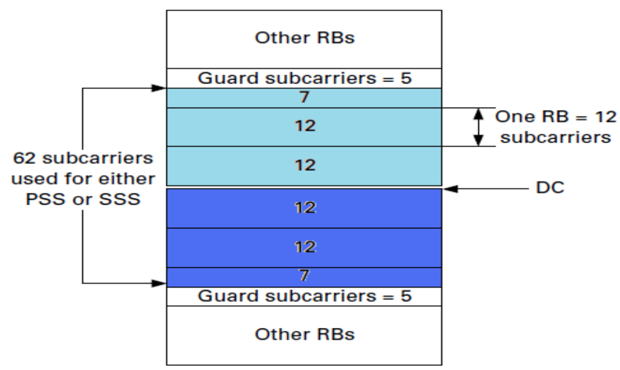

Figure 4.9. Subcarrier allocation for PSS and SSS signals.

In the 3GPP LTE system, 504 unique cells can be distinguished by combining three physical layer cell-identities provided by PSS; additionally 168 physical layer cell identity groups are provided by SSS. In the first step of *downlink* synchronization the MS uses PSS with a period of 5ms, which has been transmitted twice in a frame, to estimate symbol timing and CFO. PSS is also used to detect the physical layer cell identity. In the second step of *downlink* synchronization, SSS is used to detect the physical layer cell ID group and frame timing [23].

The three PSS sequences are selected of a three length-63 Zadoff – Chu (ZC) sequences (roots M = 25, 29 and 34), that simultaneously is extended with five zeros at the edges and mapped to the center 73 subcarriers. The structure of SSS is based on the frequency interleaving of two length-31 *m*-sequences X and Y, each one can represent 31 different values (31 different shifts of the same *m*–sequence like a Gold Sequence) [23, 43]. The set of valid combinations of X and Y are 168, allowing for detection of the physical layer cell identity.

4.3 Design of Synchronization Sequences

4.3.1 Pseudo-Noise Sequence

A pseudo noise sequence can be generated by using a linear feedback shift register (LSFR) [32-36]. A shift–register sequence with the maximum possible period for an L – stage register is called *maximal length sequence* or *m*–sequence, having a period equal to $L_{pn} = 2^r - 1$. The *m*-sequence of length $2^r - 1$ has the following attributes;

- *Balance property*: the sequence contains one more 1 than 0 in each period, that is, 2^{L-1} 1's and $2^{L-1} - 1$ 0's.
- *Two level autocorrelation:* the periodic *auto-correlation* function for the *m*-sequence $x(n)$ has two-level, (Figure 4.10a), defined by:

$$R_m(k) \triangleq \frac{1}{M} \sum_{n=0}^{M-1} x(n)x(n+k). \tag{4.3}$$

The periodic *auto-correlation* function $R_m(k)$ equals:

$$R_m(k) = \begin{cases} 1.0 & k = pM \\ -\dfrac{1}{M} & k \neq pM \end{cases}, \tag{4.4}$$

The *auto-correlation* of an *m–sequence* is 1 for zero–lag, and nearly zero (-1/ M, where M is the sequence length) for all other lags. In other words, the *auto-correlation* of the *m*–sequence can be said to approach unit impulse function as *m*–sequence length increases.

An important characteristic of *m*-sequence is the aperiodic correlation; this advantage is also used for synchronization of spread spectrum systems, [32-36], where the synchronization window is one period long, Figure 4.10b. The PAPR of an *m*–sequence with length L=31 is around 3dB, as is shown in Figure 4.10c.

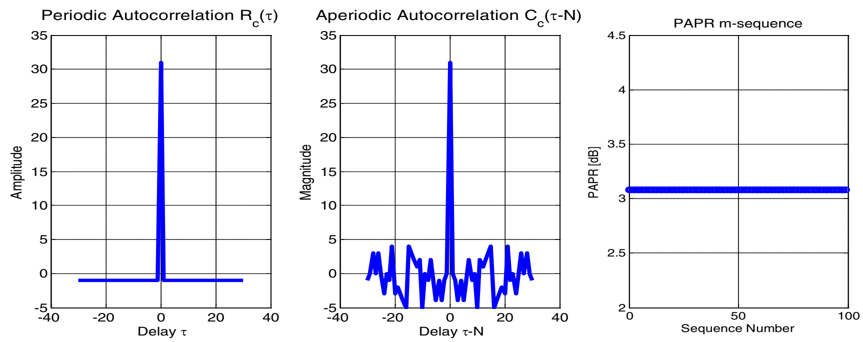

(a) (b) (c)

Figure 4.10. (a) Periodic *auto-correlation m*-sequence; (b) Aperiodic *auto-correlation m*-sequence; (c) PAPR of *m*-sequence.

4.3.2 Gold Sequence

The Gold sequence has been proposed by Gold in 1967 [33-34, 38, 45]. We consider an *m*-sequence that is represented by a binary vector b of length *N*, and a second sequence $\hat{b}$ obtained by decimating every *q*-th symbol of b, (i.e., $\hat{b} = b[q]$). When a *m*-sequence is decimated and is obtained another *m*-sequence, so it is possible to corroborate that $\hat{b} = b[q]$ has period *N* with the greatest common divisor $\gcd(N, q) = 1$.

For example, given the periodic sequence b=0010111 0010111 0010111, of period *N*=7, applying a decimation by 2 and 3 we get the corresponding decimated sequences $\hat{b}_2 = b[2] = 0111001\ 0111001\ 0111001$ and $\hat{b}_3 = b[3] = 0011101\ 0011101\ 0011101$. From the resulting sequences, it is possible to observe that $\hat{b}_3$ is also an *m*–sequence of period 7 and $\hat{b}_2$ is simply a cyclically shifted version of b. Gold proved that certain pairs of sequences of length *N* exhibit three–valued cross–correlation function with the values $\{-1, -t(L), t(L)-2\}$, they are called *preferred pairs* or *preferred sequences*, where *t* depends only on the length of the linear feedback shift register (LSFR) used, with *L* memory elements [33, 43],

$$t(L) = \begin{cases} 2^{(L+1)/2} + 1, & L, \quad odd \\ 2^{(L+2)/2} + 1, & L, \quad even \end{cases}. \tag{4.5}$$

From a pair of preferred sequences, say a_k and b_k, we construct a set of sequences of length N by taking the modulo-2 sum of a_k with the N cyclic shifted versions of b_k or vice versa. Then, we obtain N new periodic sequences with a period $N = 2^L - 1$. We may also include the original sequences a_k and b_k to get a set of $N+2$ sequences, which are named *Gold sequences.*The auto–correlation properties of Gold sequences are not as good as that of *m*–sequences (auto–correlation is not two valued), but these sequences provide some better characteristics compared to *m*–sequences, [33].

A Gold sequence of degree 5 with a period $N = 2^5 - 1 = 31$ is generated by two preferred sequences, described by the parity polynomials: $h_1(X) = X^5 + X^3 + 1$ and $h_2(X) = X^5 + X^4 + X^3 + X + 1$. In this case, there are 33 different sequences, corresponding to the 33 relative phases of the two *m*-sequences. The generated sequences have three–valued cross–correlation values of $\{-1, -t(5), t(5) - 2\}$, where $t(5) = 2^{5+1/2} + 1 = 9$, resulting in the cross–correlation values of $\{-1, -9, 7\}$, as is shown in Figure 4.11a and 4.11b, respectively. Additionally we can observe the highest PAPR of Gold sequence of almost 6.5dB in Figure 4.11c.

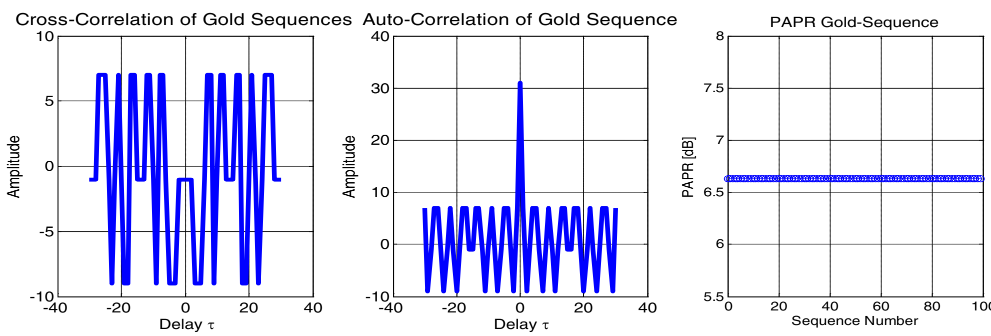

(a) (b) (c)

Figure 4.11. (a) Periodic *auto-correlation* m-sequence; (b) Aperiodic *auto-correlation* m-sequence; (c) PAPR of m-sequence.

4.3.3 CAZAC Sequence

Wireless signals interfere among them in the air, for that reason, it is necessary to code individual sequences that can be uniquely identified, even when mixed with other sequences. Additionally, a code sequence having a low correlation with shifted versions of the same code, ideally, they should have constant amplitudes.

A Zadoff – Chu (ZC) sequences (also known as generalized chirp–like (GCL) sequences or polyphase sequences) are non–binary unit amplitude sequence, (Figure 4.12a), which satisfies a constant amplitude zero *auto-correlation* (CAZAC) property, Figure 4.12b, [37, 43, 45]. CAZAC sequences are complex signals of the form $e^{j\alpha_k}$. A basic Zadoff – Chu sequence is generated by selecting an appropriate “root”. In the frequency domain, expressed as follows,

$$X_{ZC}^{u}\left(k\right)=e^{-j\pi u\frac{k(k+1)}{M_{ZC}}}, \tag{4.6}$$

where M_{ZC} is the sequence length (preferably a prime number),

u is the sequence root (an integer number relatively prime to M_{ZC}).

An important property of ZC sequence consist on the “ideal” cyclic *auto-correlation*, (Figure 4.12c), where the correlation of the root sequence with its circularly shifted version is a delta function, expressed as the zero *auto-correlation* function defined by,

$$R_{zc}\left(k\right)=\sum_{n=0}^{N_{ZC}-1}x_{zc}\left(n\right)x_{zc}^{*}\left(n+k\right)=\delta\left(k\right), \tag{4.7}$$

where $R_{zc}\left(\bullet\right)$ is the discrete periodic *auto-correlation* function of $x_{zc}\left(n\right)$ at lag k.

This property is of major interest when the received signal is correlated with a reference sequence and the received reference sequences are misaligned. The main benefit of the CAZAC property is that it allows multiple orthogonal sequences, [25].

Cyclic shifted versions of the CAZAC sequence do not cross–correlate with each other, because the shift *delay* of the root sequence creates a zero-correlation zone (ZCZ), between orthogonal shifted sequences (it is possible to derive multiple preamble sequences from a single Zadoff-Chu sequence by using cyclic shifts).

A CAZAC sequence has a constant amplitude in time and frequency, and because of that, the constant amplitude property limits the PAPR, (Figure 4.12d), which generates bounded interference to other users. The DFT of a CAZAC sequence $x_{zc}(n)$ will be a CAZAC sequence, this property allows generate the CAZAC sequence directly in the frequency domain.

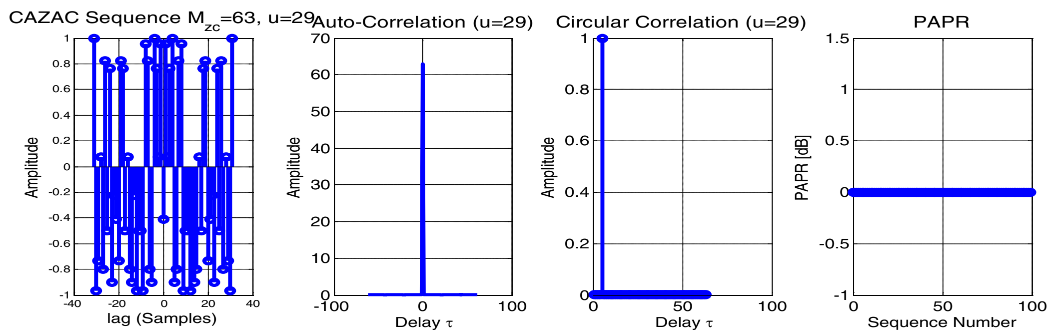

(a) (b) (c) (d)

Figure 4.12. (a) CAZAC-sequence; (b) *auto-correlation* CAZAC-sequence; (c) Circular correlation of CAZAC; (d) PAPR of CAZAC.

4.3.4 Golay Sequence

Preambles designed for *random* access based consider the application of CAZAC sequences, as well as binary sequences from the Golay complementary pairs (GCP), [45-53]. The major property of the binary sequences that form the Golay complementary pair is that, the sum of their aperiodic auto–correlation functions equals to zero for all non–zero time shifts.

The GCP exhibits low *auto-correlation* of the sidelobes that make them attractive as synchronization codes, especially on multiple access synchronization and spread spectrum systems. Golay complementary sequences have a length $L = 2^N$ (where N is any positive integer). A general method for the construction of this kind of polyphase complementary pairs of sequences were introduced by Shapiro in 1951, [48] and Rudin in 1959, [49], and is known as the Rudin-Shapiro polynomials, these kind of polynomials can be generated recursively as follows, A Rudin-Shapiro polynomials pair $Ps_n(t)$ and $Qs_n(t)$, n =0,1,2,…, are defined recursively,

$$\begin{aligned} &Ps_0(t) = Qs_0(t) = 1, \\ &Ps_{n+1}(t) = Ps_n(t) + e^{2\pi i 2^n t} Qs_n(t), \\ &Qs_{n+1}(t) = Ps_n(t) - e^{2\pi i 2^n t} Qs_n(t), \end{aligned} \tag{4.8}$$

The number of terms in the n-th polynomial, $Ps_n(t)$ or $Qs_n(t)$, is 2^n of (± 1), where $t \in [0,1)$. The sequences Ps_n and Qs_n of length n form a Golay complementary pair if the sum of their aperiodic auto-correlations is null except in zero [46], as shown in Figure 4.13a and 4.13b. A complementary pair of sequence of length L are obtained of a Rudin–Shapiro sequence Ps_n with length *n=2*L*, (Figure 4.13c), (i.e. two sequences Ps_n and Qs_n with length *L= 8* are obtained of a sequence Ps_n of length *n=16*). Golay Sequences have low PAPR, in this case has a value of 2.4dB, Figure 4.13d. e.g. for *n*=16, we have:

$$P_{16} = \underbrace{1\ 1\ 1\ -1\ 1\ 1\ -1\ 1}_{P_8}\ \underbrace{1\ 1\ 1\ -1\ -1\ -1\ 1\ -1}_{Q_8}. \tag{4.9}$$

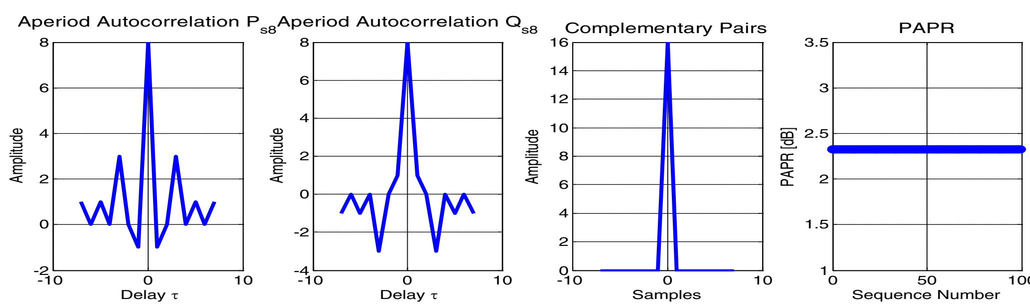

(a) (b) (c) (d)

Figure 4.13. (a) APeriodic *auto-correlation* Ps_8; (b) Aperiodic *auto-correlation* Qs_8; (c) Complementary pairs; (d) PAPR Golay sequence.

The Golay Rudin Shapiro (GRS) sequences have a uniform upper bound for the peak-to-average power ratio (PAPR), with a magnitude of the PAPR independent of the length of Golay sequence. GRS sequence is considered as a flat polynomial getting properties of a spread spectrum sequence, [53]. Additionally the GRS polynomial is orthogonal and its amplitude is on the unit circle, [50].

4.3.5 Summary of chapter four

Synchronization based on data-aided methods uses a training sequence or pilot symbol for estimation. This kind of method detects the start of the frame, define the symbol timing, and perform the estimation of the carrier frequency offset. In a timing synchronization scheme, the initial estimation is evaluated over a wide range of samples depending on the estimation method. In the case of frequency synchronization, coarse frequency synchronization acquisition finds the correct tone numbering and fine frequency acquisition the fractional offset, from the available receiver subcarriers.

The preamble is classified in short or long preamble. The short preamble is applied to make coarse carrier frequency offset estimation with a large unambiguous range, and the long preamble can be used for estimation of timing, fine frequency offset, and channel estimation. The functionality of preambles depends on sequences with good properties of autocorrelation and cross-correlation. A reduced PAPR is important in a preamble, in order to avoid nonlinearity degradation during synchronization. The most important sequences used are m-sequences, Gold, CAZAC and Golay sequences.

The OFDM synchronizer for the IEEE 802.11a WLAN standard uses two symbols for the detection of the start of the packet, timing, and frequency offset. The preamble designed for OFDMA (WiMAX) is allocated in the *downlink* subframe. The first step on synchronization process is to detect the preamble and estimate the coarse symbol timing, and the carrier frequency offset (CFO).

The cell search procedure in LTE begins with a synchronization procedure, which makes use of two specially designed preamble signals, which are broadcast in each cell. The primary goal of the cell search procedure is to enable the acquisition of the received timing and frequency of the *downlink* signal. In the first step of *downlink* synchronization the MS uses PSS with a period of 5ms, which has been transmitted twice in a frame, to estimate symbol timing and CFO.

Chapter 5

TIMING METRICS

In the present chapter is reviewed the state of the art of synchronization algorithms based on preamble signals, which by means of a timing metrics algorithm synchronize the received data. The analyzed methods correspond to the schemes based on correlation of data aided, and they allow the joint estimation of the timing and frequency offset.

5.1 Estimation Techniques for Timing Offset

The estimation techniques for timing offset are applied to determine where starts the FFT symbol at the receiver, trying to avoid ISI and ICI, and can be implemented in the time or frequency domain:

- Time domain
  - Symbol timing offset estimation based on using *cyclic prefix* (ML method) [54].
  - Symbol timing offset estimation based on training symbol, (MC method) [39].
  - Symbol timing offset estimation based on training symbol (MMSE method) [55].
- Frequency-domain
  - Symbol timing offset estimation based on the phase difference between subcarriers, (MC method) [56].

5.2 Estimation Techniques for Frequency Offset

The estimation techniques for frequency offset are used to determine the carrier frequency of the received signal, with a approximating to the value employed in the transmitter. The carrier frequency offset is also performed either in time or frequency domain:

- Time Domain
  - Carrier frequency offset estimation based on *cyclic prefix*, (ML method), [57]
  - Carrier coarse an fine frequency offset estimation based on training symbol, (MC method) [39]

- Frequency domain
  - Carrier frequency offset estimation based on training symbols, (MC method) [58, 59].

5.3 Jointly estimation of Timing and Frequency offset

The jointly estimation of timing and frequency offset is carried out by maximum correlation methods, and can be divided in auto-correlation and cross-correlation methods. These methods are designed to maximize a correlation metric, (e.g., the function given in the equation 5.1),

$$C(d) = \sum_{m=0}^{L-1} \left(r_{d+m}^{*} \cdot r_{d+m+l} \right) \tag{5.1}$$

where L is the length of the repeated pattern in the training symbol,

r is the received time-domain sequence with a time index as subscript

(*) denotes the conjugate of received value.

The time index of the sample with the maximum *auto-correlation* of the received signal is defined by,

$$\hat{d} = \arg\max_{d} \left| C(d) \right| \tag{5.2}$$

By considering the sequence $r\left(m\right) = r\left(m+l\right)$,

$$S_d = \sum_{m=0}^{L-1} r_{d+m}^{*} r_{d+m} = \sum_{m=0}^{L-1} \left| r_{d+m} \right|^2 \tag{5.3}$$

The carrier frequency offset can be calculated as follows,

$$\hat{\varepsilon} = -\frac{1}{2\pi} \angle S_{\hat{d}} \tag{5.4}$$

This method has some drawbacks. First, the peak magnitude of the $C(d)$ in different samples may fluctuate, because of the power of r_d varies with time. Secondly, when the correlation window moves away from the repeated periods, the output magnitude of the correlation may not fall off as expected.

5.4 Maximum Likelihood

The idea of using cyclic extension for symbol synchronization appeared first in [13], and later, many other schemes were developed in [54, 57, 60-63]. The proposal of using cyclic extension for estimation of symbol synchronization was first given in [60, 61]. The proposal of using a cyclic extension for frequency-offset estimation was defined in [57]. Based on previous results, a scheme of using a *cyclic prefix* and maximum likelihood method is applied to estimate timing and frequency offset in AWGN channels, which was proposed in [62].

The log-likelihood function working under the assumption that the received samples $r(k)$ are uncorrelated except for the replicas, it is evaluated with the following metric,

$$\Lambda(\theta,\varepsilon) = \left|\gamma(\theta)\right| \cos\left(2\pi\varepsilon + \angle\gamma(\theta)\right) - \rho\Phi(\theta) \tag{5.5}$$

where it is assumed that the interval of observation for the received signal are $2N_c + L$ consecutive samples. These samples contain a complete symbol with length $N_c + L$, where L samples belong to the *cyclic prefix*. The position of the symbol in the observation interval is unknown, and θ denotes the timing offset of the symbol in the interval. Thus the samples in the *cyclic prefix* have indexes $\mathrm{I} \equiv \{\theta,...,\theta + L - 1\}$ and the samples with the indexes of $\mathrm{I}' \equiv \{\theta + N_c,...,\theta + N_c + L - 1\}$, are the replica samples of the *cyclic prefix*. All the received samples in the observation interval are defined in $r = \left[r(1)...r(2N_c + L)\right]^T$.

$$\gamma(m) = \sum_{k=m}^{m+N_g-1} r(k)\, r^*(k + N_c), \tag{5.6}$$

$\gamma(m)$ is the sum of N_g consecutive correlations between pairs of N_c spaced samples apart.

$$\Phi(m) = \frac{1}{2} \sum_{k=m}^{m+N_g-1} \left|r(k)\right|^2 + \left|r(k + N_c)\right|^2 , \tag{5.7}$$

$\Phi(m)$ is the power of N_g consecutive pairs of samples.

$$\rho = \frac{\sigma_s^2}{\sigma_s^2 + \sigma_n^2} = \frac{SNR}{SNR + 1}. \tag{5.8}$$

The value θ that maximizes the function is defined by,

$$\hat{\Theta}_{ML} = \arg\max\left\{\left|\gamma\left(\Theta\right)\right| - \rho\Phi\left(\Theta\right)\right\}, \tag{5.9}$$

The peak of the correlation between samples in I and I' can be used to estimate the timing offset, Figure 5.1.

Assuming that the carrier frequency offset normalized to subcarrier spacing is ε, that is, the local carrier frequency is $f_c + \varepsilon / T$, then the complex envelope of the down converter output will be equal to $s\left(t\right)e^{j2\pi\varepsilon t/T}$, where $s\left(t\right)$ is the complex envelope of the transmitted signal. The signal is sampled at *N* times the symbol rate, it is $s\left(t\right)e^{j2\pi\varepsilon k/N}$ in the discrete form.

The fact that the correlation is $\sigma_s^2 e^{-j2\pi\varepsilon}$, for m=N_c can be used to estimate the frequency offset. The normalized CFO estimated can be calculated as,

$$\hat{\varepsilon}_{ML} = -\frac{1}{2}\angle\gamma\left(\hat{\Theta}_{ML}\right). \tag{5.10}$$

Since the CFO depend on the angle in equation 5.9, (Figure 5.2), it will be periodic with the upper limit of the CFO estimated as,

$$\left|\Delta f\right| \leq \frac{1}{N_c T_{sym}} = \Delta f_{\max}, \tag{5.11}$$

where, N_c is the *delay* between the correlated samples and T_{sym} is the sampling time.

If the frequency offset is greater than $\Delta f_{\max}$ the resulting estimate will be unable to detect the integer part of the CFO, with an integer distance between the carriers. The complexity of the ML algorithm is quite high because of the hardware for estimating ρ. Besides, error in signal to noise ratio (*SNR*) estimation often renders it less reliable than other methods.

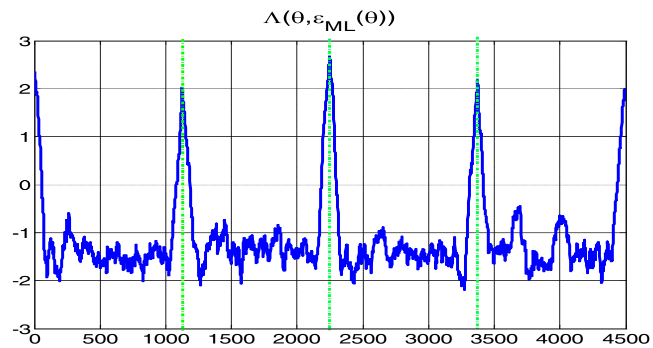

Figure 5.1. Maximum Log-likelihood.

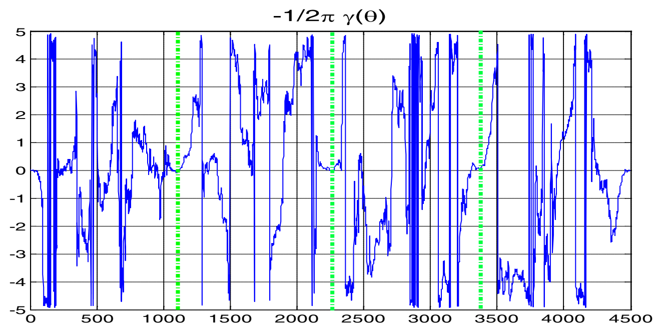

Figure 5.2. CFO estimated.

The advantage of the cyclic prefix method lies on non-included additional data. However, the peak value of the correlator output varies significantly from symbol to symbol, due to the randomness data of the cyclic prefix.

5.5 Timing metrics

The less complex but less accurate algorithms are based on the correlation of the cyclic prefix and the end part of the corresponding OFDM symbol. Schmidl and Cox proposed the first power normalized timing metric in [39], where this method uses a preamble that consists of two identical segments, each of $N_c/2$ samples. In a similar form in the literature exist timing metrics based on the idea of Schmidl and Cox, the review of the literature allow us to understand the design of this kind of metrics, with their particular characteristic of designed preamble, complexity, and accuracy on the estimation of the timing and frequency offset.

5.5.1 Schmidl and Cox timing metric

The Schmidl and Cox timing metric synchronizer relies on two training symbols, [13, 39]. The first one is used for frame and symbol timing, as well as coarse frequency offset estimation. The second one is used for fine frequency estimation.

The first training symbols consist of two identical halves sequence in the time domain, they are a pseudo noise (*PN*) sequence on the even frequencies, while zeros are used on the odd frequencies. The first training symbol is used for two purposes; first, the correlation between the two identical halves can be used for frame/symbol timing. Second, the two identical halves will remain identical after passing through the channel, except that there will be a phase difference between them caused by the carrier frequency offset. This can be used for a coarse estimate of the carrier frequency offset.

The second training symbol consists of two PN sequences; one is on the odd frequencies for measuring these sub channels, and other is on the even frequencies to help determine the fine frequency offset.

The received complex envelope at time t in the first half of the symbol is defined by,

$$r\left(t\right)=u\left(t\right)e^{j2\pi t\Delta f+\theta\left(t\right)}, \tag{5.12}$$

where Δf is the carrier frequency offset,

$\theta\left(t\right)$ is the phase shift caused by the channel in a slow *fading* environment,

The second half $T_{sym}/2$ seconds is determined by,

$$r\left(t+T_{sym}/2\right)=u\left(t+T_{sym}/2\right)e^{j2\pi t\Delta f+\theta\left(t+T_{sym}/2\right)+\pi T_{sym}\Delta f}. \tag{5.13}$$

Since $u\left(t\right)=u\left(t+T_{sym}/2\right)$

$$r^{*}\left(t\right)r\left(t+T_{sym}/2\right)=\left|u\left(t\right)\right|^{2}e^{\pi T_{sym}\Delta f+\theta\left(t+T_{sym}/2\right)-\theta\left(t\right)}\approx\left|u\left(t\right)\right|^{2}e^{\pi T_{sym}\Delta f}. \tag{5.14}$$

We can observe that the effect of the channel $\theta\left(t\right)$ is cancelled, and the result has a phase of $\phi=\pi T_{sym}\Delta f$, which is proportional to the frequency offset.

Let there be L complex samples in one-half of the first training symbol (excluding the length of the *cyclic prefix*); it is possible to define a sum of pairs of products as,

$$P(d)=\sum_{m=0}^{L-1}\left(r_{d+m}^{*}r_{d+m+L}\right), \tag{5.15}$$

where $P(d)$ is the correlation function between samples of the first half and the second half, Figure 5.3.

d is a time index of the first sample in a window observation of $2L$ samples.

At the start of the frame, the products of each of these pairs of samples will have approximately the same phase, so the magnitude of $P(d)$ will be a large value.

The received energy for the second half-symbol is defined by,

$$R(d)=\sum_{m=0}^{L-1}\left|r_{d+m+L}\right|^{2}, \tag{5.16}$$

where $R(d)$ is used as a part of an automatic gain control (AGC) loop.

The timing metric of Schmidl and Cox can be defined as,

$$M(d)=\frac{\left|P(d)\right|^{2}}{\left|R(d)\right|^{2}}, \tag{5.17}$$

where the normalization by $\left|R(d)\right|^{2}$ is necessary because the received signal power is typically time variant, Figure 5.4.

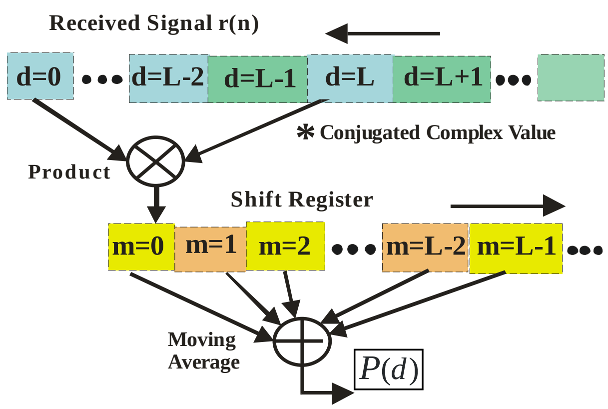

Figure 5.3. Cross-correlation of Schmidl & Cox metric.

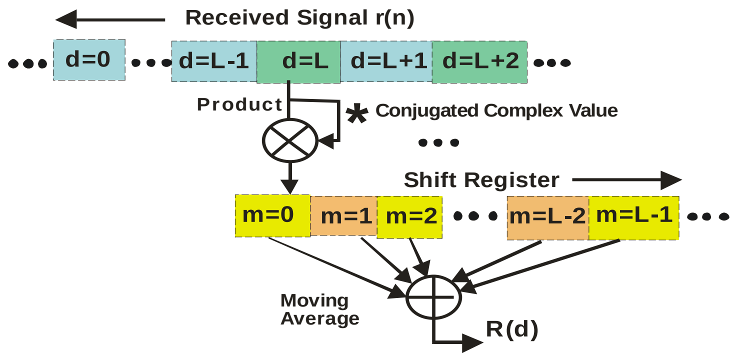

Figure 5.4. Auto-correlation of Schmidl & Cox metric.

The timing metric proposed by Schmidl and Cox reaches a "plateau", this plateau has a length equal to the length of the guard interval minus the length of the channel impulse response, where the ISI do not exists to distort the signal. The plateau starts when $d = -G$, where G is the length of the guard interval, and the plateau end when $d = 0$. If the channel has an impulse response of length τ, the plateau should starts at the index $d = -G + \tau$ and ends when $d = 0$, Figure 5.5. In conditions of high signal to noise ratio (SNR) is possible determine the starting point of the frame within the rear edge of the plateau.

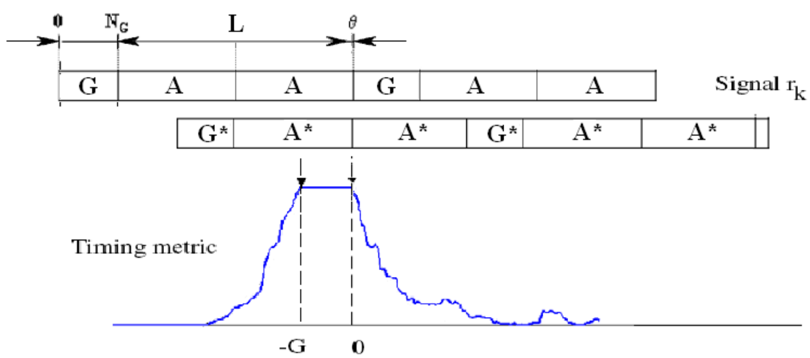

Figure 5.5. Plateau of Schmidl & Cox metric.

The principal characteristic of the metric proposed on [39] is its robustness against carrier frequency offset, as well as its robustness against *fading* (due to the "AGC" existing in the denominator of the metric).

A disadvantage of the Schmidl and Cox method is the plateau originated by the timing metric, which gives rise to a relatively high uncertainty on the starting time of the symbol.

This methods is based on one bit quantization of the received signal, and has two major benefits, first, the complexity of the digital part is very low, but perhaps most important, one can design specific synchronization circuits with 1 bit analog to digital converters, and hence lower the power consumption significantly while waiting for an incoming burst.

5.5.2 Frequency offset estimation with Schmidl & Cox

The correlation between two samples, are separated in a period of $T_{sym}/2$, within the first training symbol, and has an angle of,

$$\phi = \pi T_{sym} \Delta f . \tag{5.18}$$

where ϕ is proportional to the carrier frequency offset Δf. The $P(d)$ is a sum of these correlations so that its angle is also ϕ. If $|\phi| < \pi$ can be estimated near the best timing point, as follows,

$$\Delta \hat{f} = \frac{\hat{\phi}}{\pi T_{sym}} = \frac{angle\left(P(d)\right)}{\pi T_{sym}}, \tag{5.19}$$

$P(d)$ can not reflect the total ϕ since the angle of a complex number is limited to the range of $[-\pi, \pi]$. The complete angle of $P(d)$ would be $\phi + 2\pi q$, where q is an integer, and the frequency offset would be,

$$\Delta \hat{f} = \frac{\hat{\phi}}{\pi T_{sym}} + \frac{2q}{T_{sym}}. \tag{5.20}$$

The second term is the integer part can be found using the second training symbol.

Once the two training symbols are partially corrected in frequency, and obtained their FFT's, the existent differentially encoded related of the PN sequences of each training symbol is applied, with the objective of estimate the complete frequency offset.

The variance of the estimator for the fractional part is defined as,

$$\operatorname{var}\left(\hat{\phi}/\pi\right) = \frac{1}{4\pi^2 L \cdot \mathrm{SNR}}. \tag{5.21}$$

where equation 5.21 defines also the Cramer-Rao bound.

Once reviewed the Schmidl & Cox metric, a CAZAC sequence is selected to design the preamble, and will be evaluated on the receiver by the metric. The simulated CAZAC sequence is shown in Figure 5.6.

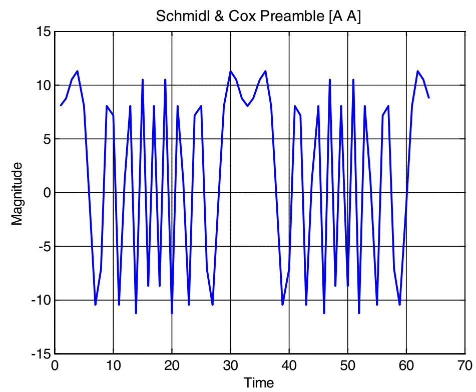

Figure 5.6. Schmidl & Cox preamble.

5.5.3 Minn et al. timing metric

In order to avoid the plateau of the timing metric in the Schmidl & Cox metric, Minn et al. [40] proposed a modified preamble structure. This preamble has identical segments and variable polarities; the sign of each segment is assigned to achieve the steepest possible roll-off correlation. For a typical Minn's preamble the following form is considered,

$$S_{Minn} = [A,A,-A,-A], \tag{5.22}$$

where A is a pseudo noise sequence with $N/4$ samples. The timing detection metric for this preamble is given by,

$$M_{Minn}(d) = \frac{\left|P_{Minn}(d)\right|^2}{(R_{Minn}(d))^2}, \tag{5.23}$$

$$\hat{\varepsilon}_{Minn} = \arg\max_{d} M_{Minn}(d), \tag{5.24}$$

$$P_{Minn}(d) = \sum_{k=0}^{1}\sum_{m=0}^{L-1}(r^{*}_{d+2Lk+m} \cdot r_{d+2Lk+m+L}), \tag{5.25}$$

$$R_{Minn}(d) = \sum_{k=0}^{1}\sum_{m=0}^{L-1}\left|r_{d+2Lk+m+L}\right|^2, \tag{5.26}$$

where $P_{Minn}(d)$ is the cross-correlation of four equally spaced received samples, (Figure 5.7) , and $R_{Minn}(d)$ is the power of the correlated samples, as shown in Figure 5.8.

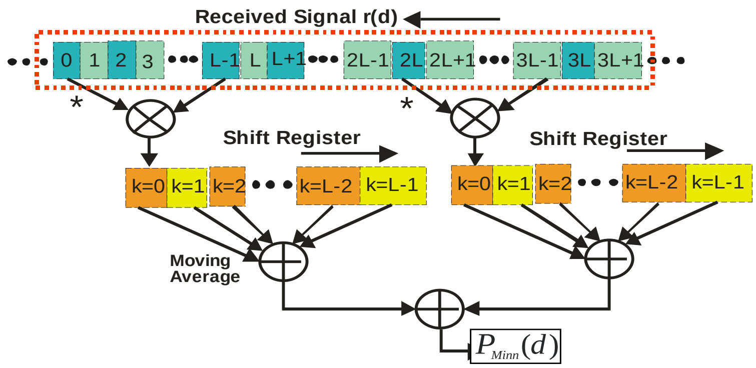

Figure 5.7. P_{Minn} Component of the Minn metric.

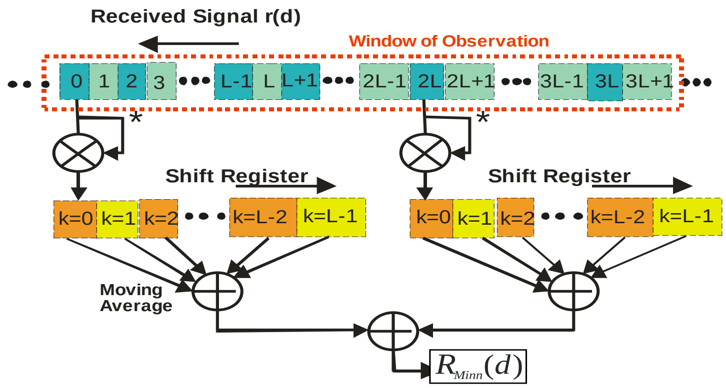

Figure 5.8. R_{Minn} Component of the Minn metric.

Based on the characteristics of Minn's metric is designed a preamble with CAZAC sequences, Figure 5.9.

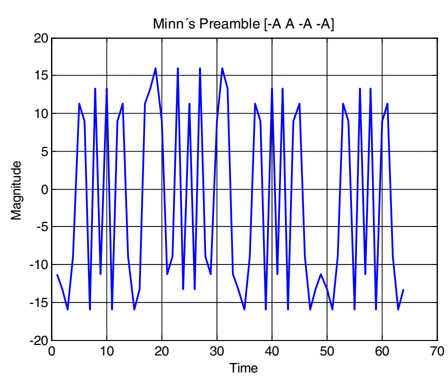

Figure 5.9. Minn's preamble.

5.5.4 Park's timing metric

In Minn's method, the negative-valued samples are used at second-half training symbol to reduce the timing metric plateau. Correlation of these negative samples, results in decrease of the accuracy defined by the timing metric at the incorrect starting point. The mean square error (MSE) of estimator is quite large in ISI channel. It is because timing metric value at only one sample off from the correct starting point is almost same to peak timing metric value. Therefore, from the observation of the two adjacent value of timing metric, it is clear that they have the same sum of the pairs of product, except only two pair of products. To enlarge the difference between the two adjacent values of timing metric, it is necessary to maximize different products between them. For this reason, Park's modified the training signal proposed by Minn, where the new preamble consist of four parts, [41]. The half part is formed by the symbols A and B, and the conjugate values of A and B, as is shown in following integrate the second part,

$$S_{Park's} = [A, B, A^*, B^*]. \tag{5.27}$$

The timing metric proposed by Park's is as follows,

$$M_{Park's}(d) = \frac{\left|P_{Park's}(d)\right|^2}{(R_{Park's}(d))^2}, \tag{5.28}$$

$$\hat{\varepsilon}_{Park's} = \arg\max_d M_{park's}(d), \tag{5.29}$$

$$P_{Park's}(d) = \sum_{k=0}^{N_c/2} (r_{d-k} \bullet r_{d+k}) , \tag{5.30}$$

The $P_{Park's}(d)$ is designed to have $N_c / 2$ different pair of products between two adjacent values, Figure 5.10. The power of the received samples is defined by equation 5.31, and is shown in Figure 5.11.

$$R_{Park's}(d) = \sum_{k=0}^{N/2} \left|r_{d+k}\right|^2. \tag{5.31}$$

To estimate the frequency offset Park's method use equation 5.19, which was applied by Schmidl & Cox.

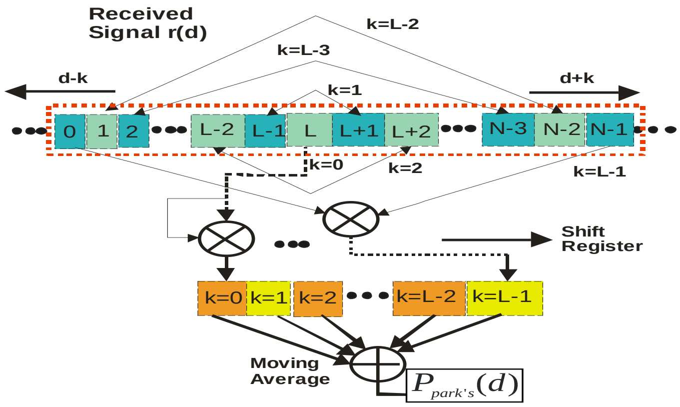

Figure 5.10. $P_{Park's}$ Component of Park's metric.

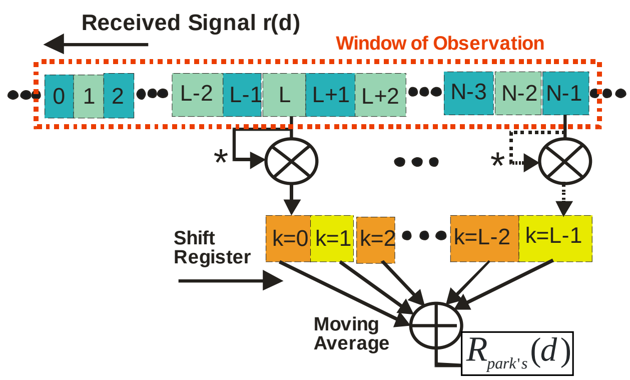

Figure 5.11. $R_{Park's}$ Component of Park's metric.

Park's method has been evaluated by simulation using a CAZAC sequence instead of a PN sequence, as was proposed in the Park's method and the result is shown in Figure 5.12.

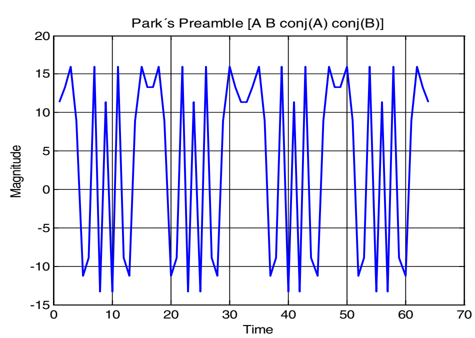

Figure 5.12. Park's preamble.

5.5.5 Shi-Serpedin timing metric

Shi and Serpedin proposed a timing metric in [63], which is based on a preamble pattern defined by,

$$S_{\text{Shi-S}}=[B,B,-B,B], \tag{5.32}$$

where B stands for a time-domain sequency of $N_c/4$ training samples with constant power (e.g. a PN sequence), and it can be generated by using an $N_c/4$-point IFFT of an PN sequence.

The received samples $r(n)$ are evaluated over a window of observation, this window includes the whole training preamble, as well as include a prefix of length p and a suffix of length q. If the starting index is determined at $t=0$, then it is possible to define the observation vector as follows,

$$R=\left[r(-p),r(-p+1),...,r(0),...,r(N_c-1),...,r(N_c+q-1)\right]^T, \tag{5.33}$$

Observation samples in a sliding window of N_c samples are taken to calculate the timing metric and defining the following sub vectors,

$$R_i=\left[r(l+(i-1)N_c/4),...,r(l+i\,N_c/4-1)\right]^T,\ i=1,2,3,4 \tag{5.34}$$

The estimation defined by the timing metric at any time instant l, is defined in equation 5.35,

$$Q(l)=\frac{P_{Shi-S}(l)}{V(l)}, \tag{5.35}$$

where,

$$P_{Shi-S}(l)=\left|R_1^H R_2-R_2^H R_3-R_3^H R_4\right|+\left|R_2^H R_4-R_1^H R_3\right|+\left|R_1^H R_4\right|, \tag{5.36}$$

and

$$V(l)=\frac{3}{2}\sum_{i=1}^{4}\left|R_i\right|^2, \tag{5.37}$$

The six terms in $P_{Shi-S}(l)$ are all the possible combinations of correlations between the four parts of the training symbol, (Figure 5.13). The negative terms are due to the negative sign of the third part. The terms in each group have a common phase, due to the same index difference between two R_i 's in each correlation. $V(l)$ defines the power of the correlated parts within the window of observation, Figure 5.14. The method of Shi-Serpedin can produce a similar response as Schmidl & Cox and Minn's metric, by selecting a correlation between specially parts of the used preamble. Applying the method of Shi-Serpedin the timing offset is estimated in the receiver, by means of search of the peak of $Q(l)$ (or simply $P_{Shi-S}(l)$) in a slow-varying channel). The start of the frame $l = d$ is estimated as,

$$\hat{d} = \arg\max_{l} Q(l). \tag{5.38}$$

and the carrier frequency offset is defined in equation 5.39,

$$\hat{\varepsilon} = \frac{2}{\pi} \arg P_1(\hat{d}) \ , \tag{5.39}$$

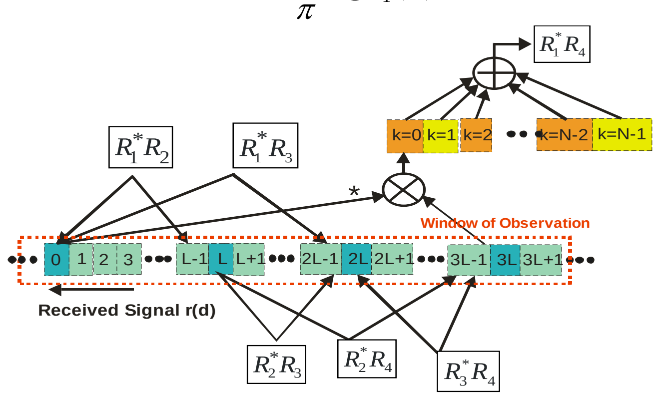

Figure 5.13. P_{Shi-S} Components of Shi-Serpedin Metric.

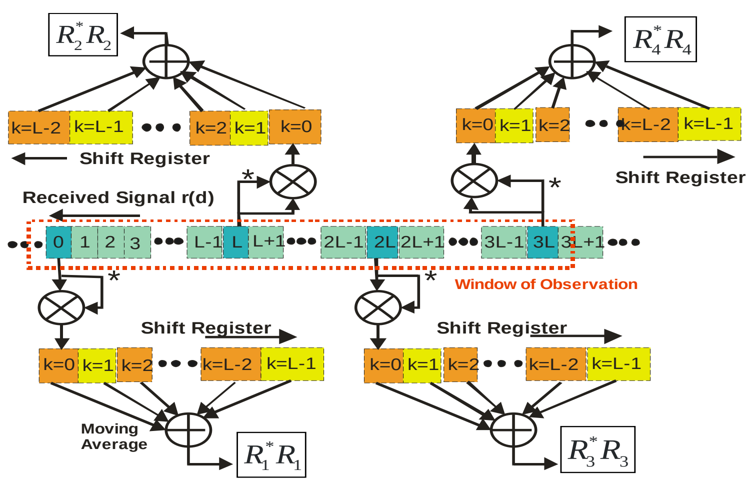

Figure 5.14. $V(l)$ Components of Shi-Serpedin Metric.

The Shi-Serpedin preamble was designed with a CAZAC sequence, considering the initial design proposed in [63], depicted in Figure 5.15.

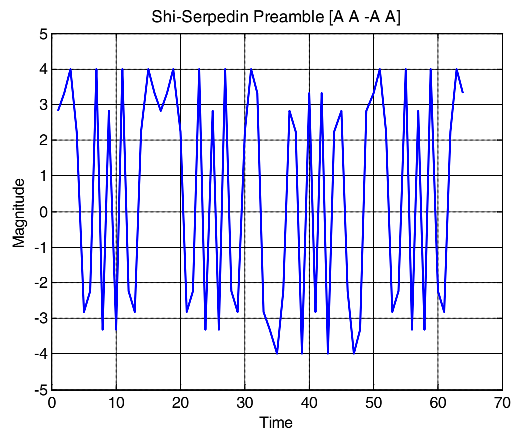

Figure 5.15. Shi-Serpedin Preamble.

5.5.6 Ren et al. timing metric

Using a similar pattern like [39], Ren. et al. proposed in [42] a long preamble, with a constant envelope preamble designed with a CAZAC sequence weighted by a PN sequence. The constant envelope preamble is generated by applying the discrete Fourier transform (DFT) of a CAZAC sequence, which has a length N_c, is symmetric in the time domain, and satisfies the following condition,

$$A_i = A_{i+N_c/2} = C \cdot e^{\theta_i}, \quad i = 0,1,\ldots,N_c/2-1, \tag{5.40}$$

$$\left\| A_k \right\| = C, \quad k = 0,1,\ldots,N_c-1, \tag{5.41}$$

where C is a constant amplitude,

θ_i is the phase of each sample of the preamble sequence.

Each sample of the sequence is multiplied by a weighting factor, using a PN sequence, and the preamble proposed by Ren's is defined as,

$$\mathrm{S}_{REN} = \left[A \ A \right] \circ s_k, \quad k = 0,1,\ldots,N_c-1, \tag{5.42}$$

where s_k is the PN sequence weighting factor of the k-th sample of the preamble.

"$\circ$" operator indicates Hadamard multiplication of the two vectors. The value of the PN sequence is +1 or -1, [21].

The timing metric proposed by Ren's is based on a modified Schmidl and Cox metric, and is defined as,

$$M_{\mathrm{Ren}}(d) = \frac{\left|P_{\mathrm{Ren}}(d)\right|^2}{\left(R_{\mathrm{Ren}}(d)\right)^2}, \tag{5.43}$$

$$\hat{\varepsilon}_{\mathrm{Re}n} = \arg\max_{d} M_{\mathrm{Ren}}(d), \tag{5.44}$$

where $P_{\mathrm{Ren}}(d)$ is the correlation of the received samples in an interval of observation, Figure 5.16, and $R_{\mathrm{Ren}}(d)$ is autocorrelation of received samples, Figure 5.17. The timing offset is determined by the maximum peak obtained by $\hat{\varepsilon}_{\mathrm{Re}n}$.

A modified timing metric is applied to remove the weighted factor, where the received signal is multiplied with the original PN sequence used in the transmitter, given by equation 5.45.

$$P_{\mathrm{Ren}}(d) = \sum_{m=0}^{L-1} s_m s_{m+L} r_{d+m}^{*} r_{d+m+L}, \tag{5.45}$$

$$R_{\mathrm{Ren}}(d) = \left(1/2\right) \sum_{m=0}^{L-1} \left|r_{d+m}\right|, \tag{5.46}$$

The PN weighted factors improve the accuracy to detect the maximum peak value of the Ren's metric. The frequency offset estimation of Ren's method is given as follows,

$$\hat{v}_R = \frac{1}{\pi N_c} \arg\left(P_R\left(\hat{d}\right)\right). \tag{5.47}$$

The total frequency offset of the received signal can be estimated by using the resulting value $\hat{v}_R$ and compensating the value of the constant envelope preamble, [39].

The Cramer-Rao bound for $\hat{v}_R$ in an AWGN channel is defined as,

$$\mathrm{var}\left(\hat{v}_R\right) \geq \frac{2}{\pi^2 N_c \cdot \mathrm{SNR}}. \tag{5.48}$$

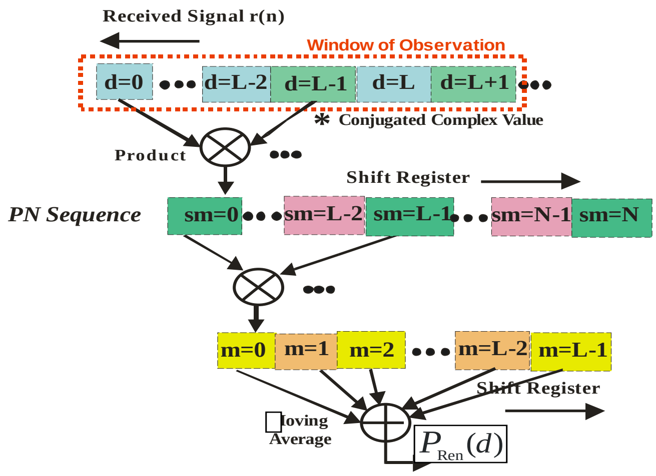

Figure 5.16. P_{Ren} Component of Ren's metric.

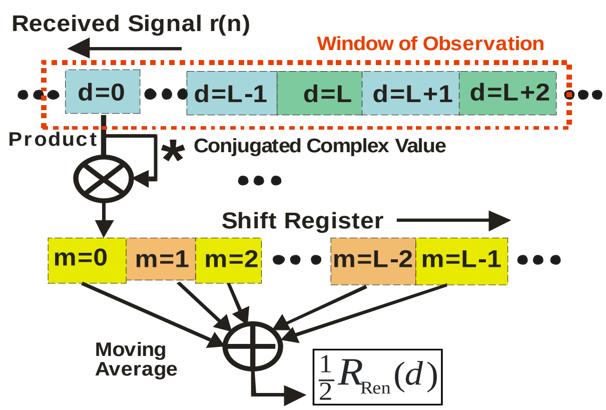

Figure 5.17. R_{Ren} Component of Ren metric.

The designed preamble applied for the Ren et al. metric is shown in Figure 5.18.

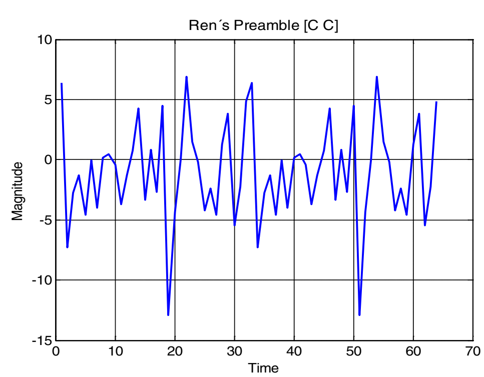

Figure 5.18. Ren et al. preamble.

5.5.7 Seung timing metric

Based on Park's et al, a modified timing metric was proposed by Seung et al in [64], this method is based on the time domain preamble given by,

$$\mathrm{S}_{\mathrm{Seung}} = [C_{N_c/2}, D^{*}_{N_c/2}], \tag{5.49}$$

where $C_{N_c/2}$ represents the sequence of the length $N_c/2$, generated by the inverse fast Fourier transform (IFFT) of the CAZAC sequence.

$D^{*}_{N_c/2}$ is a complex conjugate of $D_{N_c/2}$, which is the time reversed version of $C_{N_c/2}$.

This method requires a zero padding elements like *cyclic prefix* in the preamble. The timing metric proposed by Seung et al. is shown as follows,

$$M_{Seung}(d) = \frac{\left|P_{Seung}(d)\right|^2}{(R_{Seung}(d))^2}, \tag{5.50}$$

$$\hat{\varepsilon}_{Seung} = \arg\max_{d} M_{Seung}(d), \tag{5.51}$$

where,

$$P_{Seung}(d) = \sum_{k=0}^{N_c/2-1} (r_{d-k} \bullet r_{d+k+1}), \tag{5.52}$$

and

$$R_{Seung}(d) = \frac{1}{2}\sum_{k=0}^{N_c/2} \left|r_{d+k-N/2}\right|^2, \tag{5.53}$$

where the components of the timing metric $M_{Seung}(d)$ are; $P_{Seung}(d)$ the cross-correlation of the received samples, Figure 5.19, and $R_{Seung}(d)$ is the power energy of received samples, as is shown in Figure 5.20. The carrier frequency estimation is achieved by means of the Schmidl and Cox method

$$\hat{v} = \frac{1}{\pi N_c} angle\left(P(\hat{\varepsilon}_{Seung})\right), \tag{5.54}$$

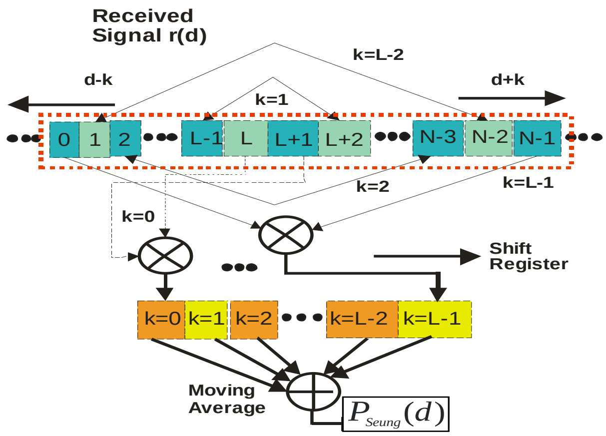

Figure 5.19. P_{Seung} component of Seung's metric.

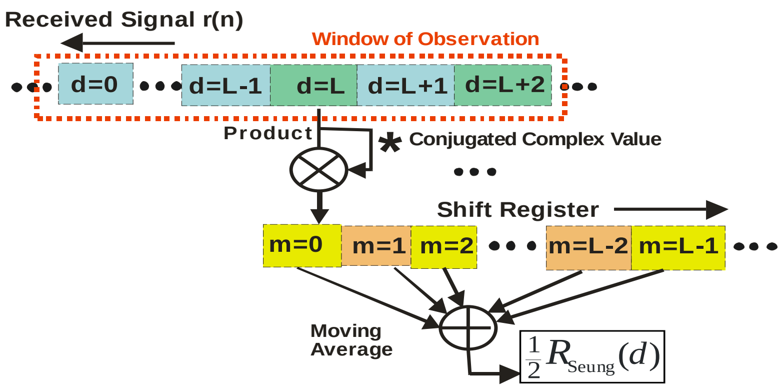

Figure 5.20. R_{Seung} component of Seung's metric.

The preamble simulated in MATLAB used by the Seung metric is shown in Figure 5.21.

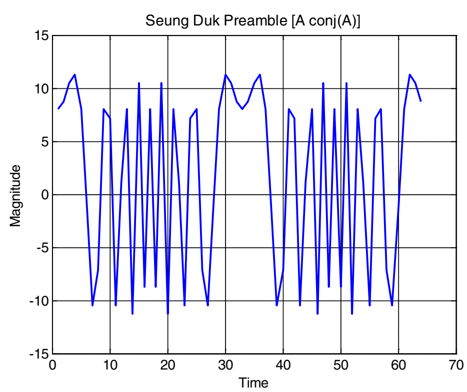

Figure 5.21. Seung's preamble.

5.5.8 Zhou et al. timing metric

The timing metric proposed by Zhou et al. in [65] is based on a modified preamble, and it is designed taking in consideration the operations of symmetric and *delay* correlation between the constitutive samples of the preamble, defined in equation 5.55.

$$S_s = [C, D, C, D], \tag{5.55}$$

where C represents a CAZAC sequence.

D is a sequence C conjugated and reversed in time.

The Zhou's timing metric combines the merits of delayed and symmetric correlation profile, defined by,

$$M(d) = \frac{|\Gamma_S(d)| . |\Gamma_d(d)|}{(P_d(d))^2}, \tag{5.56}$$

where the symmetric correlation profiles is calculated in equation 5.57, and shown in Figure 5.22.

$$\Gamma_s(d) = \sum_{n=0}^{N_c/2-2} (r_{d+N_c/2-1-n} \bullet r_{d+N_c/2+1+n}). \tag{5.57}$$

and the delayed correlation profile, Figure 5.23, can be obtained as following,

$$\Gamma_d(d) = \sum_{k=0}^{N_c/2-1} (r^*_{d+k} \bullet r_{d+N/2+k}). \tag{5.58}$$

The received signal power is defined in equation 5.59, and is depicted in Figure 5.24.

$$P_d(d) = \sum_{k=0}^{N_c/2-1} |r_{d+k}|^2. \tag{5.59}$$

The metric of Zhou et al., it is characterized by a threshold resulting of the correlations, and over which is possible to detect the correct timing point. However, the resulting peaks require defining every maximum point of the resulting metric.

The frequency estimation is not defined in [39], but it is possible to apply the equation defined by the Schmidl and Cox metric.

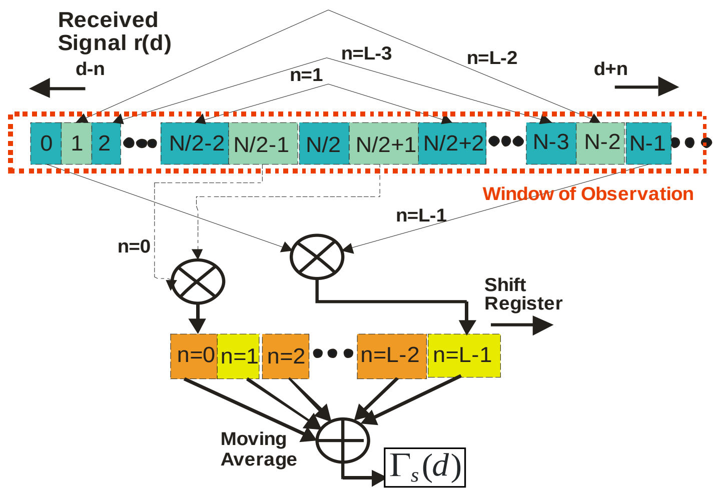

Figure 5.22. Symmetric correlation of Zhou's metric.

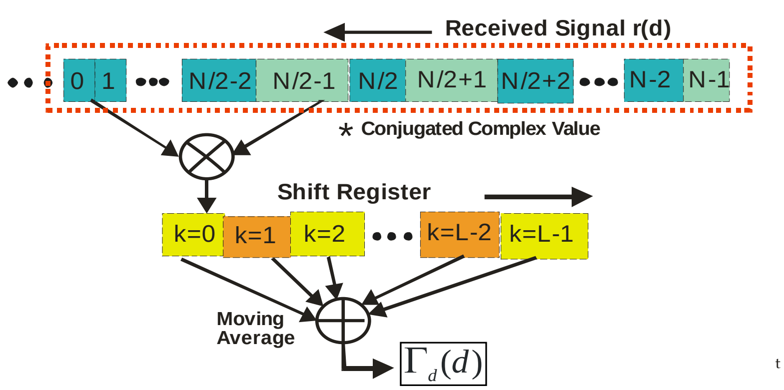

Figure 5.23. Delayed correlation of Zhou's metric.

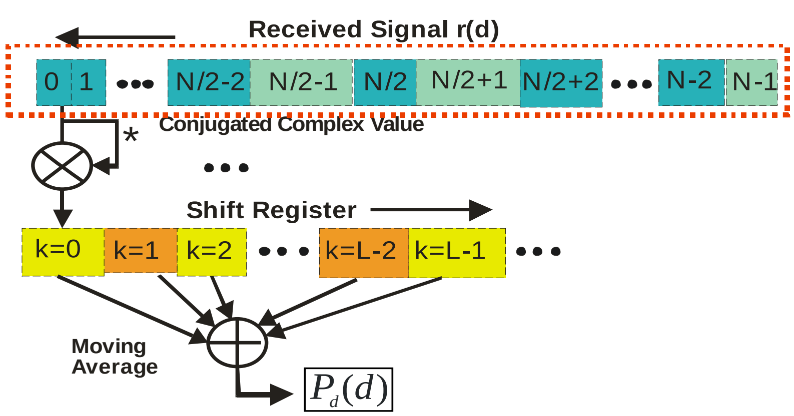

Figure 5.24. P_d component of Zhou's metric.

The simulated preamble applied for Zhou's metric is shown in Figure 5.25.

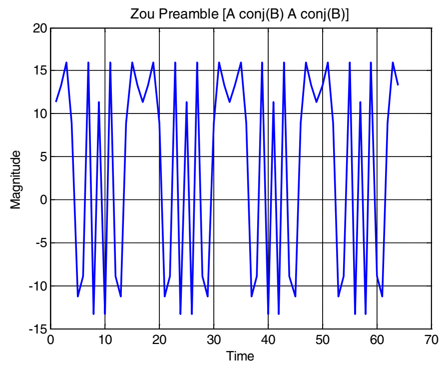

Figure 5.25. Zhou's preamble.

5.5.9 H. Wang et al. timing metric

The preamble designed by Minn *et al*. [40], with a repetitive period of length $L_L = N_c / 4$ uses a PN sequence. H. Wang et al. in [66] proposed a modified timing metric with its corresponding preamble, which is a partial weighted sequence to improve the timing and frequency estimation of [39].

The designed preamble follows the same considerations as the long preamble; with selected periods for apply the weighted PN sequence, and is defined by,

$$\text{Preamble}_W = \left[D \;\; A_{HW} \;\; D \;\; A_{HW} \right], \tag{5.60}$$

where D is a CAZAC sequence of length $L_L = N_c / 4$. A_{HW} is a CAZAC sequence weighted by a PN sequence $pn(k),\ k = 0,1,\ldots,N_c/4-1$.

The preamble proposed by H. Wang, select two periods in the preamble with the finality of estimate the fractional frequency offset, and the coarse frequency offset estimated is carry out by the CAZAC sequence once suppressed the weighting factors.

The corresponding timing metric algorithm proposed by H. Wang et al. uses the following timing metric equations,

$$M_W(d) = \frac{\left|P_W(d)\right|^2}{\left(R_W(d)\right)^2}, \tag{5.61}$$

$$P_W(d) = \sum_{m=0}^{L-1} pn_m \cdot r_{d+m}^{*} \cdot r_{d+m+3*L}, \tag{5.62}$$

$$R_W(d) = \frac{1}{4} \cdot \sum_{i=0}^{3} \sum_{m=0}^{L-1} \left| r_{d+m+i*L} \right|^2 . \tag{5.63}$$

where $M_W(d)$ is the timing metric proposed by H. Wang et. al., $P_W(d)$ is the cross-correlation of received samples in the observation window, (Figure 5.26), and $R_W(d)$ is the power energy of the signal, as is depicted in Figure 5.27.

The frequency offset proposed by H.Wang estimate the fractional frequency offset, by means the following equation.

$$\hat{\nu}_W = -angle\left[r^*_{\hat{d}+m} \cdot r_{\hat{d}+m+2*L} \right] \Big/ \pi . \tag{5.64}$$

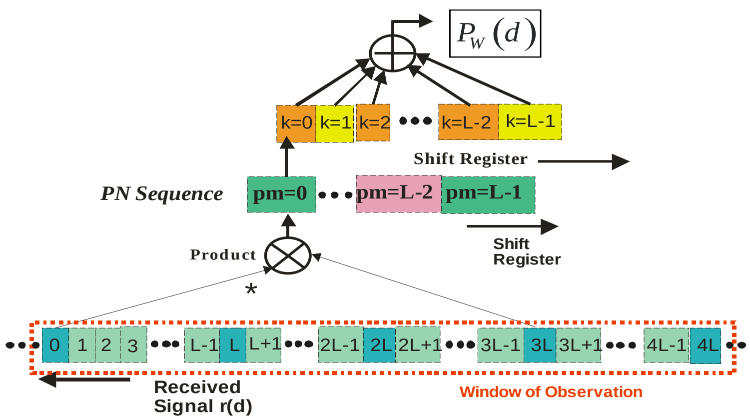

Figure 5.26. P_W component of H. Wang's metric.

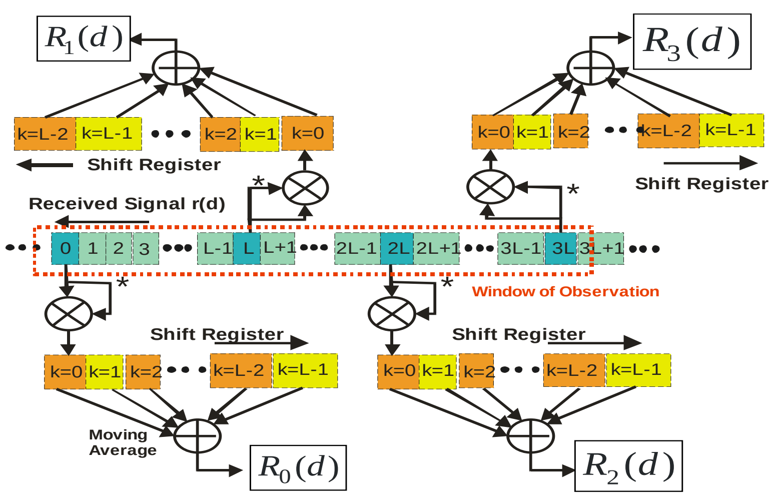

Figure 5.27. R_W component of H. Wang's metric.

The preamble used for H. Wang metric is plotted in Figure 5.28.

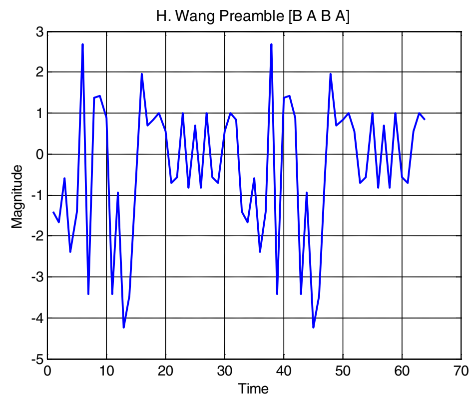

Figure 5.28. H. Wang's preamble.

5.5.10 Summary of chapter five

Timing and frequency offset estimation can be implemented in the time or frequency domain, where the estimation can be defined independent or jointly. The joint estimation of timing and frequency offset is carried out by maximizing correlation methods, which can be divided in auto-correlation and cross-correlation methods. These methods are designed to maximize a correlation metric.

The state of art of timing metrics and preambles has been studied along this chapter. The review starts with the analysis of the Schmidl and Cox Metric, and its corresponding preamble design. Schmidl and Cox timing metric synchronizer relies on two training symbols. The first one is used for frame and symbol timing, as well as coarse frequency offset estimation. The second one is applied for fine frequency estimation.

Schmidl and Cox metric is the base of more accurate timing metrics later developed, these methods adopt a preamble in a configuration of short or long preamble. The existing timing metrics varies the following design characteristics; use a different sequence, modify the preamble structure, increase the number of evaluated samples in the correlation, or scramble the transmitted symbol.

The reviewed timing metric of Minn et al., proposed a preamble with identical segments and variable polarities to improve the existing plateau in Schmidl and Cox method. Parks et al., developed an improved method in comparison with Minn´s method. Park's preamble is designed with conjugate values of the preambles, increasing the difference between the two adjacent values, which maximize different part products of the preamble. Other method like, Shi-Serpedin's timing metric, were designed, applying all the possible combinations of correlations between the four parts of a short preamble.

Ren et al, proposed an interesting method, where the developed timing metric detects a constant envelope preamble, which one is a CAZAC sequence weighted by a PN sequence. Seung et al, apply a long preamble, which is a modified version of Park's method. Zhou's method designed a metric considering symmetric and delay correlation between the parts of a short preamble. Finally, H. Wang applied a timing metric, which has a partial weighted sequence, improving the timing and frequency estimation.

Chapter 6

CONTRIBUTIONS

Once reviewed the state of art of timing metrics, the present chapter will state the major contributions derived of this dissertation. The first part of the chapter is focused on corroborate the functionality of each metric by simulation, and a comparative study was carried out. The accuracy of each estimator is measured by obtaining the mean square error (MSE). In addition, a whole performance evaluation of the system is achieved by defining the bit error rate (BER).

The second part of this chapter consists of the proposed algorithms, where two timing metrics are proposed. One metric is based on a weighted long preamble, and the second one is based on a weighted short preamble. The performance of proposed metrics is evaluated by the MSE and BER, and they are compared with the reviewed timing metrics existing on the literature. The chapter ends with the evaluation of the optimal preamble to estimate the frequency-offset, which is based on minimizing the Cramer-Rao bound (CRB).

6.1 Comparative study of existing timing metrics

A comparative study of existing metrics has been an important part of this thesis, it has provided the tools needed for obtaining, processing, analyzing and comparing their functionality, determining the best characteristics. In this chapter, we will report the results of the simulation in MATLAB of the reviewed metrics. The corresponding parameters for simulation of the OFDM preamble are summarized in Table VII,

Table VII. OFDM parameters of simulation.

OFDM parameters of simulation			
OFDM Subcarriers	Cyclic Prefix	Timing Offset	Normalized Frequency Offset
64	16	10 samples	2
256	64	25 samples	0.36

The channel model applied during the simulation is a Rayleigh fading channel selective on frequency, with a length of 16 taps and an exponential power delay profile, additive white Gaussian noise (AWGN) and a range of signal to noise ratio (SNR) from 0 to 20dB, [22, 31].

6.1.1 Simulation of Schmidl and Cox metric

The simulated Schmidl and Cox preamble with $N_c = 64$ subcarriers is evaluated, and the resulting timing and frequency-offset estimation are shown in the Figure 6.1a and 6.1b, respectively.

We can observe the detection of the maximum peak in Figure 6.1a, where the beginning of the symbol is located at $N_c/2$ samples of the preamble and a timing delay of 10 samples is detected. The frequency offset estimated in [39] has an available frequency range from -5π to 5π. Once detected the maximum peak the estimated coarse frequency is evaluated in an interval of length $N_c/2$ samples, as is shown in Figure 6.1b.

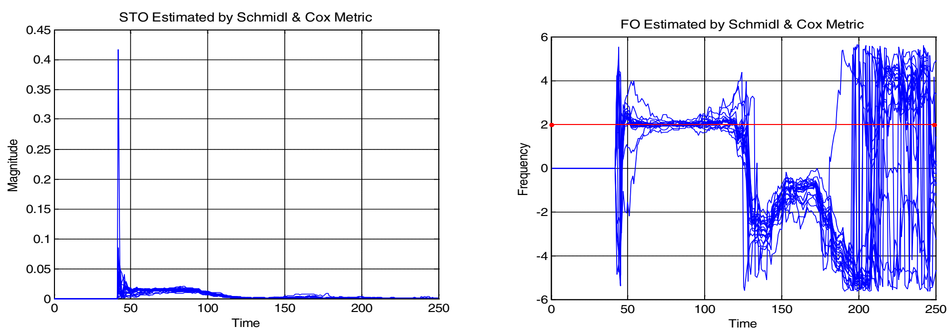

(a) (b)

Figure 6.1. (a) STO estimated and (b) CFO estimated by Schmidl & Cox, $N_c = 64$, $TO = 10$, $FO = 2$.

In the same way, the estimated timing offset for a preamble of $N_c = 256$ samples exhibits a better definition of the detected peak, which is achieved by increasing the number of samples in the preamble (Figure 6.2a). Additionally, we can observe that, the increased interval of comparison originates a reduction in the available frequency range, within a valid interval from -1.5π to 1.5π. The estimated frequency offset is shown in Figure 6.2b.

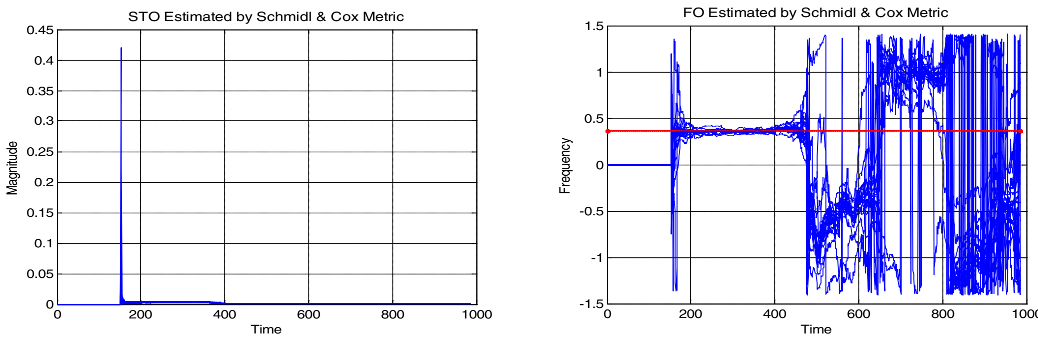

(a) (b)

Figure 6.2. (a) STO estimated and (b) CFO estimated by Schmidl and Cox, N_c=256, *TO*=25, *FO*=0.36.

6.1.2 Simulation of Minn's metric

The simulated Minn's metric, [40], is performed using the same parameters and conditions like Schmidl & Cox metric, in order to compare their respective responses. The simulated timing and frequency offset applying a preamble with a length of $N_c = 64$ are shown in Figure 6.3a and 6.3b, respectively. Note that the estimated frequency offset is obtained from a reduced number of samples, and the range of estimation is increased from -10π to 10π.

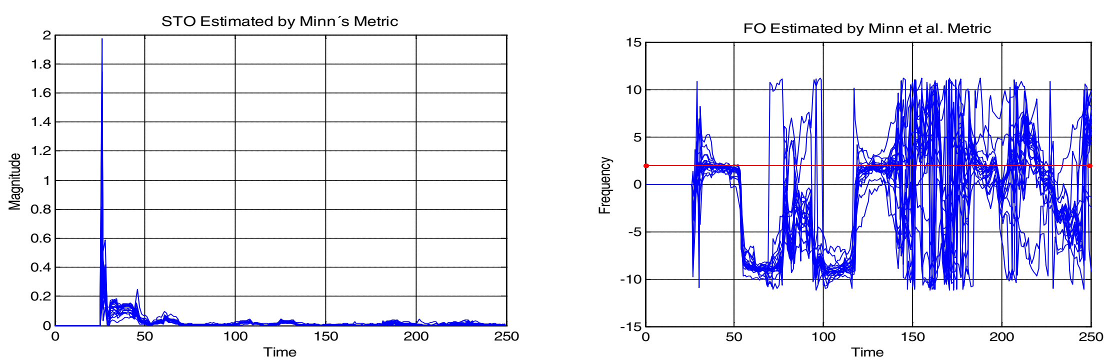

(a) (b)

Figure 6.3. (a) STO estimated and (b) CFO estimated by Minn Metric, N_c=64, *TO*=10, *FO*=2.

The timing offset estimated for a coarse delay of 25 samples is shown in Figure 6.4a, and the estimated fractional frequency offset normalized of 0.36 is plotted in Figure 6.4b. We observe a reduced range of estimation from -2.5π to 2.5π.

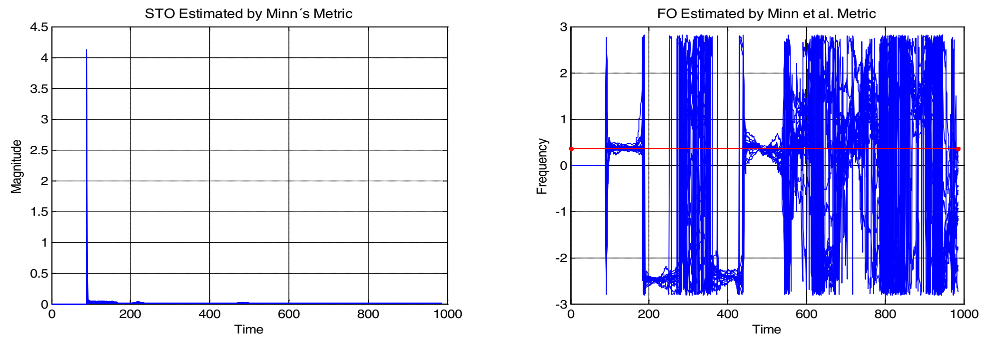

(a) (b)

Figure 6.4. (a) STO estimated and (b) CFO estimated by Minn's metric, N_c=256,*TO*=25, *FO*=0.36.

6.1.3 Simulation of Park's metric

The resulting coarse timing offset for the Park's metric [41] for N_c=64, is shown in Figure 6.5a, where is notable an improved detection of timing offset with a well defined maximum peak response. However, the frequency estimated is not so well detected with a variable frequency interval of estimation, within a range from -10π to 10π, as is illustrated in Figure 6.5b.

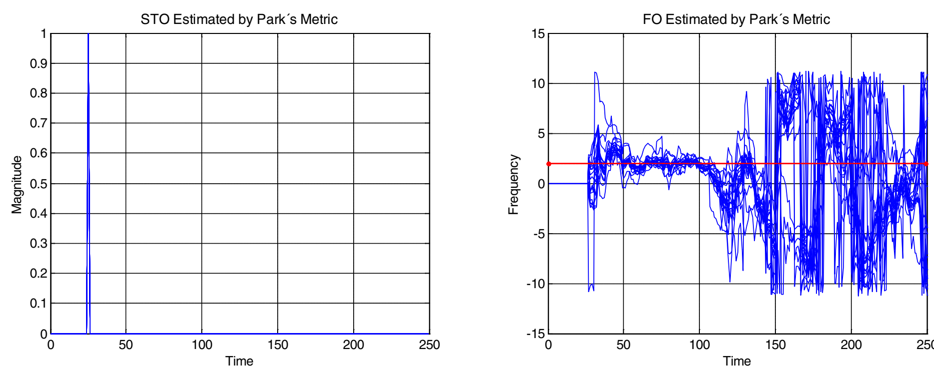

(a) (b)

Figure 6.5. (a) STO estimated and (b) CFO Estimated by Parks metric, N_c=64, *TO*=10, *FO*=2.

In a similar way, the resulting timing offset for a preamble with N_c=256 samples, (Figure 6.6a), exhibits a maximum detected peak well defined. However the fractional frequency offset shows a not well defined value, where the interval to estimate the fractional offset is not consistent, within a range of estimation from -2.5π to 2.5π, (Figure 6.6b).

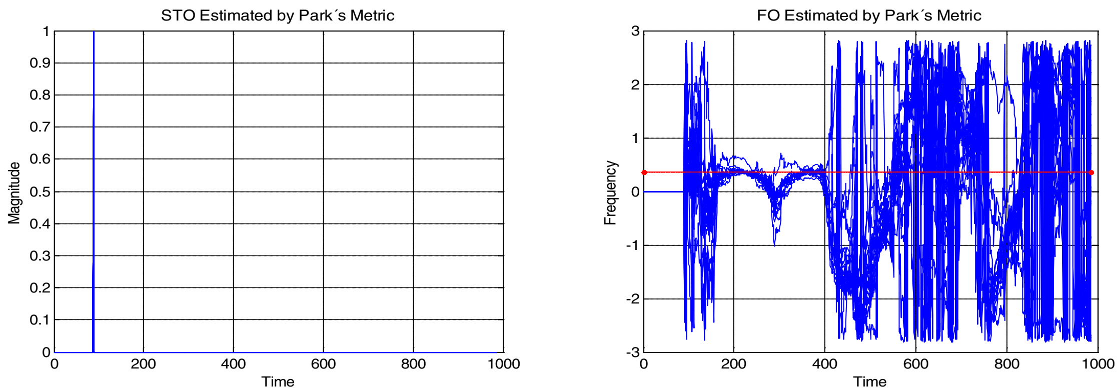

(a) (b)

Figure 6.6. (a) STO Estimated and (b) CFO Estimated by Parks Metric, N_c=256,TO=25, FO=0.36.

6.1.4 Simulation of Shi-Serpedin metric

The estimated timing and frequency offset for a preamble of length N_c=64, which is affected with timing offset of 10 samples, a normalized frequency Offset of 2 are shown in Figure 6.7a and 6.7b, respectively. The estimated timing offset is not well defined due to the lateral components, which originates uncertainty in the selection of the maximum detected peak. The coarse frequency is estimated in range from -10π to 10π, with a reduced time interval of observation, as is observed in Figure 6.7b.

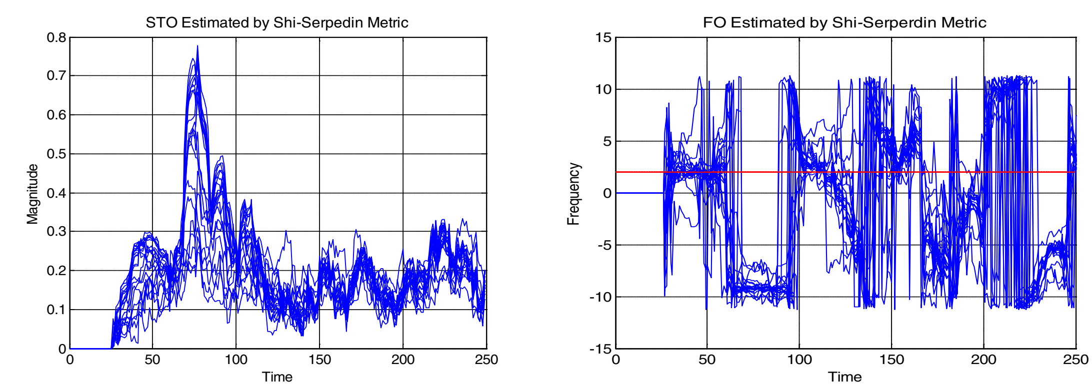

(a) (b)

Figure 6.7. (a) STO Estimated and (b) CFO Estimated by Shi-Serpedin Metric, N_c=64, TO=10, FO=2.

The estimated timing offset with a preamble of length N_c=256 is shown in Figure 6.8a, with a better estimation of the maximum peak than a preamble of length N_c=64. However, the estimated point remains with lateral peaks defined by response of the Shi-Serpedin metric. The fractional frequency offset is plotted in Figure 6.8b with the estimation range from -2.5π to 2.5π.

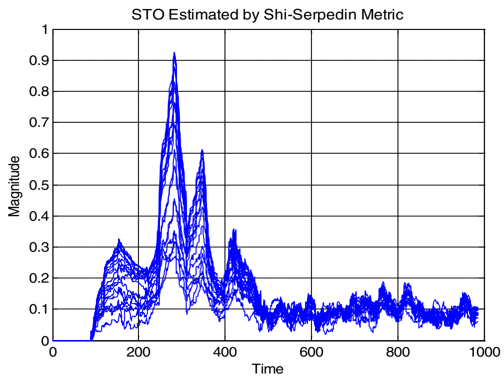

(a)

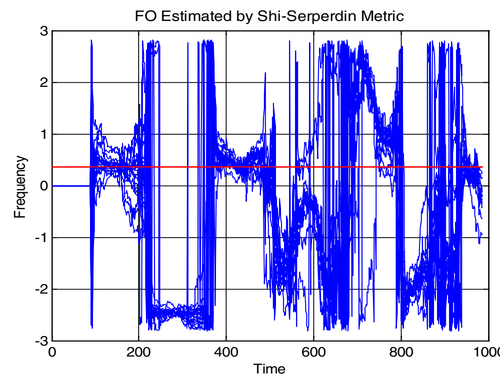

(b)

Figure 6.8. (a) STO estimated and (b) CFO estimated by Shi-Serpedin metric, N_c=256, *TO*=25, *FO*=0.36.

6.1.5 Simulation of Ren et al. metric

The resulting coarse timing estimation for a preamble with length N_c=64 is shown in Figure 6.9a, and the estimated normalized coarse frequency offset with a value of 2, it is plotted in Figure 6.9b. The estimated timing offset which indicates the starting point of the symbol exhibits a lateral peak, but is not comparable with the maximum resultant peak. The obtained frequency offset is not accurately estimated, within an offset range from -5π to 5π.

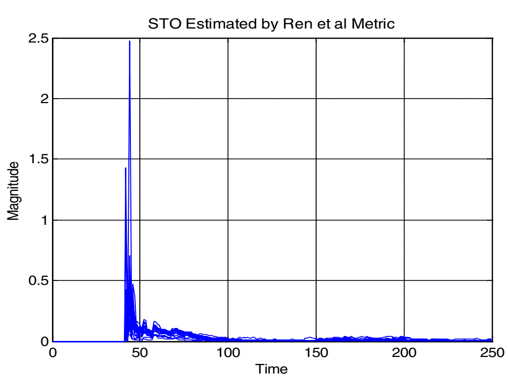

(a)

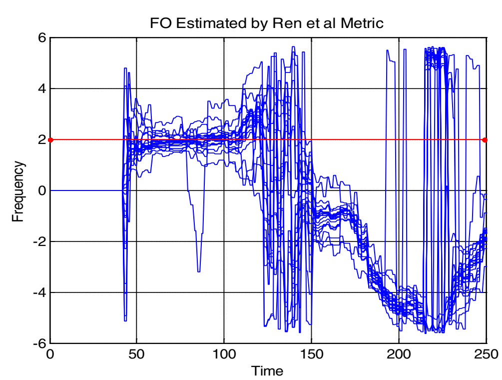

(b)

Figure 6.9. (a) STO estimated, (b) CFO estimated by Ren's metric, N_c=64,*TO*=10, *FO*=2.

The accuracy of the Ren's metric with a preamble of length N_c=256 is shown in the Figures 6.10a and 6.10b, respectively. The estimated coarse timing is shown in Figure 6.10a, where is observable a well-defined maximum peak. The estimated fractional frequency offset of a normalized value of 0.36 is well detected, within the available range from -1.5π to 1.5π, Figure 6.10b.

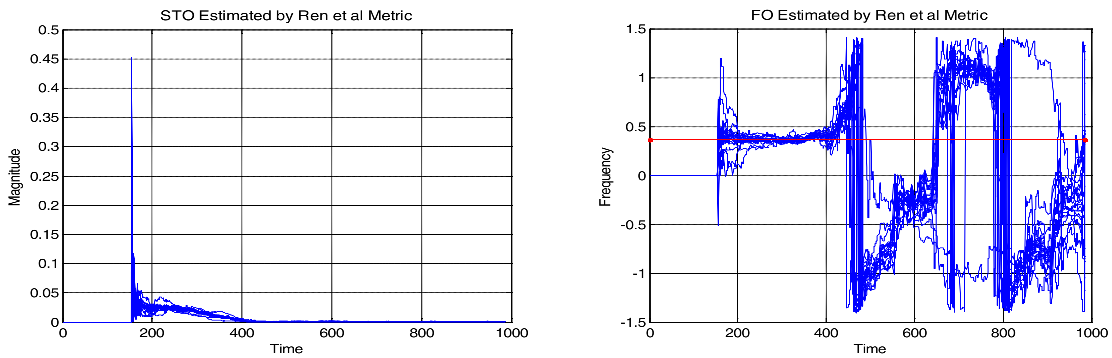

(a) (b)

Figure 6.10. (a) STO estimated, (b) CFO estimated by Ren's metric, N_c=256,*TO*=25, *FO*=0.36.

6.1.6 Simulation of Seung's metric

The timing and frequency offset resulting of the Seung's metric [64], shows a good defined coarse timing offset for a preamble of length N_c=64 (Figure 6.11a), and a precise estimation for a preamble with length N_c=256, (Figure 6.12a). However, the coarse and fractional frequency offset are not well defined for N_c=64, (Figure 6.11b), and N_c=256 (Figure 6.12b).

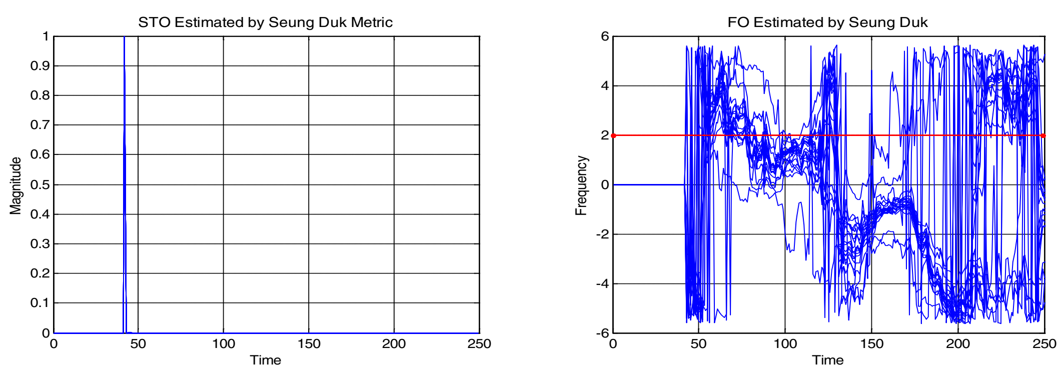

(a) (b)

Figure 6.11. (a) STO estimated, (b) CFO estimated by Seung's metric, N_c=64, *TO*=10, *FO*=2.

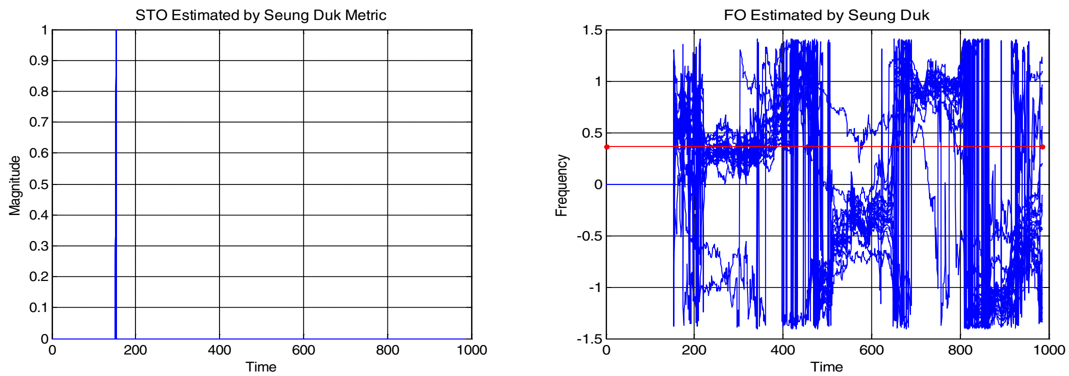

(a) (b)

Figure 6.12. (a) STO estimated, (b) CFO estimated by Seung's metric, N_c=256,TO=25, FO=0.36.

6.1.7 Simulation of Zhou's metric

The simulations of the resulting estimations in time and frequency of Zhou's metric, [65], are shown in Figure 6.13a and 6.13b, respectively, where is notable the good estimation for coarse timing, that can be obtained using a preamble of length N_c=64. The resulting coarse frequency offset is good estimated in the interval of observation, within an estimation range from -10π to 10π.

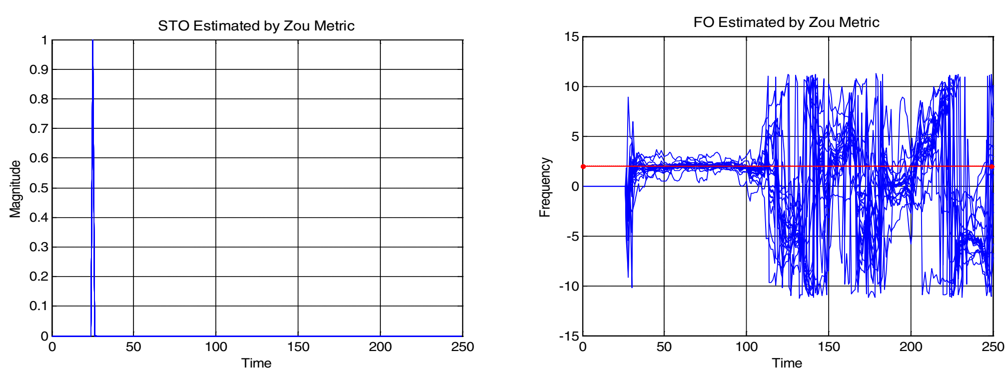

(a) (b)

Figure 6.13. (a) STO estimated and (b) CFO estimated by Zhou's metric, N_c=64, TO=10, FO=2.

In the case of a preamble with length N_c=256 the timing estimated is shown in Figure 6.14a, and the estimated fractional frequency offset of 0.36 is shown in Figure 6.14b. It is possible observe an excellent accuracy in the estimation of the timing offset, with a well-defined maximum peak without lateral side lobes. Once estimated the timing offset, the fractional frequency offset is estimated within an available interval from -2.5π to 2.5π, it is probably to detect the frequency offset over a wide range of received samples with the Zhou's metric, which have a good approximation to the expected frequency offset, as is represented in Figure 6.14b.

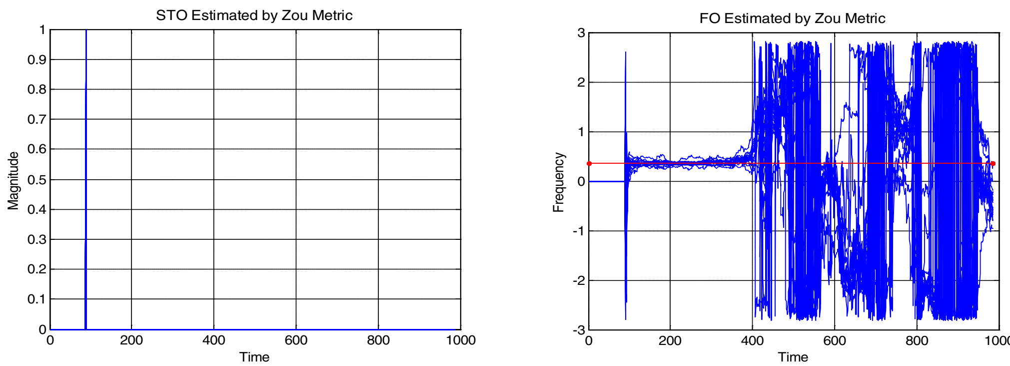

(a) (b)

Figure 6.14. (a) STO estimated and (b) CFO estimated by Zhou's metric, N_c=256,*TO*=25, *FO*=0.36.

6.1.8 Simulation of H. Wang's metric

The H.Wang metric proposed in [66], it is evaluated by simulation in MATLAB. Firstly, a preamble with length of N_c=64 and normalized frequency offset of 2 samples is used, as is shown in Figures 6.15a and 6.15b, respectively. It is notable on the simulation that the estimation of the coarse frequency offset is not well defined, thus obtaining estimated values with scattered values over the expected frequency offset.

Secondly, it is presented the estimated timing offset for a preamble of length N_c=256, (Figure 6.16a). The simulation shows that even increasing the length of the preamble, the accuracy of timing offset has only a slight improvement. However, the estimated fractional frequency offset is considerably improved, as shown in the Figure 6.16b, where the estimation has low dispersion, this in comparison with the estimation achieved by the preamble of length N_c=64.

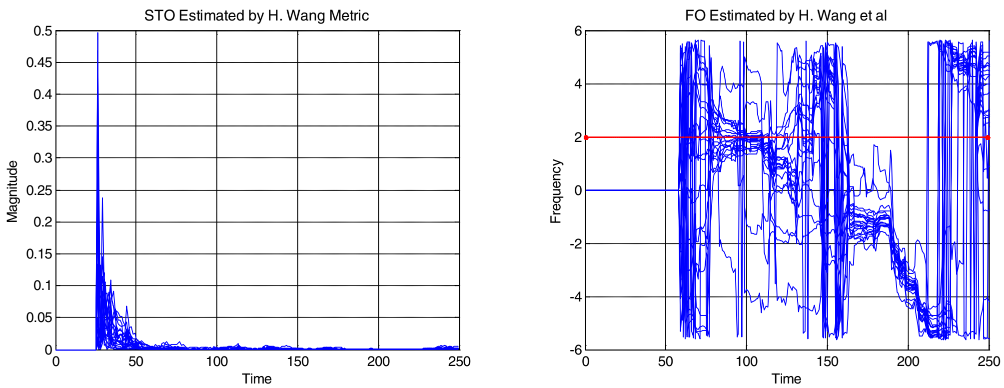

(a) (b)

Figure 6.15. (a) STO Estimated and (b) CFO Estimated by H. Wang Metric, *N*=64, *TO*=10, *FO*=2.

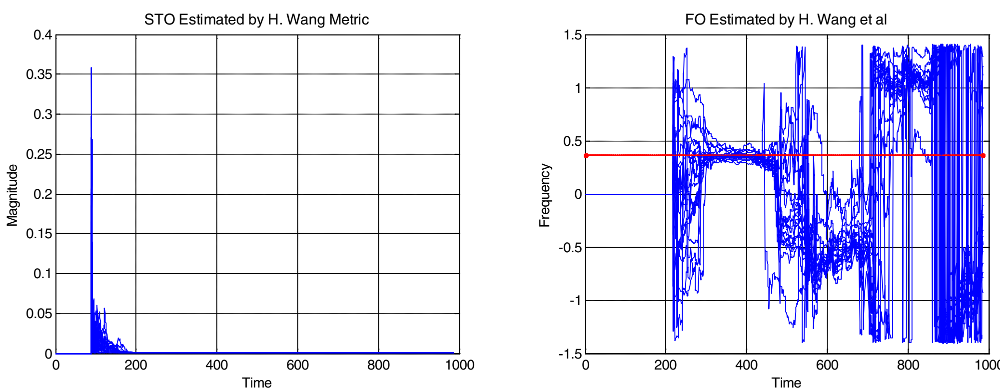

(a) (b)

Figure 6.16. (a) STO Estimated and (b) CFO Estimated by H. Wang Metric, *N*=256,*TO*=25, *FO*=0.36.

The obtained simulations varying the length of the symbol, allows to define a different range of estimation for the carrier frequency offset, and is different for a long or short preamble, as is detailed in Table VIII.

Table VIII. Range of Estimation

Preamble	Length of Preamble	Designed Sequence
Short	64	-2.5π to 2.5π
Long	64	-10π to 10π
Short	256	-1.25π to 1.25π
Long	256	-2.25π to 2.25π

6.2 Performance evaluation of the reviewed metrics

Once analyzed and simulated the reviewed timing metrics, it is possible to evaluate the mean square error (MSE) of the estimators, and the bit error rate (BER) performance of the complete OFDM system. The mean square error (MSE) reflects the bias and the variance of an estimator, which is an important criterion of comparison. The MSE of the parameter estimated is the expected squared difference between the estimated and the original value, [67].

In order to corroborate the correctly received signal, and once estimated the timing and frequency offset, the bit error rate (BER) is evaluated, [44]. In addition, it is necessary to apply channel estimation with the finality of reducing the affectations originated by the multipath channel. Comparing the best performance between the reviewed metrics is possible obtain the more accurately timing metric.

6.2.1 Simulation results and discussion

The performances of the reviewed metrics is reviewed by simulations in MATLAB, by evaluating the MSE of the timing offset, the frequency offset, and the BER of the received signal. The characteristics of simulation are shown in Table IX,

Table IX. Characteristics of simulation

Length of Preamble N_c	Cyclic Prefix	Timing Offset (samples)	Normalized Frequency Offset
64	16	10	2
64	16	20	3.5
128	32	20	2
128	32	16	1.34
256	64	22	0.46
256	64	25	0.36

The evaluated timing estimation for a preamble of length N_c=64 is shown in Figure 6.17, with a coarse timing offset (TO) of 10 samples. The better timing estimation is achieved by the metrics of Park, Zhou and Seung, which are not plotted in the Figure 6.17 because the measured error in the estimation is null.

The estimated frequency offset obtained by simulation is shown in Figure 6.18, with a normalized carrier frequency offset (CFO) of 2, where is notable the best frequency estimation achieved by the Zhou's metric, and is followed by the timing metrics of Schmidl and Cox, Ren et al, H. Wang and Minn.

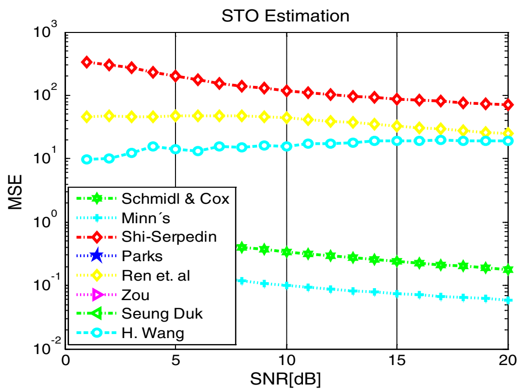

Figure 6.17. STO, N=64, TO=10, FO=2.

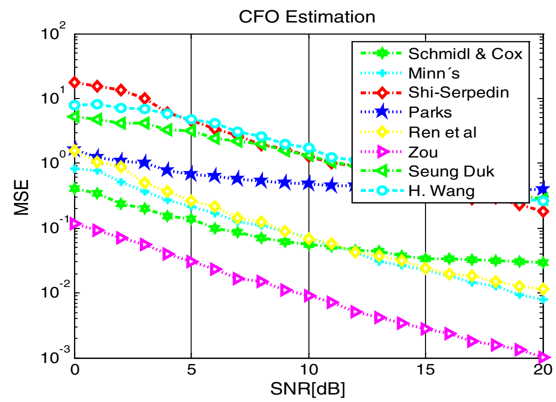

Figure 6.18. CFO N=64, TO=10, FO=2.

The obtained bit error rate shown in Figure 6.19 is simulated in conditions of Rayleigh fading channel, where the best approximation to the Analytic BER has been obtained by Zhou's metric, and a good estimation is achieved by the Schmidl and Cox, Seung and Ren et al. timing metrics.

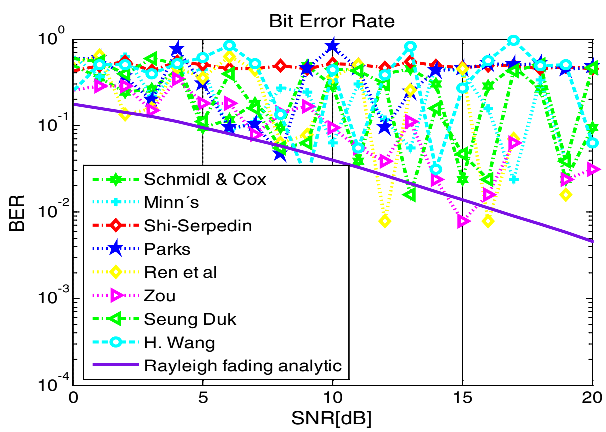

Figure 6.19. BER for N_c=64, TO=10, FO=2.

The timing estimation obtained with a preamble of length N_c= 64, TO of 20 samples and a normalized CFO of 3.5 is shown in Figure 6.20. The resulting estimation shown that the more accurately estimation were obtained by Parks, Zhou, and Seung's metrics, which are not displayed in the Figure 6.20, because the estimation is like an impulse response and the integer timing offset is correctly estimated.

The estimated carrier frequency offset is plotted in Figure 6.21, with the best estimation obtained by the Zhou's metric, having similar results with Ren et al., Park's and Schmidl & Cox timing metrics.

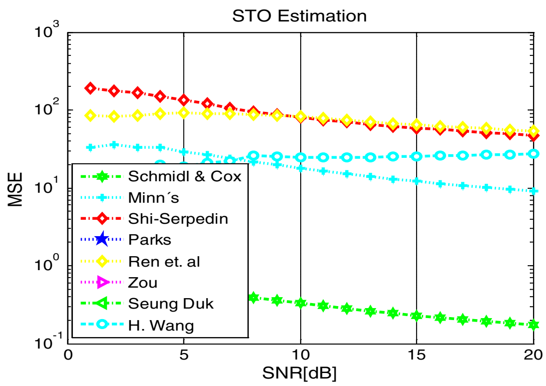

Figure 6.20. Timing Offset, *TO*=20.

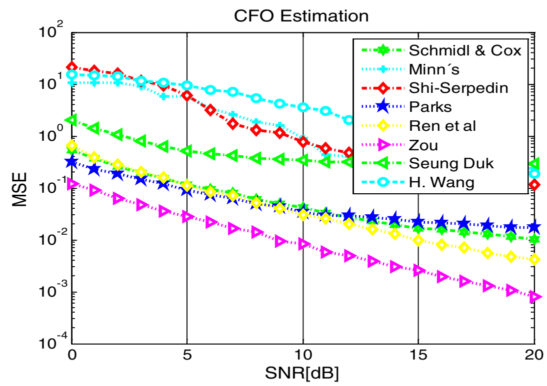

Figure 6.21. Frequency Offset, *FO*=3.5.

The Seung's metric obtains the best resultant BER in the simulation, as is shown in Figure 6.22. The simulation results indicate that, with an integer part and fractional frequency offset, the estimation is not well defined by the metrics, and because of that it is necessary a fine estimation.

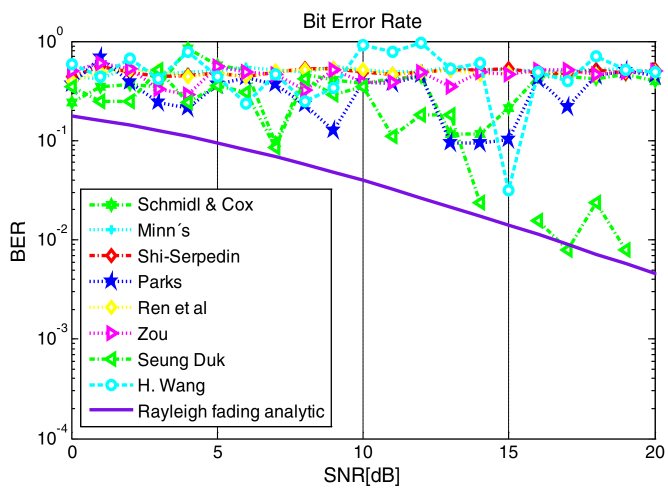

Figure 6.22. BER for *N*=64, *TO*=20, *FO*=3.5.

The estimation obtained for a preamble of length N_c=128, with a TO of 20 samples and a normalized CFO of 2, is depicted in Figure 6.23, where the best timing estimation is achieved by the metrics proposed by Seung, Zhou, and Park's.

The Zhou metric determines the better frequency estimation in comparison with other reviewed metrics, and its response is followed by the estimation obtained by Schmidl & Cox and Ren et al. metrics, as is depicted in Figure 6.24.

The obtained BER for the evaluated metrics is shown in Figure 6.25. The Parks Metric obtains the best joint estimation. The estimation achieved by Seung and the Schmidl and Cox exhibit also good BER results.

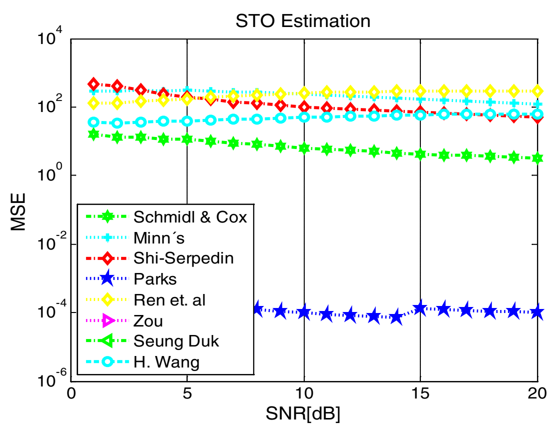

Figure 6.23. STO, *N*=128, *TO*=20, *FO*=2.

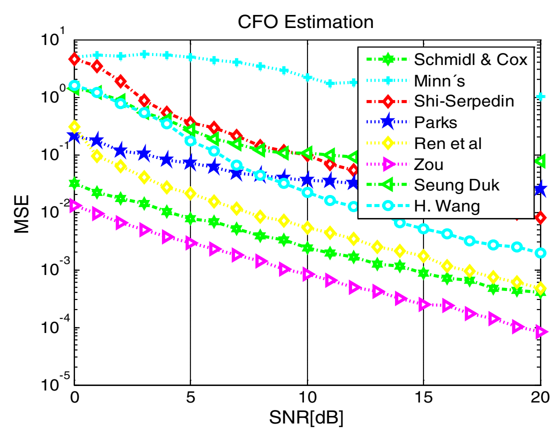

Figure 6.24. CFO, *N*=128, *TO*=20, *FO*=2.

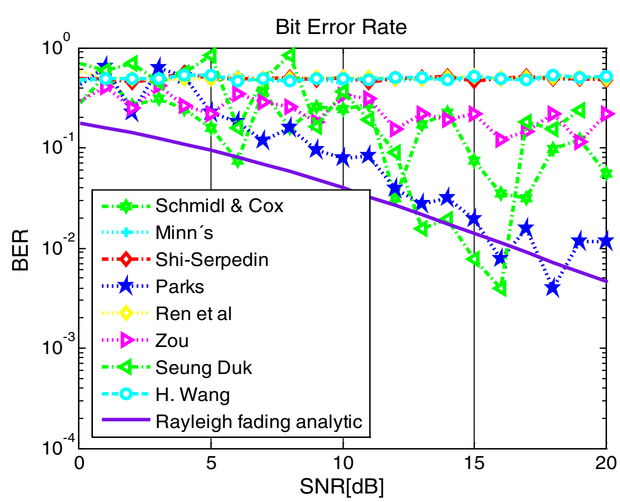

Figure 6.25. BER for *N*=128, *TO*=20, C*FO*=2.

The estimated timing and frequency offset for a preamble of length *N*=128, *TO*=16 and normalized FO of 1.34 are plotted in Figures 6.26 and 6.27, respectively. We observe that the best timing estimations are the responses of Zhou, Seung and Park's metric. The estimated integer and fractional frequency offset is well defined by the metrics of Zhou, Schmidl & Cox, and quite similar to the response obtained by Ren et al. metric.

The resulting BER of the jointly estimation is depicted in Figure 6.28, where we can observe the best response achieved by the Zhou metric. The BER determined by the modified Schmidl & Cox is similar to Ren et al, and H. Wang metric is quite similar to Zhou Metric.

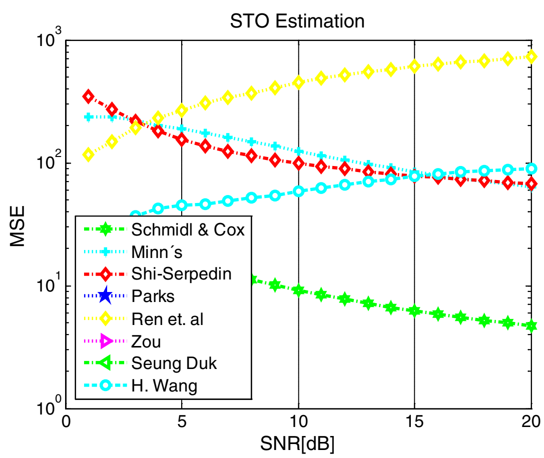

Figure 6.26. STO, *N*=128, *TO*=16, *FO*=1.34.

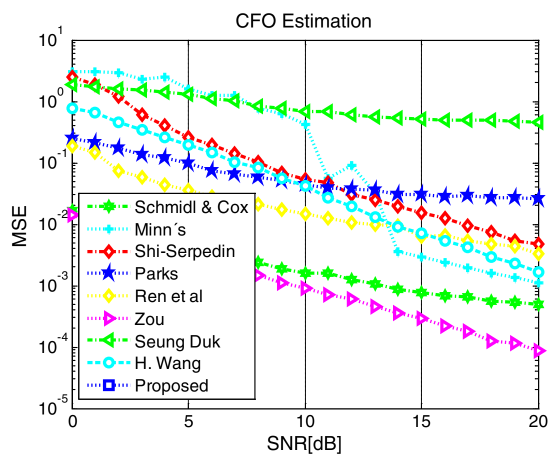

Figure 6.27.CFO, *N*=128, *TO*=16, *FO*=1.34.

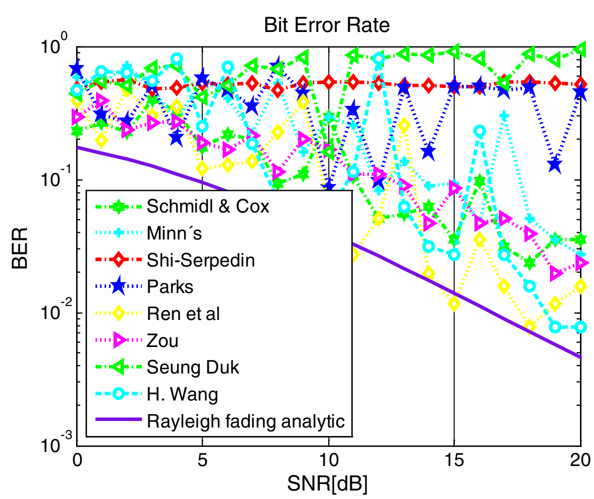

Figure 6.28. BER for *N*=128, *TO*=16, *FO*=1.34.

Considering a preamble of length N_c=256, *TO*=22 and *FO*=0.46. The simulation of the estimated timing offset is shown in Figure 6.29, where the best estimation is given by the Zhou's metric, having a similar response to Seung and Park's metrics.

The best estimation of the frequency offset is determined by applying the Zhou´s metric, and is very similar to the Schmidl and Cox metric, as is observed in Figure 6.30. The jointly estimation of the Zhou's metric results in a good BER; it was obtained by simulation and illustrated in Figure 6.31.

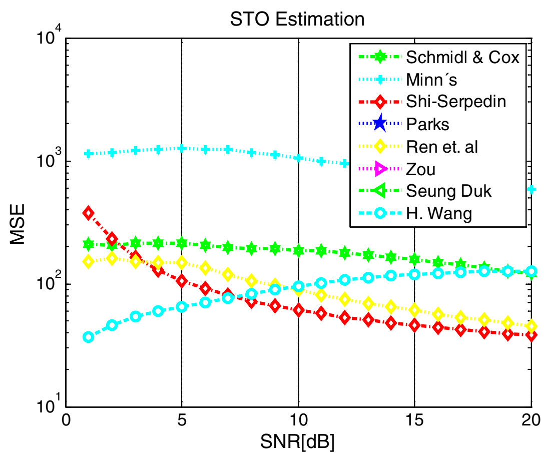

Figure 6.29. STO, *N*=256, *TO*=22, *FO*=0.46.

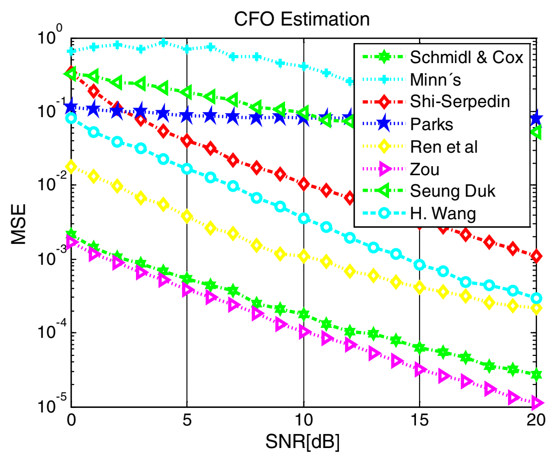

Figure 6.30.CFO, *N*=256, *TO*=22, *FO*=0.46.

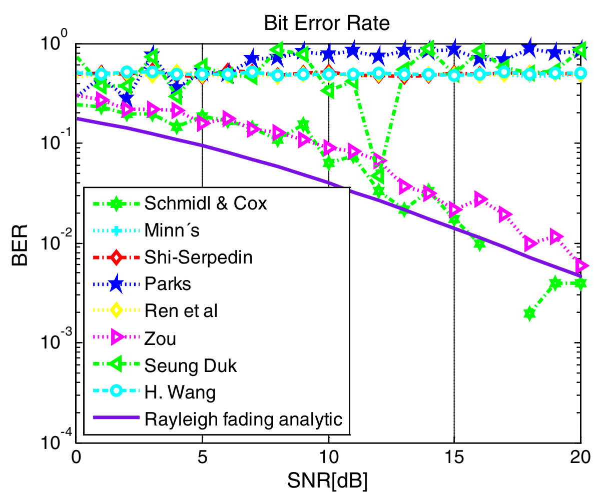

Figure 6.31. BER for *N*=256, *TO*=22, *FO*=0.46.

The timing estimation obtained for a preamble of length *N*=256, *TO*=25 and normalized *CFO*=0.36 is plotted in Figure 6.32, where the better estimations are obtained by Zhou, Seung Duk and Parks metrics, obtaining a null error, which causes shall not displayed in the Figure.

The estimated frequency offset is shown in Figure 6.33, where the best response is obtained by the Zhou metric, followed by the estimation of Ren et al., Schmidl & Cox, and H.Wang metrics. The Figure 6.34 illustrates the resulting BER obtained by simulation; it is notable that the H.Wang and Zhou's metrics achieve the best responses.

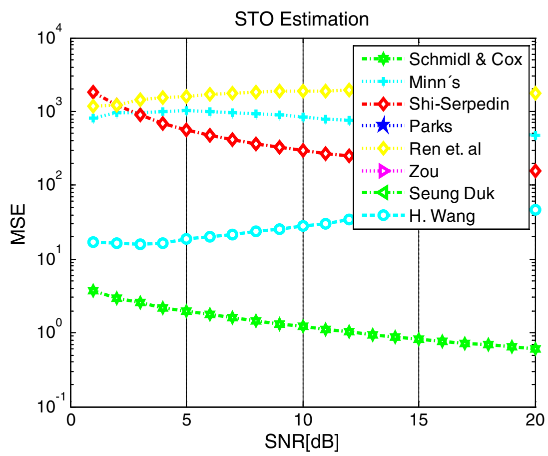

Figure 6.32. STO, *N*=256, *TO*=25, *FO*=0.36.

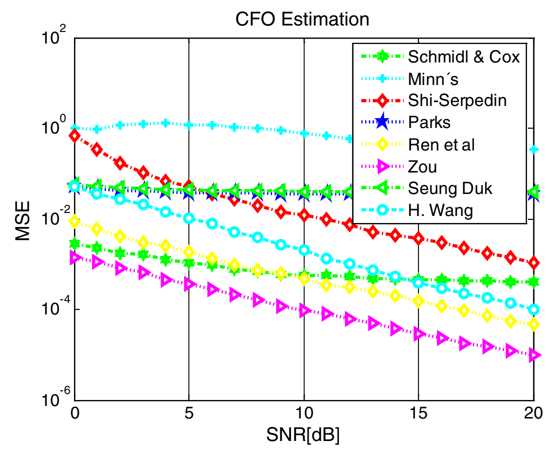

Figure 6.33.CFO, *N*=256, *TO*=25, *FO*=0.36.

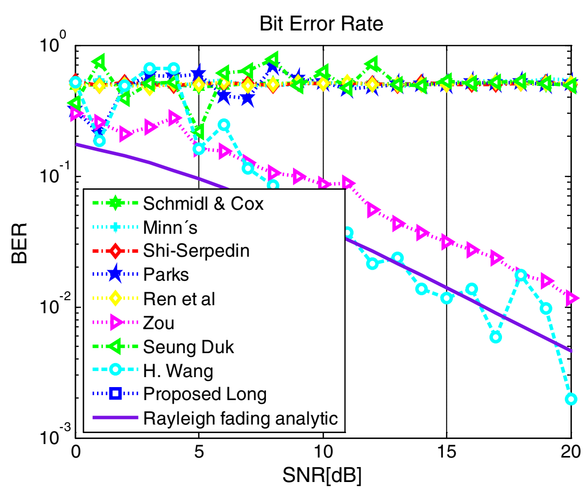

Figure 6.34. BER for *N*=256, *TO*=25, *FO*=0.36.

The comparison of resulting BER is shown in Table X, where is possible to observe that, when a Rayleigh fading channel and synchronization errors are present, the BER performance is reduced. The best results are obtained by the most recently developed timing metrics, where the Zhou and Seung metrics are characterized by a multiple correlations between different parts of the preamble, which increase the time process to obtain the estimation. However, improved results are obtained by the weighted metrics proposed by Ren et al., and H. Wang.

Table X.- Resulting BER of analyzed metrics.

Metric	N_c	STO	CFO	SNR	BER
Schmidl & Cox	64	20	3.5	5dB	$10^{-0.5}$
	128	16	1.34		$10^{-0.9}$
	256	25	0.36		$10^{-0.5}$
Minn	64	20	3.5	5dB	$10^{-0.5}$
	128	16	1.34		$10^{-0.6}$
	256	25	0.36		$10^{-0.5}$
Shi-Serpedin	64	20	3.5	5dB	$10^{-0.5}$
	128	16	1.34		$10^{-0.5}$
	256	25	0.36		$10^{-0.5}$
Parks	64	20	3.5	5dB	$10^{-0.7}$
	128	16	1.34		$10^{-0.5}$
	256	25	0.36		$10^{-0.5}$
Ren et al.	64	20	3.5	5dB	$10^{-0.6}$
	128	16	1.34		10^{-1}
	256	25	0.36		$10^{-0.5}$
Zhou	64	20	3.5	5dB	$10^{-0.5}$
	128	16	1.34		$10^{-0.9}$
	256	25	0.36		$10^{-0.9}$
Seung Duk	64	20	3.5	5dB	$10^{-0.7}$
	128	16	1.34		$10^{-0.6}$
	256	25	0.36		$10^{-0.9}$
H. Wang	64	20	3.5	5dB	$10^{-0.6}$
	128	16	1.34		$10^{-0.8}$
	256	25	0.36		$10^{-0.9}$

6.3 Proposed preamble and timing metric

Once reviewed the state of art of timing metrics, and in order to get more accurate timing and frequency estimation, in the following section are explained the most important contributions of the present thesis to the timing metrics.

The first contribution of this thesis is the proposal of a weighted modified long preamble; it is based on a CAZAC sequence weighted by a Golay Rudin Shapiro (GRS) sequence.

The second contribution consists of the proposal of a synchronization algorithm, based on the idea proposed by Ren et al [42]. The third contribution consist on a modified short preamble and its corresponding timing metric, based on the idea proposed by H. Wang et al [66].

6.3.1 Proposed long preamble and timing metric

The proposed long preamble consists on applying a GRS sequence for weighting a CAZAC sequence and is designed as follows; First, the CAZAC sequence of length $L=N_c\ /2$ is scrambled with a GRS sequence Ps of the same length, (Figure 6.35), and then the resulting sequence is up-sampled by two, to get a symmetric sequence, Figure 6.36.

$$Cz_T = [A_T \;\; A_T], \tag{6.1}$$

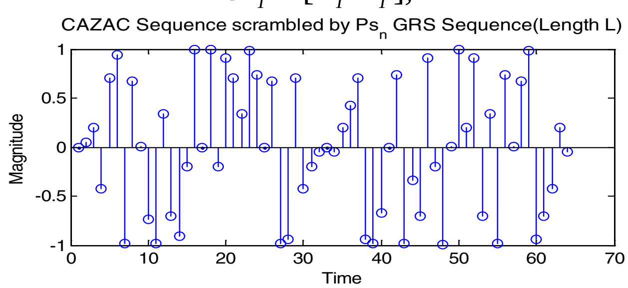

Figure 6.35. CAZAC scrambled sequence with P_s sequence.

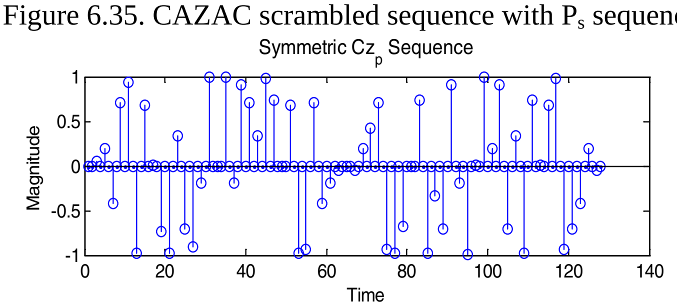

Figure 6.36. Cz_p sequence.

Next, once defined symmetric sequence, each component of the preamble Cz_T is multiplied by the GRS complementary pair sequences, represented by,

$$S_{long} = [Dl_P \; Dl_Q], \tag{6.2}$$

where Dl_P represents the sequence of length $N_c/2$, which is generated by the discrete Fourier transform (DFT) of the sequence Cz_T and then multiplied by $P(k), k = 1, 2, ..., N_c / 2$. In the same way, Dl_Q represents the sequence of length $N_c/2$, generated by the DFT of the Cz_P sequence, and later is multiplied by $Q(k), k = L+1, L+2, ..., N_c / 2$. The resulting proposed preamble is show in Figure 6.37.

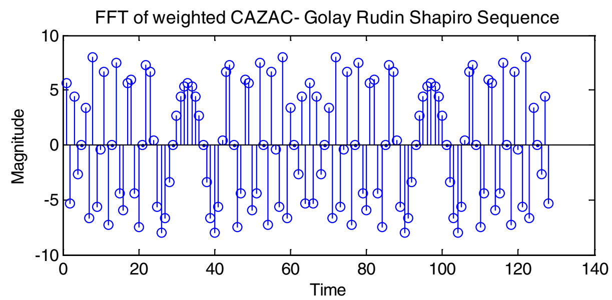

Figure 6.37. Proposed preamble.

The proposed timing metric that detects the proposed preamble was developed as follows,

$$P_E(d) = \sum_{m=0}^{L-1} Ps_m Ps_m r^*_{d+m} r_{d+m+L}, \tag{6.3}$$

$$R_E(d) = \left(\tfrac{1}{2}\right) \sum_{m=0}^{L-1} \left| r_{d+m+L} \right|, \tag{6.4}$$

where Ps_m is the Golay Rudin-Shapiro sequence, which is used to de-spread the received signal in the correlators of the timing metric (this is the same sequence used to scrambling the CAZAC sequence on the transmitted preamble). $P_E(d)$ is the cross-correlation of the received samples, Figure 6.38, and $R_E(d)$ is the power energy of the delayed correlated samples (Figure 6.39).

The estimation of timing offset is defined in equation 6.6,

$$M_E(d)=\frac{P_E(d)}{R_E(d)}, \tag{6.5}$$

$$\hat{d}=\arg\max_{d}\left(M_E(d)\right), \tag{6.6}$$

The frequency offset can be estimated as,

$$\hat{v}_E=\frac{1}{\pi N_c}\arg\left(P_E\left(\hat{d}\right)\right), \tag{6.7}$$

where $\hat{d}$ is the timing point of the started symbol, and the length of the period of estimation depend on the length of the preamble. The proposed preamble estimates the integer and fractional frequency offset in the range of [-5π, 5π] for a length of N_c=*64*.

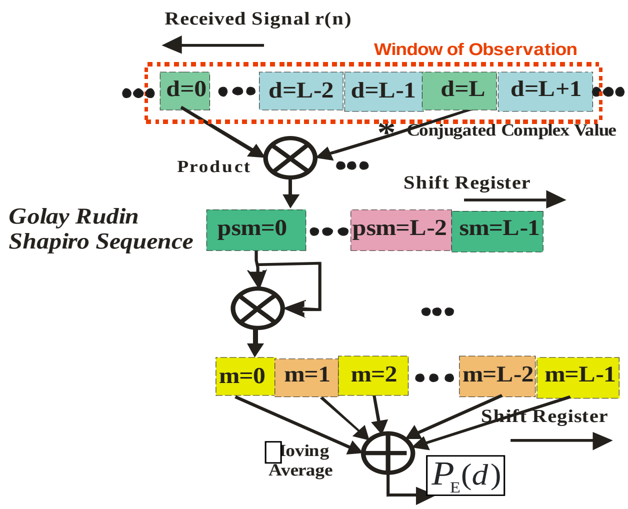

Figure 6.38. P_E Component of the proposed long metric.

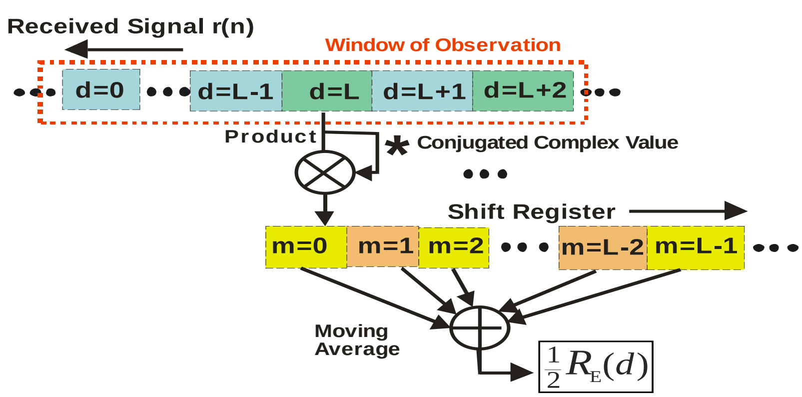

Figure 6.39. R_E component of the proposed long preamble.

6.3.2 Proposed short preamble and timing metric

In a similar way like the long preamble, the short preamble is designed with a repetitive period of length $L_L = N_c / 4$, using the same procedure applied for the long preamble, where the weighted sequence $\left[Ps_s(k)\ Qs_s(k) \right], k = 0,1,...,L/4$ is used over two repetitive periods in the preamble. The designed short preamble is defined by,

$$S_{short} = [Ds_{Ps}\ Ds_{Qs}\ Ds_{Ps}\ Ds_{Qs}], \tag{6.8}$$

where Ds_{Ps} and Ds_{Qs} are the weighted CAZAC sequence of length $L_L = N_c / 4$. We have proposed a synchronization algorithm with its corresponding timing metric, defined as,

$$M_{E_{short}}(d) = \frac{\left|P_{E_{short}}(d)\right|^2}{\left(R_{E_{short}}(d)\right)^2}, \tag{6.9}$$

$$P_{E_{short}}(d) = \sum_{m=0}^{L-1} Ps_{s_m} Ps_{s_m} r_{d+m}^{*} \cdot r_{d+m+L_L}, \tag{6.10}$$

$$R_{E_{short}}(d) = \frac{1}{4} \cdot \sum_{i=0}^{3} \sum_{m=0}^{L-1} \left| r_{d+m+i*L} \right|^2, \tag{6.11}$$

where the receiver timing metric uses a synchronized replica of the Ps_{s_m} sequence, with the finality of de-spread the received signal, allowing the recovery of the transmitted CAZAC sequence. $P_{E_{short}}(d)$ is the correlation of the actual and the $N_c/4$ delayed sample, Figure 6.40. $R_{E_{short}}(d)$ defines the power of the samples in the window of observation, Figure 6.41.

The frequency offset estimated for the short preamble is carried out as following,

$$\hat{v}_{E_{short}} = \frac{1}{\pi N_c} angle\left(r_{\hat{d}+m}^{*} \cdot r_{\hat{d}+m+L} \right), \tag{6.12}$$

where $\hat{d}$ is the estimated maximum point of the timing metric.

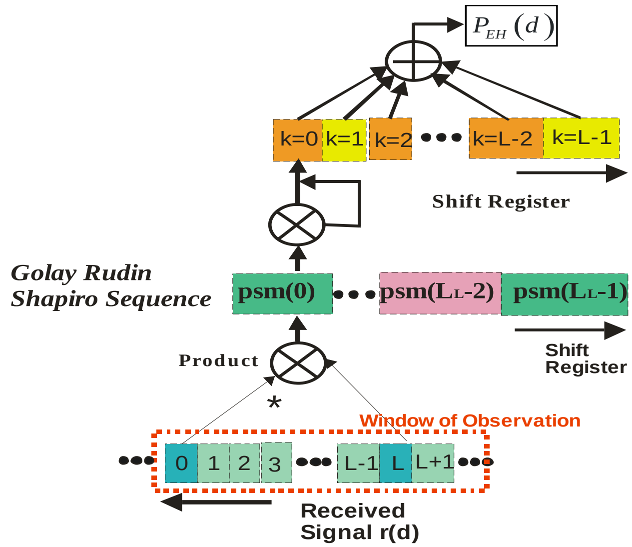

Figure 6.40. $P_{E_{short}}$ component of the proposed short preamble.

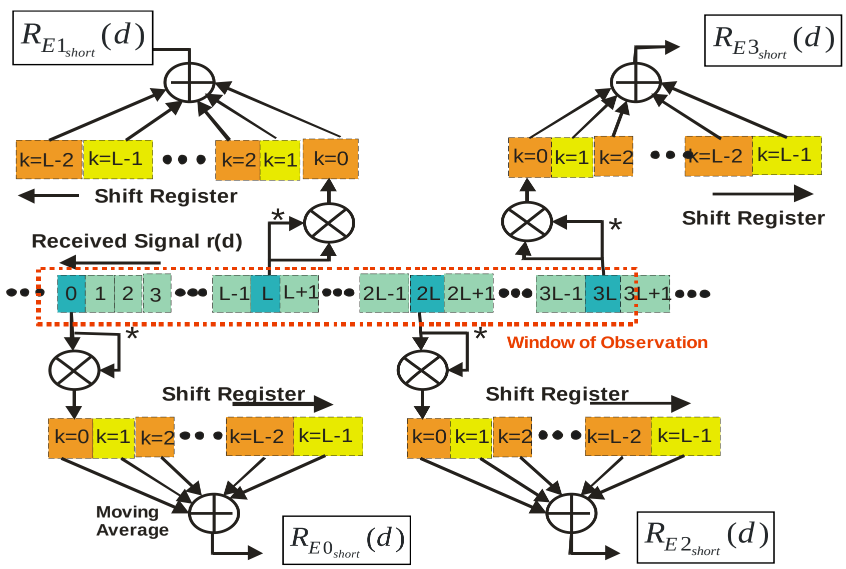

Figure 6.41. $R_{E_{short}}$ Component of the proposed short preamble.

6.3.3 Performance evaluation of weighted metrics

Simulations are carried out in MATLAB to evaluate the performance of the Ren et al., H. Wang, and the proposed weighted timing metrics. The considered channel model is a Rayleigh fading channel selective on frequency with AWGN, and 16 taps with an exponential power delay profile. Additionally, the channel estimation is applied to improve the performance of evaluated Bit Error Rate of the transmitted OFDM data.

6.3.4 Simulation results and discussion of weighted timing metrics

We evaluated the timing metrics algorithms by simulation with the characteristics of frequency offset, timing offset shown in Table XI, in conditions of multipath channel and the response of each estimator has been evaluated to a SNR of 0-20dB, simulating 1000 preamble sequences for each noise of the corresponding dB.

Table XI. Timing and Frequency offset

Length of Preamble N_c	Cyclic Prefix	Timing Offset (samples)	Normalized Frequency Offset
64	16	20	0.5
64	16	10	3
128	32	20	0.3
128	32	20	1.5
256	64	30	0.25

The timing offset obtained by simulation for all the evaluated timing metrics is shown in Figure 6.42. The timing offset is 20 samples, where their started timing point is in the sample 52 for the preamble of Ren et al (Figure 6.42a) and the proposed long timing metric (Figure 6.42b). In case of H. Wang and the proposed metric with a short preamble, the beginning of the symbol is in the sample 36, (Figure 6.42c and 6.42d, respectively). In all reviewed metrics, the index time started at zero, taking in consideration the *cyclic prefix*.

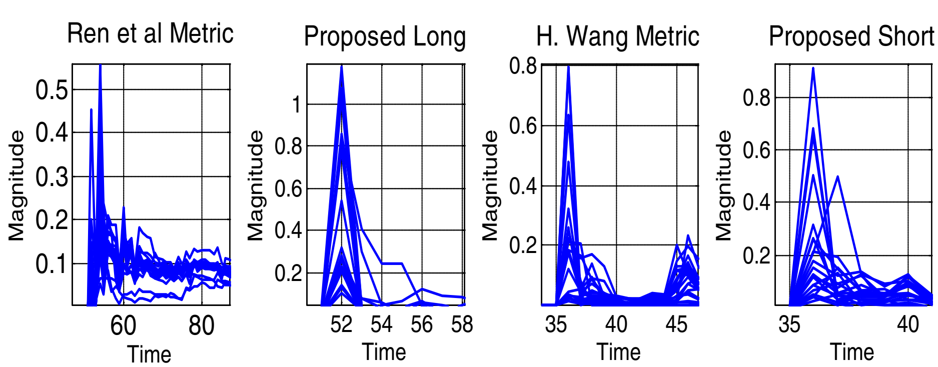

(a) (b) (c) (d)

Figure 6.42. STO estimated by the evaluated metrics.

The estimated frequency offset obtained by Ren *et al*. timing metric is shown in Figure 6.43a, and the estimation obtained by the proposed long preamble with its corresponding timing metric is shown in Figure 6.43b. In a similar way, in Figure 6.43c is shown the estimated CFO for the H. Wang metric, and in Figure 6.43d it is possible to observe the CFO estimated by the proposed short timing metric.

The accuracy achieved by the proposed metrics results in best peak detection. However, it is necessary to evaluate the mean square error (MSE) of the reviewed timing metrics, this to verify the improved detection. In a similar way, for frequency estimation is necessary to evaluate the MSE of each method.

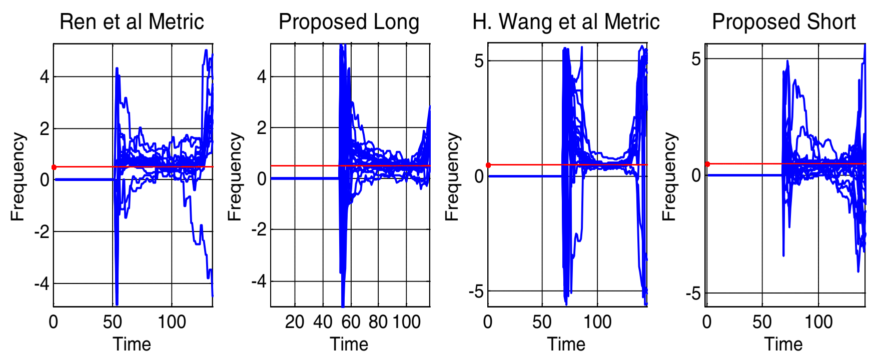

(a) (b) (c) (d)

Figure 6.43. CFO estimated by the evaluated metrics.

The mean square error (MSE) reflects the bias and the variance of an estimator. Figure 6.44 shows the plot of the MSE of the reviewed timing metrics and the resulting timing offset estimation, where the best result corresponds to the proposed short preamble with the lower MSE.

The resulting MSE of the frequency offset for the reviewed methods is given in Figure 6.45. Observing that the best estimation is achieved by the proposed short and long preambles, this in comparison with the existing weighted synchronization algorithms.

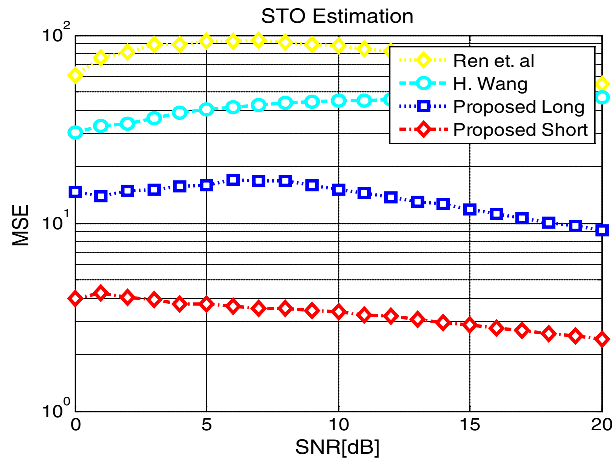

Figure 6.44. MSE of STO.

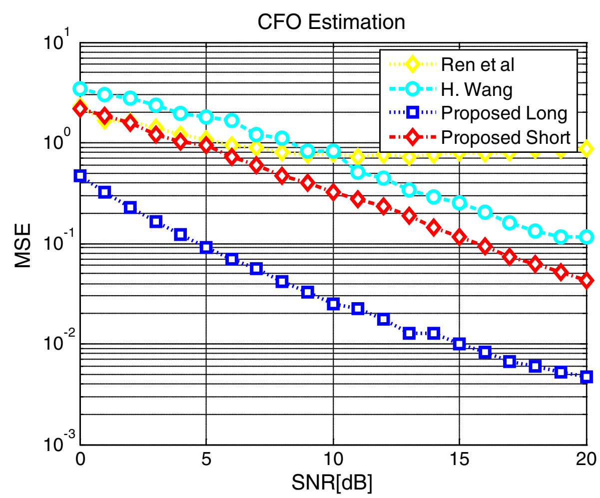

Figure 6.45. MSE of CFO.

A complete evaluation of preambles with different lengths in the OFDM system is achieved by means of measuring the bit error rate. The transmitted data are QPSK symbols.

The process of evaluate the performance is developed as follows: In the first step, the received samples are evaluated to define the starting point of the transmitted preamble, taking in consideration the maximum peak detected. The following step consists in multiply the received symbol by the negative value of the estimated frequency offset. Additionally it is applied a channel estimation to suppress the effects of the channel.

In following are detailed the resulting bit error rate, which has been achieved by the synchronization methods, and they were evaluated over different lengths of preamble symbols.

Figure 6.46 shows the resulting BER for a preamble of length N_c=64, timing offset equals to 20 and normalized frequency offset of 0.5. The resulting estimation shows that, the proposed synchronization algorithms with a short and long preamble achieve the best response. The monotony of the BER of the resulting H. Wang metric is due to an incorrect estimation of the time or frequency, which originates an increase of the error of the received symbols, as observed at the evaluated MSE, shown in Figures 6.44 and 6.45.

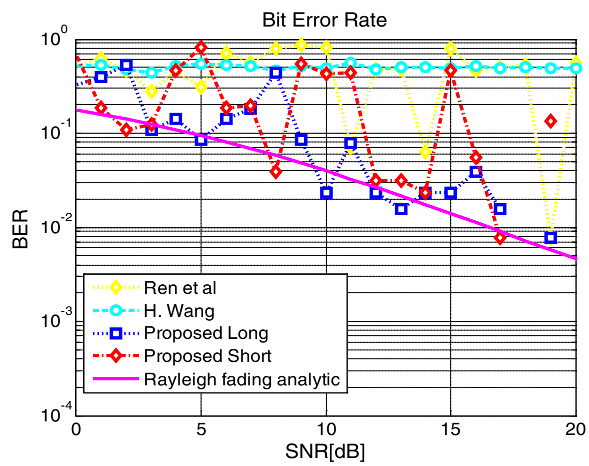

Figure 6.46. BER, N_c*=64,TO=20,FO=0.5*.

The BER obtained for a preamble with length N_c=64, timing offset of 10 and normalized frequency offset of 3 is shown in Figure 6.47. The proposed synchronization long preamble algorithm exhibits a good response and approximation to the analytic BER for OFDM symbol, which has been evaluated over Rayleigh channels.

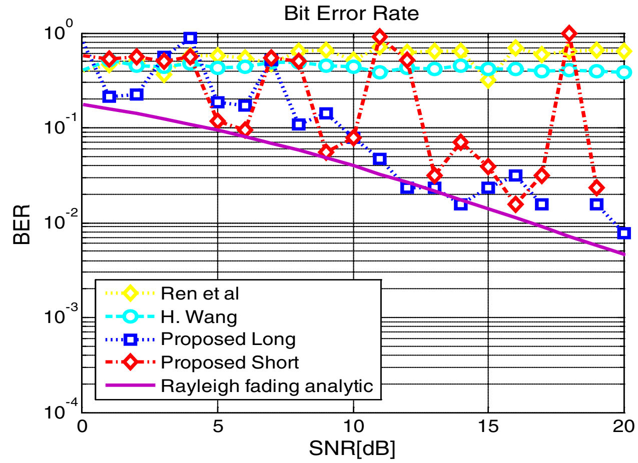

Figure 6.47. BER, N_c=64,TO=10,FO=3.

Figure 6.48 shows the BER obtained for a preamble of length N_c=128, timing offset of 20 and a fractional frequency offset of 0.3. We observe that, the better response is obtained by the proposed long preamble with its corresponding timing metric, which are designed in specific to estimate fractional frequency offset.

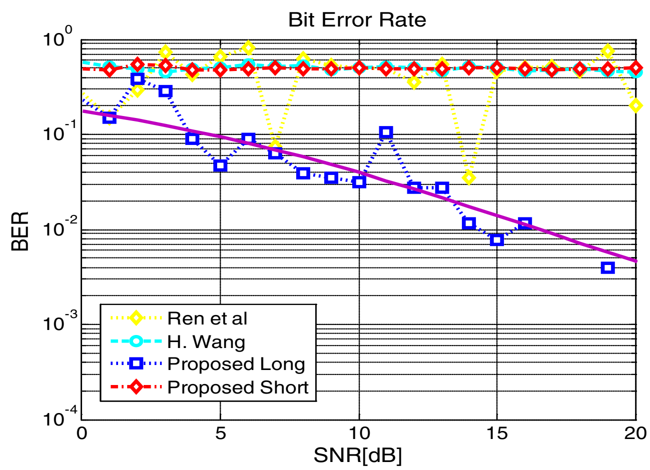

Figure 6.48. BER, N_c=128,TO=20,FO=0.3.

The obtained BER for a preamble of length N_c=128, timing offset of 20 samples and a normalized frequency offset of 1.5 is plotted in Figure 6.49, where it is possible to observe the improved response achieved by the proposed long preamble. In a similar way, it is observable a monotony of the resulting BER, which was obtained by the metrics of H. Wang, Ren's and the proposed short preamble metric, the measuring results are originated by an incorrect estimation of the integer and fractional frequency offset.

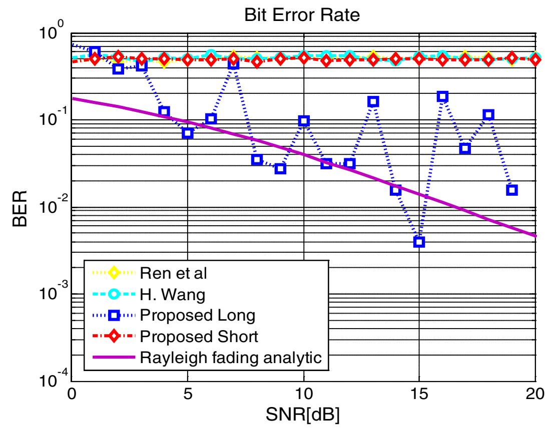

Figure 6.49. BER. N_c=128,TO=20,FO=1.5.

The BER for a preamble with length N_c=256 samples and CP of 64 samples are show in Figure 6.50, where the normalized frequency offset is 0.25 and the coarse timing offset is 30 samples. The result shows a good approximation of the proposed timing metrics to the analytic BER for Rayleigh channels, where the timing and frequency offset is achieved with good results in both expected estimates.

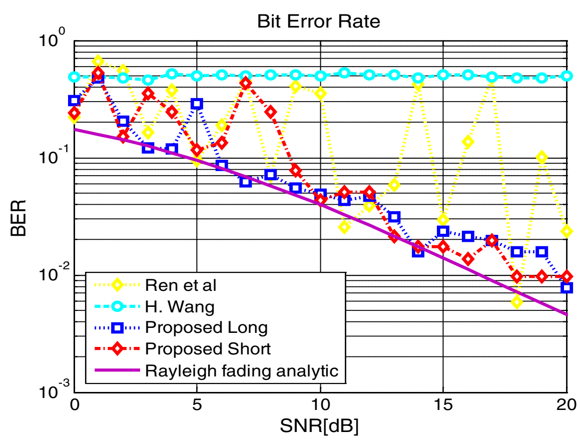

Figure 6.50. BER *N=256,TO=30,FO=0.25*.

The comparison of resulting BER is shown in Table XII, which was obtained by the reviewed and proposed weighted metrics. It is notable that, a considerable improvement is achieved with the application of the proposed long preamble, this taking in consideration a range of timing and frequency offsets.

Table XII.- Resulting BER of weighted metrics.

Metric	N_c	STO	CFO	SNR	BER
Ren et al.	64	20	0.5	5dB	$10^{-0.8}$
	128	20	1.5		$10^{-0.6}$
	256	30	0.25		10^{-1}
H. Wang	64	20	0.5	5dB	$10^{-0.6}$
	128	20	1.5		$10^{-0.6}$
	256	30	0.25		$10^{-0.6}$
Proposed Long	64	20	0.5	5dB	10^{-1}
	128	20	1.5		10^{-1}
	256	30	0.25		$10^{-0.8}$
Proposed Short	64	20	0.5	5dB	$10^{-0.2}$
	128	20	1.5		$10^{-0.6}$
	256	30	0.25		$10^{-0.1}$

6.4 Performance of preambles

An important contribution of the thesis consist on evaluate by simulation the limit Cramer-Rao bound, [67], of the existing and proposed preambles. The properties of auto-correlation of the reviewed preambles are evaluated by using the Schmidl & Cox timing metric.

The functionality of the data-aided synchronization methods depend on well designed pilot tones or preambles, where the synchronization methods based on auto-correlation of a training symbol enable the use of special sequences; where the most common sequences are PN and CAZAC sequences [32-38, 43-45].

The period of repetitive structures defines a long preamble, with a symmetric sequence defined by a half OFDM symbol and period $L_S = N_c / 2$, and in similar way, a short preamble is a repetitive period sequence of length $L_L = N_c / 4$. The reviewed and proposed preambles evaluated are shown in Table XIII.

Table XIII. Preamble design.

Method	Designed Preamble		
	Sequence	Short, $L_s = N_c / 4$	Long, $L_L = N_c / 2$
Schmidl and Cox, [39]	A = PN sequence		$\mathbf{S}_s = [A\,A]$
Minn, [40]	A_q = PN sequence	$\mathbf{S}_s = [A_q, A_q, -A_q, A_q]$	
Shi-Serpedin, [63]	B = PN sequence	$\mathbf{S}_s = [B, B, -B, B]$	
Park, [41]	A_q, B = PN sequences (*) Conjugated valued	$\mathbf{S}_s = [A_q, B, A_q^*, B^*]$	
Ren, [42]	C = CAZAC seq. B = PN sequence		$\mathbf{S}_s = [C\,C]\bullet B$
Seung, [64]	C = CAZAC seq. D=Time reversed version of C.		$\mathbf{S}_s = [C\,D]$
Zhou, [65]	C = CAZAC seq. E=Rotated Conjugated version of C.	$\mathbf{S}_s = [C_z, E, C_z, E]$	
Wang, [66]	C = CAZAC seq. A=PN sequence.	$\mathbf{S}_s = [C, F, C, F]$	
Proposed	C = CAZAC seq. B_{GRS} = GRS sequence		$\mathbf{S}_s = [C\,C]\bullet B_{GRS}$

Taking in consideration the preambles of Table XI, it is possible to design each one by means of CAZAC sequence, instead of a pseudo noise (PN) sequence, with the objective of use the *auto-correlation* properties of CAZAC sequences and low PAPR.

The PAPR of the proposed preamble is shown on the Figure 6.51.

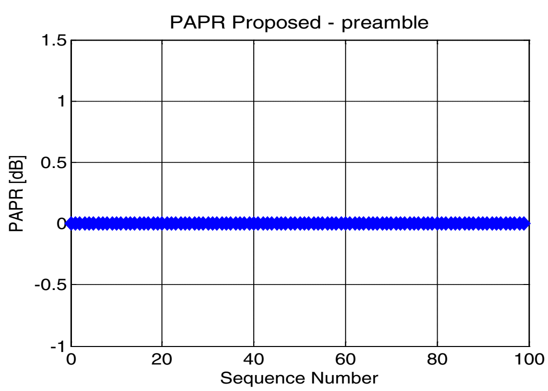

Figure 6.51. PAPR of Proposed Preamble.

Optimal periodic preambles sequences designed for timing and frequency offset estimations, which are applied in conditions of *frequency selective* Rayleigh *fading* channels is an important issue, since a good design can significantly improve the estimation response, and complexity. The optimal preamble sequence for frequency offset estimation is based on minimizing the Cramer Rao bound (CRB), which can be found in [21].

The average CRB is derived by means of an approximation in [68] of periodic signals with *cyclic prefix,* for the CFO estimation in *frequency selective* Rayleigh *fading* channels.

The CRB of the directed CFO estimation can be obtained like in [69]:

$$CRB = \frac{N_c^{'2}}{8\pi^2\left(tr\left(R^{-1}\Lambda R\Lambda\right) - tr\left(\Lambda^2\right)\right)}, \tag{6.13}$$

where $R = SC_hS^H + \sigma_n^2 I_{N'}$, with $[S]_{k,l} = s\left(k-l\right)$, for $0 \le k \le N_c^{'}, 0 \le l \le L-1$, s corresponds to the transmitted sequence, $C_h = E[hh^H] = \sigma_n^2 I_{N_c^{'}}$ is the covariance matrix of the channel, and $\Lambda = diag\left\{0,1,...,N_c^{'}-1\right\}$ a diagonal matrix with N' training signal samples.

6.4.1 Performance evaluation of preambles

The design of the existing and proposed preambles were investigated by simulations and compared by means of the Schmidl and Cox metric, and were evaluated the auto and *cross-correlation* of the sequences to estimate the timing and frequency offset.

The optimal preamble sequences for frequency synchronization are optimal only for a given estimation method or timing metric, for that reason, we considered the CRB expression for the CFO estimation in Rayleigh *fading* channels for the reviewed preamble sequences.

The performances of the existing and proposed preambles are evaluated by the MSE, and the channel estimation is not considered on the simulations.

6.4.2 Simulation results and discussion of reviewed preambles

The CRB for the different preambles evaluated is shown in Figure 6.52, with a length N_c=64, *CP*=16, and normalized frequency offset of $\hat{v} = 3.35\pi$, transmitted over a *multipath* fading channel of 16 taps. The obtained results exhibit a similar response between preambles designed with a conjugated CAZAC sequence, and preambles with an inverted sign CAZAC sequence, [40]. In contrast, the best results are obtained with preamble sequences using weighted CAZAC sequences, such as Ren et al, [42], H. Wang, [66], and the proposed preamble.

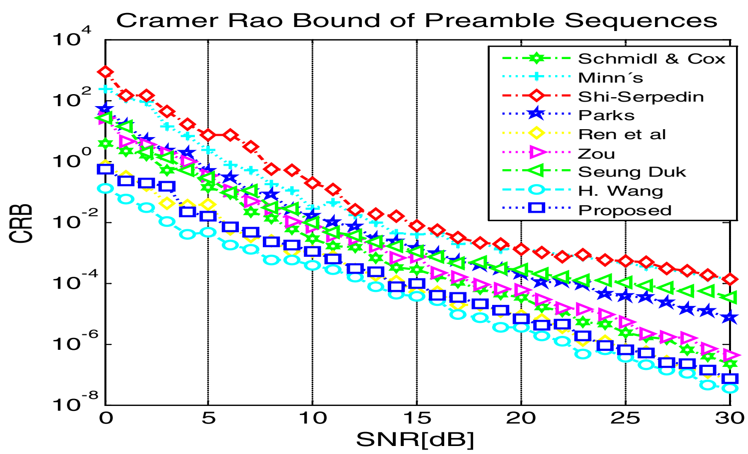

Figure 6.52. CRB of preamble sequences.

We evaluated each preamble with the Schmidl and Cox metric to obtain the Mean Square Error (MSE) and the Cramer Rao Bound (CRB) of each preamble, with a coarse timing offset equal to 10 samples, a normalized frequency offset $\hat{v} = 3.35$, and a length of N_c=64 and CP=16.

Incise (a) of the Figure 6.53 shows the SNR versus MSE of the timing offset, where is notable that, the proposed preamble has a smaller MSE, and is comparable to the weighted CAZAC sequence designed by H. Wang, the main difference is that its preamble is a short preamble and the proposed preambles is a long preamble. Taking a reduced number of samples in a period, the configuration of rotated conjugated versions of CAZAC sequence shows the much smaller MSE than others.

Figure 6.53b presents the SNR versus MSE of the frequency offset which was obtained of each evaluated preamble, where the frequency range estimation for a preamble of length N_c = 64 is -4.5π to 4.5π. In the Figure 6.53b is observable that our proposed preamble achieves the best value for MSE, this in comparison with the other metrics, and the response follows a similar way in comparison to the CRB expected.

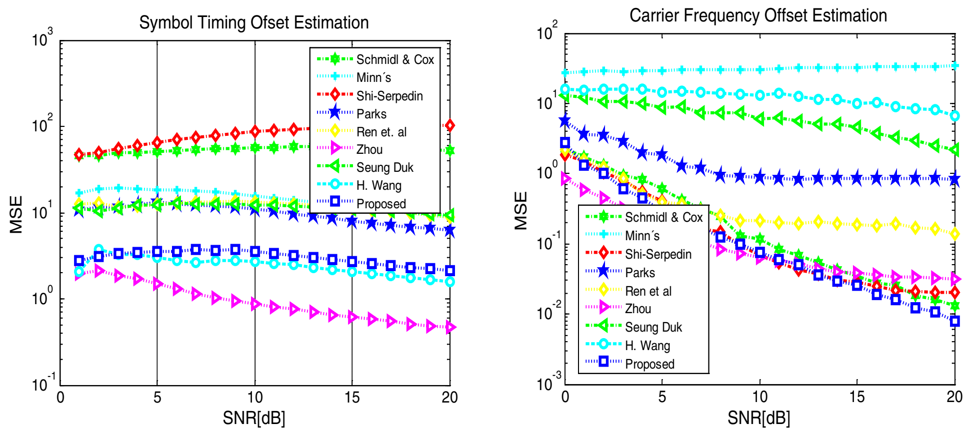

(a) (b)

Figure 6.53. (a) STO $\hat{\varepsilon} = 10$; (b) CFO Estimation $\hat{\nu} = 3.35$.

The obtained bit error rate (BER) of the transmitted data is plotted in Figure 6.54. The simulation shows similar responses between preambles due to the limitations offered by the timing metric, (channel estimation is not considered). The Figure 6.54 shows that the best BER response is achieved by the proposed preamble.

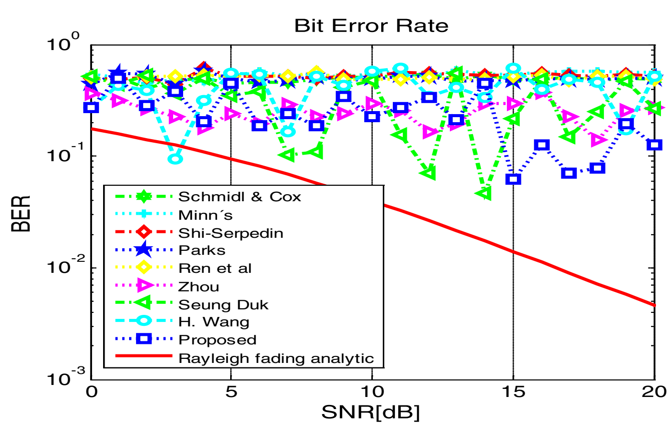

Figure 6.54. Bit Error Rate for a preamble of length N_c=64.

In order to evaluate the preambles with length N_c = 128, a coarse timing offset of 14 samples and a normalized frequency offset $\hat{\nu} = 1.25\pi$ has been simulated and the results are shown in Figure 6.55a, where the best estimated timing offset is obtained by the weighted metric proposed by H. Wang.

The frequency range estimation with the preamble of length N_c = 128 is available from -2.5π to 2.5π. Figure 6.55b shows the obtained MSE of the estimated frequency offset, where is notable that, the preamble proposed by Shi-Serpedin has the best response, and the MSE response of the proposed preamble is quite similar to Ren. et al., with a good frequency estimation, this in comparison with the others simulated methods.

The resulting BER for a preamble with length N_c =128 is given in Figure 6.56, where is observable the similar response between preambles of weighted metrics and their modified structures. The BER of each simulated preamble shows a remarkable difference in the way to estimate the timing offset and frequency offset, and it is not possible to estimate with good results in both estimations, which originates the necessity of more accurately metrics.

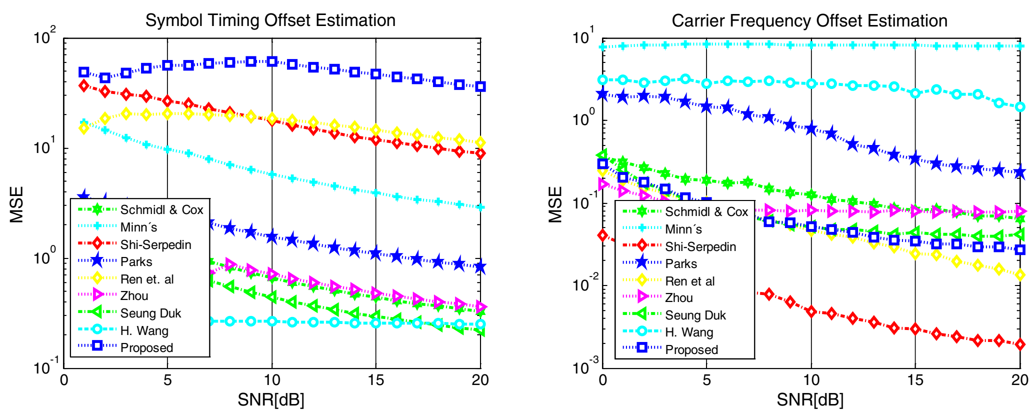

(a) (b)

Figure 6.55. (a) STO $\hat{\varepsilon} = 14$; (b) CFO Estimation $\hat{\nu} = 1.25$.

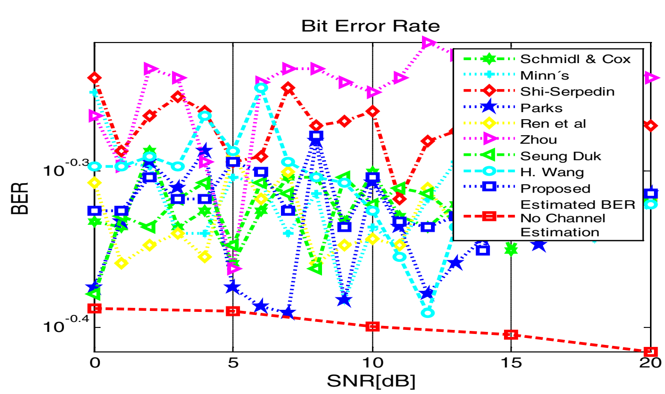

Figure 6.56. Bit Error Rate for a preamble of length N=128.

In the same way, when is increased the length of symbol to N_c = 256, a timing offset (TO) of 28 samples and a normalized carrier frequency offset (CFO) of $\hat{v} = 0.95\pi$ are applied, (with a estimation range of $-\pi$ to π). Figure 6.57a shows the obtained MSE of evaluated metrics. The metric of H. Wang achieves the best estimation, and the proposed preamble exhibits low precision.

Figure 6.57b shows the MSE for the frequency offset estimation, where the proposed metric exhibits the much smaller MSE in comparison with the other simulated metrics.

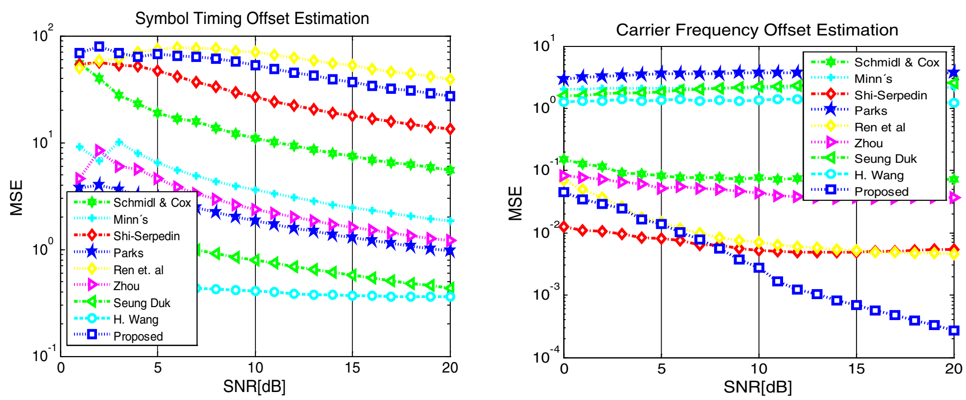

(a) (b)

Figure 6.57. (a) STO $\hat{\varepsilon} = 28$, (b) CFO Estimation $\hat{v} = 0.95$.

The BER analysis for preamble symbols of length N_c=256 is plotted in Figure 6.58, where is observable that, all the responses are quite similar to the estimation obtained with preambles of length N_c=128. However, it is expected a different response varying the length of the channel, timing and frequency offsets near to the limit range of estimation.

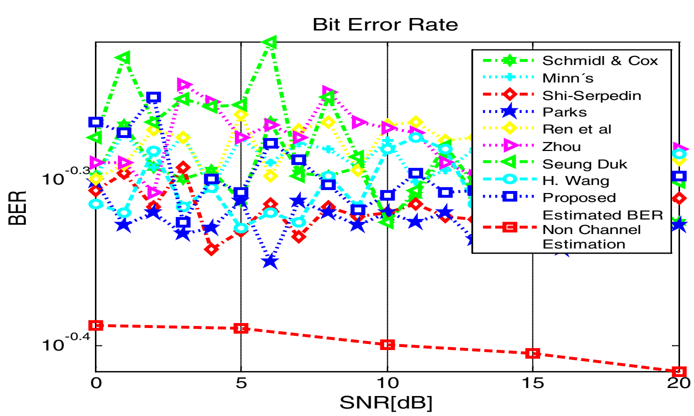

Figure 6.58. Bit Error Rate for a preamble of length N_c=256.

The MSE of the timing and frequency offset estimation for a symbol of length N_c=512 is shown in Figure. 6.59a and 6.59b, respectively, with a TO of 30 samples and a normalized frequency offset $\hat{v} = 0.49\pi$ (within a estimation range of -0.5π to 0.5π). The response of resulting MSE shows that, our preamble has better CFO estimation than timing offset estimation. The BER of simulated data is shows in Figure 6.60.

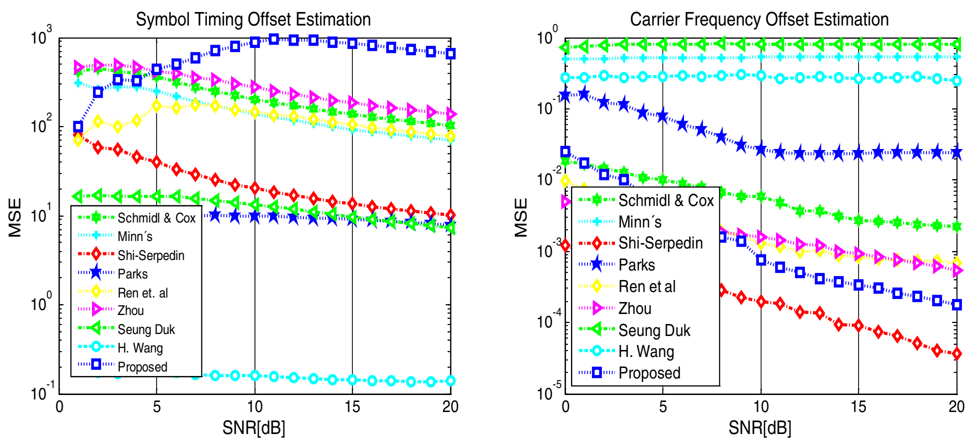

(a) (b)

Figure 6.59. (a) STO $\hat{\varepsilon} = 30$; (b) CFO Estimation $\hat{v} = 0.49$.

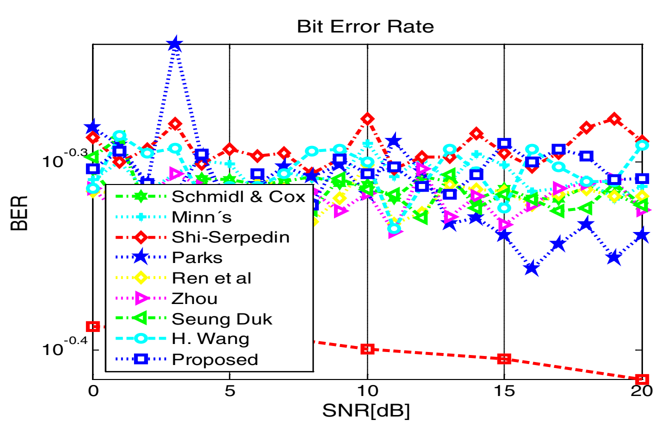

Figure 6.60. Bit Error Rate for a preamble of length N=512.

6.5 Synchronization of LTE systems

Synchronization of long-term evolution (LTE) systems is based on the Cell Search process, which is achieved with the aid of special designed sequences. A special contribution of this thesis is referred to the cell search process, which consist in a proposed normalized detection, where the objective is to get a more accurately primary synchronization signal. The sequences used in synchronization of LTE allows estimate the timing and frequency offset, and beside this, they are used to identify the mobile station (MS) or User Equipment (UE) with the base station (BS), and this process will be explained in the following section.

6.5.1 Cell search

LTE uses two OFDM based systems for its modulation channel access techniques. Orthogonal frequency division multiple access (OFDMA), which is used for the downlink transmission, and single carrier frequency division multiple access (SC-FDMA) or DFT-S-OFDMA, which is applied for the uplink, [22, 25].

The cell search procedure in LTE consists of a series of synchronization stages by which the UE determines time and frequency parameters, they are necessary to demodulate the downlink and transmit the uplink signals with the correct timing. It is also used for the acquisition of the receiver frequency of the downlink channels. Thus, the cell detection is linked to the primary synchronization (PSS), and the secondary synchronization (SSS).

The synchronization is a continuous and periodic process, which must be always active (i.e., not only when the equipment is powered on). It has to search and estimate the link quality with the neighboring cells, in order to be able of offering mobility to users.

A FDD frame is illustrated in Figure 6.61. Each slot contains 7 OFDMA symbols with short CP or 6 OFDMA symbols with long CPs. This slot partition is shown in Figure 6.62.

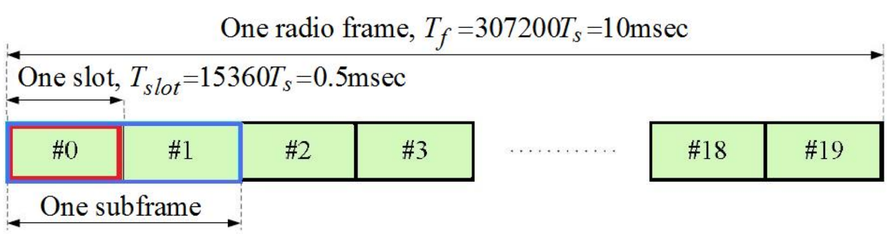

Figure 6.61. FDD Radio Frame.

The synchronization signals are transmitted periodically, twice per 10 ms radio frame. In a FDD cell the PSS is always located in the first and 11th slots of the last OFDMA symbol within the radio frame, [22-25, 28], thus enabling the UE to acquire the slot boundary timing independently of the CP length. The SSS is located in the symbol immediately preceding the PSS. This design enable coherent detection of the SSS relative to the PSS, which is based on the assumption that the channel coherence duration is significantly longer than one symbol, [23-25].

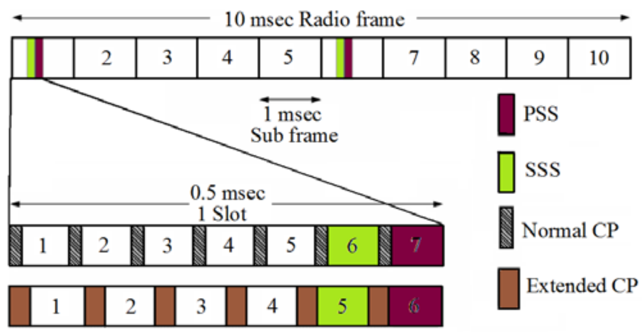

Figure 6.62. PSS and SSS signals located in a FDD Frame.

A total of four possible SSS positions must be checked if the UE is searching for both FDD and TDD cells. Symbol boundaries are first detected by a *correlator* that detects the peak correlation between the CP and its delayed replica in each OFDMA symbol, [23, 24].

In the frequency domain, the synchronization sequences occupy six blocks of resources (1 RB = 180 kHz), allowing an invariant allocation to band system (which can vary from 6 to 110 RBs). A resource block consists of 12 sub-carriers, which makes 72 sub-carriers for PSS. However, as the sequence length is 62 symbols both synchronization sequences are mapped into 62 subcarriers located symmetrically around the DC sub-carrier. A set of 10 sub-carriers are left unfilled, allowing a 64 FFT and a lower sampling frequency to be used for the synchronization process [23].

The PSS is used to detect the physical layer cell identity ($N_{ID}^{(2)}$ in the range 0-2), while detecting SSS sequence provides the cell identity group ($N_{ID}^{(1)}$ in the range 0-167) of three identities, which define 504 unique physical layer cell identities in LTE, [23, 24]. This means that the complete cell search procedure consists of two steps to identify the cell identity after the detection of synchronization sequences, applying the modulo 3 equation, defined by,

$$N_{ID}^{CELL} = 3N_{ID}^{(1)} + N_{ID}^{(2)}. \tag{6.14}$$

6.5.2 Primary Synchronization

The PSS is chosen from a class of the polyphase Zadoff-Chu (ZC) sequences [37], which satisfy constant amplitude zero *auto-correlation* (CAZAC) property. These baseband sequences are complex signals defined as,

$$ZC_u^{N_{ZC}} = e^{-j\frac{\pi un(n+1)}{N_{ZC}}}, \quad n = 0,1,2....,N_{ZC} - 1 \tag{6.15}$$

where u is the ZC root index relatively prime to N_{ZC},

N_{ZC} = 63 and u is selected from {25, 29, 34} values.

This set of roots for the ZC sequences has been selected to obtain good periodic *auto-correlation* and *cross-correlation* properties. In particular, these sequences have a low sensitivity to Doppler frequency-offset, defined as the ratio of the maximum undesired auto-correlation peak in the time domain to the desired correlation peak computed at a certain frequency offset. This characteristic allows a certain robustness of the PSS detection during the initial synchronization. The three values of $N_{ID}^{(2)}$ = 0, 1, 2 are represented by the PSS with three different ZC root indices u = 25, 29, 34 (see Figure 6.63), respectively.

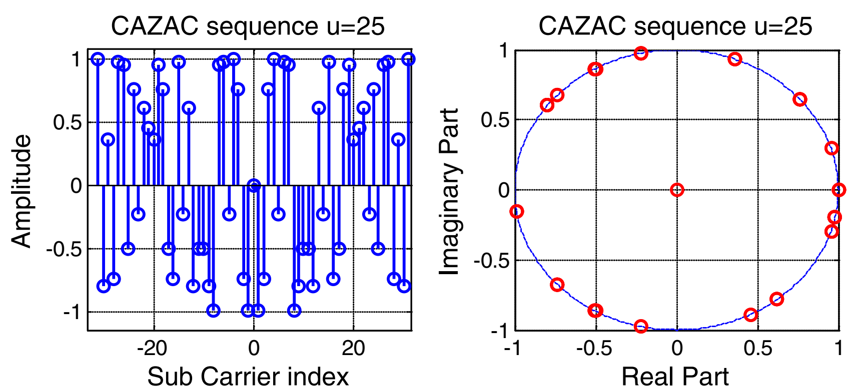

Figure 6.63. CAZAC sequence root u = 25.

Considering the transmission of the system, PSS sequences are converted from the frequency domain to the time domain by a discrete Fourier transform (DFT). The transmission over a multipath propagation channel with additive white Gaussian noise (AWGN) introduces a carrier frequency offset (CFO) due to differential velocity between platforms and frequency misalignment between transmitter and receiver oscillators. As a result, the received signal becomes, [14, 22, 70],

$$y(n) = [x(n) \otimes h(n) + w(n)]e^{-j2\pi\Delta f_n T_s}, \qquad (6.16)$$

where $x(n)$ is the transmitted signal,

$h(n)$ represents the time-varying multi-path *fading* channel,

$w(n)$ is Additive White Gaussian Noise (AWGN),

Δf_n is the carrier frequency offset,

T_s is the sampling clock period.

The algorithms for the carrier frequency were tested for frequency offsets of Δf = 0.01, and for the multipath ITU pedestrian A and ITU vehicular A channels [22, 28].

From a user equipment (UE) point of view, the selected root combination satisfies time domain root symmetry, knowing that the sequences 29 and 34 are complex conjugates of each other and can be detected with a single *correlator*, (Figure 6.64), thus allowing some complexity reduction. The UE must detect the PSS without any a-priori knowledge of the channel, so that a non-coherent correlation is required for PSS timing detection. A maximum likelihood detector defined by [25, 70, 71],

$$m_u^* = \arg\max_u \left| \sum_{i=0}^{N-1} Y\left[i+m\right] S_u^*\left[i\right] \right|^2, \qquad (6.17)$$

where *i* is the time index, *m* is the timing offset, *N* is the PSS time-domain signal length, $Y[i]$ is the received signal at time instant *i* and $S_u[i]$ is the PSS with root *u* replica signal at time *i*.

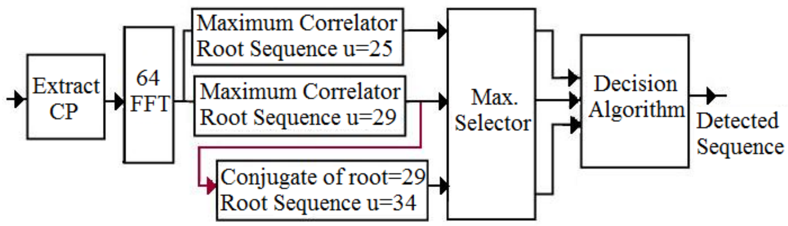

Figure 6.64. Maximum likelihood detector.

The results obtained in the detector define the selected root each 5 ms, when the emitted sequence is the root u = 25, and the received signals are affected by AWGN, a *multipath* propagation channel and frequency offset. Then the detector receives the sequences that are shown in Figure 6.65.

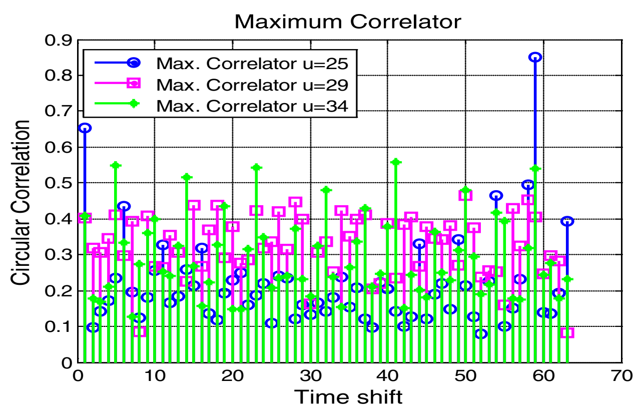

Figure 6.65. Detected signal with *multipath* channel and frequency offset.

6.5.3 Proposed Normalized Detection

In order to avoid the confused detection of the peak sequence, we proposed a normalized detection, once obtained the corresponding root of the received signal, by using the following equation,

$$\text{Normalized detection} = \frac{m_u^*}{\frac{1}{N}\sum_{i=0}^{N-1} S[i-m]Y[i]}, \tag{6.18}$$

where the denominator of equation 6.18 is the linear cross-correlation, of the replica signal $S[i]$ with the maximum peak detected and the received signal $Y[i]$. The application of this normalization is shown in the Figure 6.66.

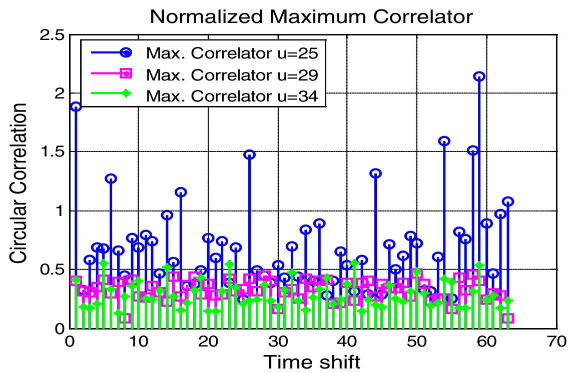

Figure 6.66. Normalized detection of the root.

6.5.4 Secondary Synchronization

After the UE has found the 5 ms timing, the second step is to obtain the radio frame timing and the cells' group identity. This information can be found from the SSS. The process starts with the generating a basic pseudo noise sequence from which the two sequences are produced. The two sequences are scrambled with $N_{ID}^{(2)}$ and $N_{ID}^{(1)}$ related parameters. After that, the sequences are interleaved into a 62-length sequence, which represents the SSS sequence. The combination of the two length-31 sequences defining the SSS, differs between slot 0 and slot 10. Figure 6.67 illustrates a graphical representation of the described process.

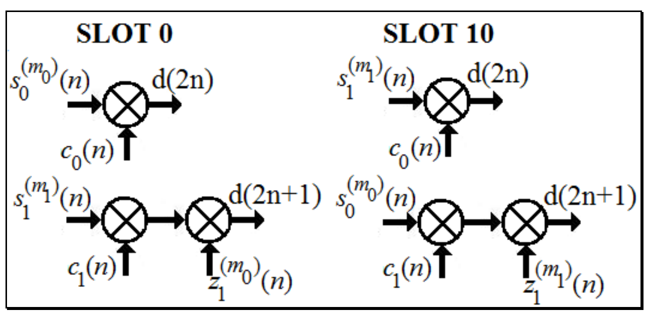

Figure 6.67. Slot 0 and 10 of the transmitted frame.

The even-numbered *d(2n)* and odd-numbered *d(2n + 1)* sequence samples are given in the equations (6.19) and (6.20), [23]:

$$d(2n) = \begin{cases} s_0^{(m_0)}(n)c_0(n) & \text{in slot 0} \\ s_1^{(m_1)}(n)c_0(n) & \text{in slot 10} \end{cases}, \tag{6.19}$$

$$d\left(2n+1\right)=\begin{cases} s_1^{(m_1)}(n)c_1(n)z_1^{(m_0)}(n) & \text{in slot 0} \\ s_0^{(m_0)}(n)c_1(n)z_1^{(m_1)}(n) & \text{in slot 10} \end{cases}. \tag{6.20}$$

The indices m_0 and m_1 are derived from the physical layer cell group $N_{ID}^{(1)}$ according to equation 6.21a and 6.21b, [23], Figure 6.68.

$$m_0 = m' \bmod 31 \tag{6.21a}$$

$$m_1 = (m_0 + \lfloor m'/31 \rfloor + 1) \bmod 31 \tag{6.21b}$$

$$m' = N_{ID}^{(1)} + q(q+1)/2,$$

$$q = \left\lfloor \frac{N_{ID}^{(1)} + q'(q'+1)/2}{30} \right\rfloor,$$

$$q' = \lfloor N_{ID}^{(1)} / 30 \rfloor$$

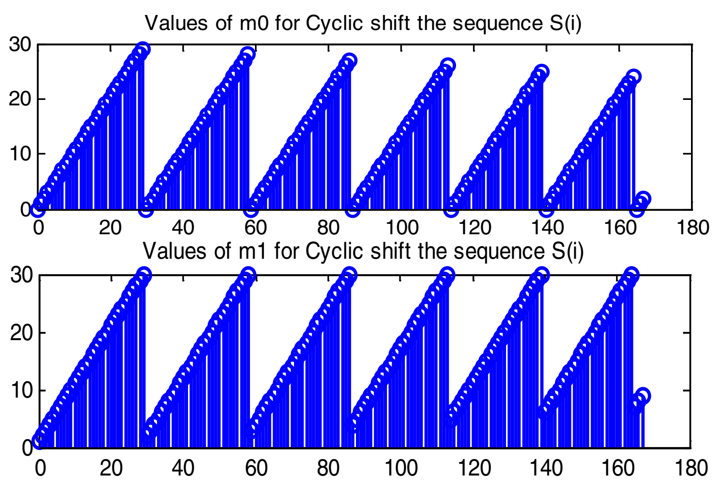

Figure 6.68. Indices m_0 and m_1.

The sequences $s_0^{(m_0)}$ and $s_1^{(m_1)}$ are defined as two different cyclic shifts of the pseudo noise sequence $\tilde{s}(i)$, where $\tilde{s}(i) = 1 - 2x(i), 0 \le i \le 30$ with $x(i)$ given as:

$$x(j+5) = (x(j+2) + x(j)) \bmod 2, \qquad 0 \le j \le 25, \tag{6.22}$$

with initial conditions $x(0) = 0$, $x(1) = 0$, $x(2) = 0$, $x(3) = 0$, $x(4) = 1$. The expression $(1-2x(i))$ converts binary 0 and 1 in $x(i)$ to +1 and −1 respectively.

The next step consists in scrambling two *pseudo noise* sequences with two physical layer cell identity $N_{ID}^{(2)}$ related sequences, called c_0 and c_1. The two sequences are produced by cyclic shifts of another basic $\tilde{c}(i)$ pseudo noise sequence.

$$\begin{cases} c_0(n) = c((n + N_{ID}^2) \bmod 31) \\ c_1(n) = c((n + N_{ID}^2 + 3) \bmod 31) \end{cases} ;c \in \{-1,1\}. \qquad (6.23)$$

The two length-31 scrambling sequences $z_1^{(m_0)}(n)$ and $z_1^{(m_1)}(n)$ are defined by a cyclic shift of the *pseudo noise* sequence $z(i)$ like $s(n)$ or $c(n)$.

The simulation of the sequences even-numbered *d(2n)* and odd-numbered *d(2n + 1)* for the slot 0 are shown in the Figure 6.69. These sequences are interleaved and mapped around the DC-carrier, forming the SSS.

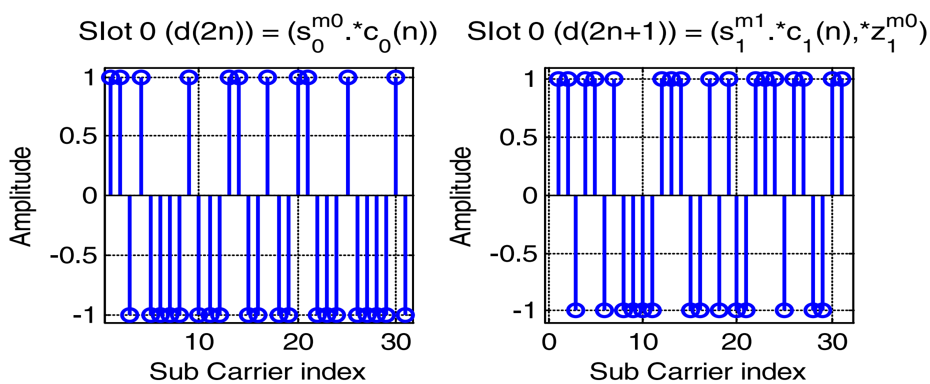

Figure 6.69. Sequences d(2n) and d(2n+1) for the slot 0.

The SSS detection is done after the PSS detection, and the channel can therefore be assumed to be known (i.e., estimation based on the detected PSS sequence). For SSS sequence detection, coherent or non-coherent techniques can be used. From a conceptual point of view, a coherent detector takes advantage of knowledge of the channel, while a non-coherent detector uses an optimization metric corresponding to the average channel statistics, [23- 25].

The sequence decoder block for the SSS in the receiver contains the following blocks:

- *De-interleaving*
- *De-scrambling*
- *Extraction* process.

The position of the sequences on the arriving frame is unknown. Where only exists the knowledge that the first symbol is always scrambled using the *C_0* sequence. Taking in consideration the known $N_{ID}^{(2)}$ obtained in the PSS detection, the process of detection of the $N_{ID}^{(1)}$ is determined in [23, 72, 73], (Figure. 6.70).

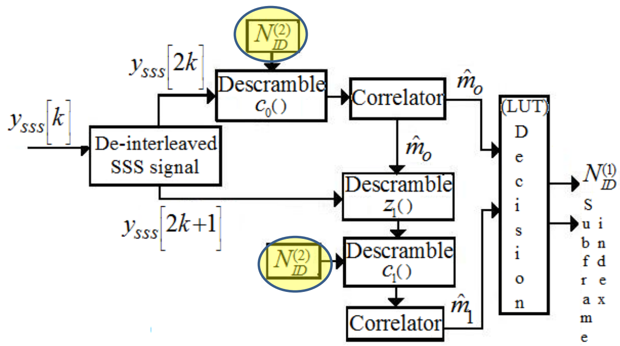

Figure 6.70. Block diagram of the SSS detector.

The received sampled signals are de-interleaved as is shown in Figure 6.71, where $y_{sss}(2k)$ is used to descramble the index m_0 by using the scrambling sequence c_0, as is illustrated in Figure 6.72. The scrambling and descrambling are done by multiplication, because all used sequences have values in the {-1, +1} space domain, [33],

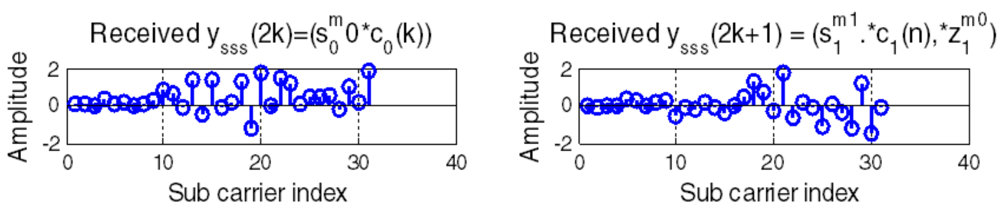

Figure 6.71. Received de-interleaved SSS signals.

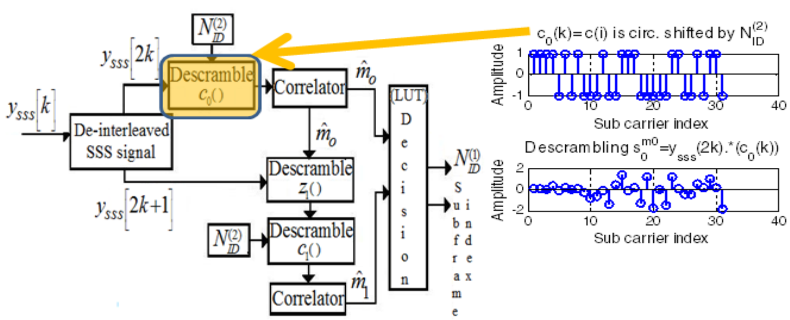

Figure 6.72. Descrambled $c_0(\cdot)$.

The received descrambled sequence *s(n)* is shifted with an unknown quantity named *m*. This value is applied to a circular correlation of the *correlator* in the SSS detector, [73, 74], defined by,

$$\text{Circ. corr }(k) = \frac{1}{M}\sum_{k=0}^{M-1} s(n) * s((n+m-k) \bmod M), \tag{6.24}$$

This circular correlation has its maximum at the zero lag, which means that if the position of the maximum can be determined at the zero lag, the shifted quantity *m* can be obtained correctly. Taking that in consideration, it is possible to detect the index m_0, by applying the correct shifted index of the circular correlation, until the maximum peak at the zero lag is detected, Figure 6.73.

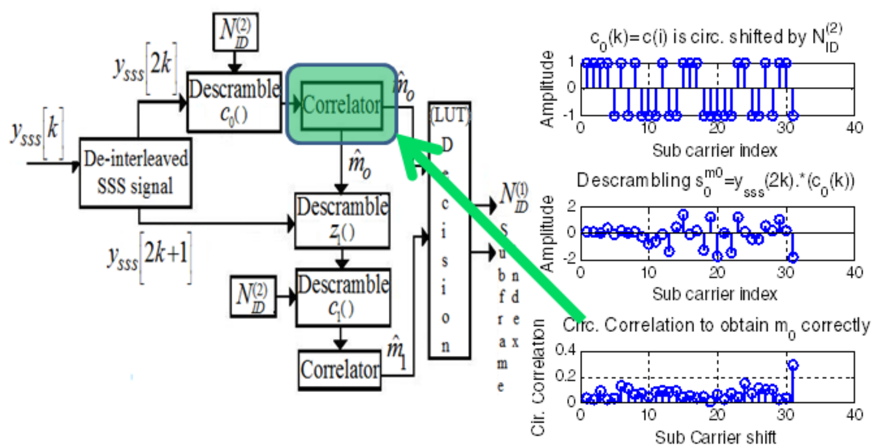

Figure 6.73. Circular Correlator to obtain m_0.

Once detected the index m_0, the next step is descramble the sequence z_1 by applying the index m_0 to the received sequence $y_{sss}(2k+1)$, which is plotted in Figure 6.74. The sequence z_1 is applied with the index $N_{ID}^{(2)}$ to descramble the sequence c_1, as is observable in Figure 6.75, and by means of circular correlation is obtained the index m_1, as is shown in Figure 6.76, which are necessary to determine the value of $N_{ID}^{(1)}$. The complete cell search procedure is achieved once the parameters $N_{ID}^{(2)}$ and $N_{ID}^{(1)}$ were obtained and then is applied the equation 6.14 in the UE to access the cell in an enodeB.

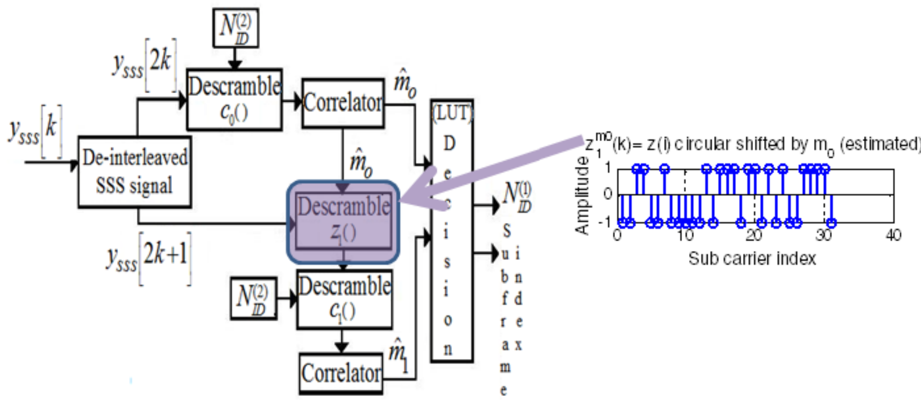

Figure 6.74. Descrambled $z_1(\cdot)$.

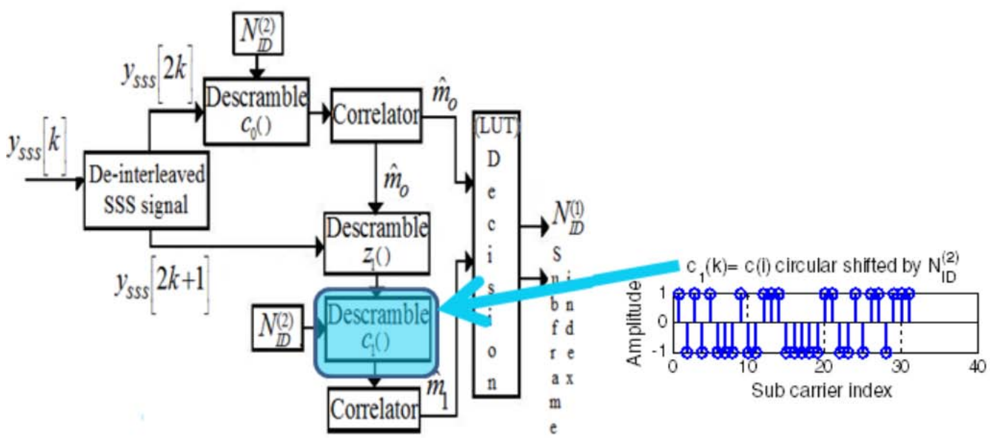

Figure 6.75. Descrambled $c_1(\cdot)$.

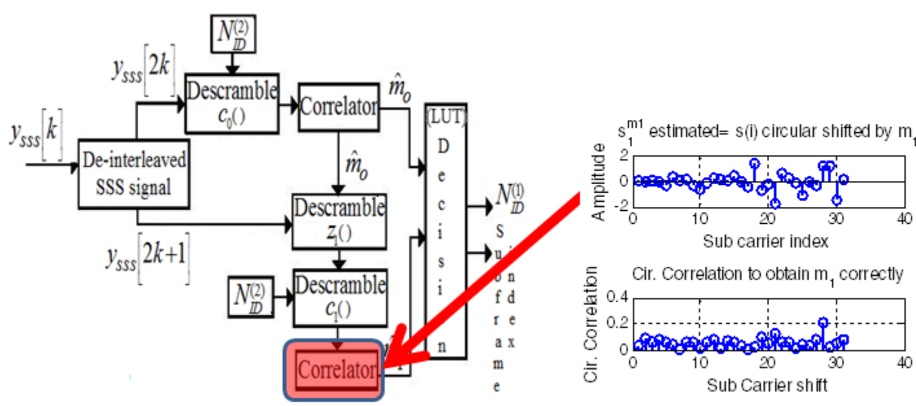

Figure 6.76. Circular Correlation to obtain m_1.

Chapter 7

CONCLUSIONS AND FUTURE WORK

7.1 Conclusions

The main results of this thesis are contributions to solve efficiently timing and frequency synchronization problems of OFDM based systems. In order to present new methods, we have simulated existing timing metric methods for synchronization. The analysis of advantages and disadvantages of such synchronization methods allows the definition of our objective, by means of modeling a modified preamble and its corresponding timing metric, to improve the existing methods used to solve the problem of synchronization.

To reach this goal, we proposed a preamble weighted by a Golay sequence. The idea is based on the weighted CAZAC sequences, which was presented by Ren et al. In propose preamble we make use of the properties of a Golay sequence instead of a pseudo noise sequence. The structure of the preamble can be designed in a short preamble and a long preamble. A properly designed timing metric algorithm was designed for each proposed preamble.

The proposed method is based on the Golay sequence used to scramble the CAZAC sequence in the transmitter. Similarly at the receiver is used a CAZAC sequence to descramble the received signal, and consequently, to define the jointly time and frequency synchronization.

The performance of the reviewed and proposed timing metrics was evaluated by means of the Mean Square Error (MSE) and the bit error rate (BER) of the data. The comparative results of simulation for each preamble and its corresponding timing metric, demonstrated improved results of the proposed designs, which were corroborated by simulation in MATLAB.

The limit of frequency estimation for the analyzed and proposed preambles is defined by means of the Cramer-Rao Bound, where the preambles were evaluated by using the Schmidl

& Cox Metric. The obtained results demonstrated a better frequency estimation of proposed preamble in comparison with the existing ones.

Finally, the important problem of improve the detection of the Primary Synchronization Signal for the LTE systems has been investigated. We propose the method to improve the detection by applying a normalized detection, where its performance was evaluated by simulation in MATLAB. Additionally the complete process of cell search for LTE system was simulated, where is explained the direct relation between the Primary and Secondary Synchronization signals.

7.2 Future work

Future work in this field can be related with the multiple requirements of OFDM systems, such as:

Channel Estimation: The orthogonality allows each subcarrier component of the received signal to be expressed as the product of the transmitted signal and channel frequency response at the subcarrier. Thus, the transmitted signal can be recovered by estimating the channel response just at each subcarrier. In general, the channel can be estimated by using a preamble or pilot symbols known to both transmitter and receiver.

Multiple Input Multiple Output (MIMO) Channel: When a wireless channel with high channel capacity is given, it is necessary to find a good technique to achieve high - speed data transmission and or high reliability. By using multiple antennas is possible to improve the transmission reliability. However, antenna diversity require a good channel estimation and synchronization in the receiver.

Random Access: The OFDMA system is ideally orthogonal when the user signals are perfectly time/frequency synchronized. However, any small synchronization error causes inter-user interference and results in a loss of the performance. Therefore, the terminals should be pre-synchronized to keep the interference below an acceptable level. The goal of the random access procedure is to synchronize the transmissions of the different terminals in the time (the remaining asynchronism must be included in the cyclic prefix).

Appendix A

Simulations in Matlab

Program for simulate Proposed preamble

```
function [xE,Ps,Qs]=PreambleE(L,N,Ng)
LE=N/2;
%% Golay Shapiro Rudin Sequence
        LG=N;
        SQ=LG-1;
        Nbits=12;
        x1=0:1:SQ;
        x1=x1.';
        for indy=1:SQ+1
            rt=x1(indy);
            y(indy,:) = dec2bin(rt,Nbits);
        end
        [m n]=size(y);

        for ii=1:m
            sq=y(ii,:);
            for ini=1:n
                a(ii,ini)=str2num(sq(1,ini));
            end
        end
        for indy=1:m
            a1=a(indy,:);
            for i=1:length(a1)-1
                b(i)=a1(i)*a1(i+1);
                c=sum(b);
                d(indy)=(-1)^c;
            end
        end
        Ps=d(1:LE);                              %P(k)
        Qs=d(LE+1:N);                            %Q(k) Complementary pair

%% PN Sequence
    p1=[1 1 0 1 1 1];                    % x^5+x^4+x^2+x^1+1        LSFR
    p1init=[1 0 0 0 0];                  % 1 for n=0     initial conditions
%     pnb = seqgen.pn('GenPoly',p1,'InitialStates',p1init);     % with initial conditions
```

```
   pnb = seqgen.pn('GenPoly',p1);
   set(pnb, 'NumBitsOut',LE);  %0<=j<=25
   pnb= generate(pnb);
   seqm1=pnb.';
   si_hat=1-2*(seqm1);                  %  value 0 to 1 and value 1 to -1 of PN sequence
    Ask=upsample(si_hat,2);               %% symmetric PN sequence in a period [sk sk+N/2]]
% Ask=[si_hat si_hat];
   sE1=Ask(1:N/2);
   sE2=Ask((N/2)+1:N);
%% CAZAC Sequence
   M=1;                              %M=root of cazac sequence
   if gcd(M,LE)==1                      %greatest common divisor
      rr=(0:LE-1).*(0:LE-1)/2;
      prb0=exp(j*2*pi*1.00*rr/LE);
   end
   A=prb0;
   Ad1a=upsample(A,2);                  %% symmetric CAZAC sequence [xk xk+n/2]
   Ad1=Ad1a.*Ask;

%%  Proposed preamble
% prb02=prb0;          %with CP on the designed preamble
prb02=prb0.*Ps;        %without CP on the designed preamble
CZac=upsample(prb02,2);
% CZac=[prb02 prb02];

Ada=CZac(1:LE).*Ps;            %CAZAC*Ps
Adb=CZac(LE+1:N).*Qs;           %CAZAC*Qs
CazacGRS=[Ada Adb];        %Proposed Preamble symbol ([CAZAC*GRS
CAZAC*COMPLEMENTARY GRS pair]

 %%  FFT of sequences   PROPOSED PREAMBLE
xe=(fft((CazacGRS)));
xE=[xe(N-Ng+1:N) xe];                                     %add CP to the designed preamble
```

PUBLICATIONS DERIVED OF THE THESIS

Eric M. Silva C., fredric j. harris, G. Jovanovic Dolecek, "Synchronization Algorithms based on Weighted CAZAC Preambles for OFDM Systems," The 13th International Symposium on Communications and Information Technologies (ISCIT 2013), Samui Island, Thailand, 4-6 September 2013.

Eric M. Silva C., fredric j. harris, G. Jovanovic Dolecek, "On Preamble Design for Timing and Frequency Synchronization of OFDM Systems over Rayleigh Fading Channels," 18th International Conference on Digital Signal Processing, Santorini , Greece, 1-3 July 2013.

Eric M. Silva C., fredric j. harris, G. Jovanovic Dolecek, "A Novel Preamble and Synchronization Algorithm based on a weighted CAZAC- Golay Rudin Shapiro Sequence for OFDM Systems," CONCAPAN XXXII, Nicaragua 2012.

Silva C, E.M., Dolecek, G.J., Harris, F.J, "Cell Search in Long Term Evolution Systems: Primary and Secondary Synchronization", IEEE Third Latin American Symposium on Circuits and Systems (LASCAS 2012) , Playa del Carmen, Quintana Roo, pp. 1- 4, Feb. 29 - March 2 2012.

Silva C. E. M. and Jovanovic. D. G., "Design and Simulation of QPSK Reconfigurable Digital Receiver", 53rd Symp. IEEE MWSCAS 2010, Seattle, Washington, pp. 656 – 659, Aug. 1-4, 2010.

Silva C. E. M., Jovanovic D. G., "Características del Sistema OFDM con Bancos de Filtros, Implementación Polifásica y Filtros Prototipo", XI Encuentro de Investigacion INAOE, Nov.2010.

Silva C. E. M., Jovanovic D. G., "Un Método de Sincronización en OFDM Mediante la Estimación Conjunta de la Sincronía del Símbolo y la Frecuencia", X Encuentro de Investigación, INAOE, Puebla, México, pp. 147-151, Nov. 4-5, 2009.

LIST OF FIGURES AND TABLES

BIBLIOGRAPHY

[1] H. F. Harmuth., "On the transmission of information by orthogonal time functions". AIEE Transactions I:248–255, 1960.

[2] Chang, R.W., ‘‘Synthesis of band-limited orthogonal signals for multichannel data transmission,’’ Bell Syst. Tech. J, vol. 45, pp. 1775–1796, December 1966.

[3] Chang, R. W., ‘‘A theoretical study of performance of an orthogonal multiplexing data transmission scheme,’’ IEEE Trans. Comm. Technol., vol. 16, pp. 529–539, August 1967.

[4] Chang, R. W., ‘‘Orthogonal frequency division multiplexing,’’ U.S. Patent 3,488,445, filed November 14, 1966, issued January 6, 1970.

[5] Saltzberg, B. R., ‘‘Performance of an efficient parallel data transmission system,’’ IEEE Trans. Comm. Technol., vol. 15, December 1967.

[6] Zimmerman, M. S., and A. L. Kirsch, ‘‘The ANIGSC-10 (KATHRYN) variable rate data modem for HF radio,’’ IEEE Trans. Comm. Technol., vol. 15, pp. 197–205, April 1967.

[7] Weinstein, S. B., and P. W. Ebert, ‘‘Data transmission by frequency division multiplexing using the discrete Fourier transform,’’ IEEE Trans. Comm. Technol., vol. 19, no. 5, October 1971.

[8] Hirosaki, B.,‘‘An orthogonally multiplexed QAM system using the discrete Fourier transform,’’ IEEE Trans. Commun., vol. 29, pp. 982–989, July 1981.

[9] Hirosaki, B., S. Hasegawa, and A. Sabato, ‘‘Advanced group band data modem using orthogonally multiplexed QAM technique,’’ IEEE Trans. Commun., vol. 34. no. 6, pp. 587–592, June 1986.

[10] Hirosaki, B., et al., ‘‘A 19.2 kbits voiceband data modem based on orthogonally multiplexed QAM techniques,’’ Proc. of MEE ICCTS, pp. 21.1.1–5, 1985.

[11] Van Nee R. Ramjee P., "OFDM for Wireless Multimedia Communications", Artech House, 2000.

[12] Engels M. (Editor), "Wireless OFDM Systems: How to Make Them Work?," Springer, 1st edition, July 31, 2002.

[13] Xiong F., "Digital Modulation Techniques," Artech House, 2nd Edition, 2006.

[14] Chiueh Tzi-D., Pei-Y. Tsai, "OFDM *Baseband* Receiver Design for Wireless Communications," Wiley, 1st Edition, Dec. 2007.

[15] Ye Geoffrey Li, Orthogonal Frequency Division Multiplexing for Wireless Communications, 1st Edition, 2006.

[16] Kalivas G., “Digital Radio System Design,” John Wiley & Sons Ltd, 1st Edition, 2009.

[17] Hui L., L. Guonqing, “OFDM Based Broadband Wireless Networks: Design and Optimization,” John Wiley & Sons, 2005.

[18] Ahmad R. S., B. R. Saltzberg, M. Ergen, “Multi-Carrier Digital Communications Theory and Applications of OFDM,” Springer Science + Business Media, Inc., 2004.

[19] Shinsuke H., R. Prasad., “Multicarrier techniques for 4G mobile communications,“ Artech House, 2003.

[20] Ke-Lin D., M. N. S. Swamy, “Wireless Communication Systems: From RF Subsystems to 4G Enabling Technologies,” Cambridge University Press, 2010.

[21] Ibnkahla M. (Editor), “Signal Processing for Mobile communications: Handbook,” CRC Press, 2005.

[22] Cho Y. S., J. Kim, W. Y. Yang, C. G. Kang, “MIMO-OFDM Wireless Communications with MATLAB”, John Wiley & Sons (Asia), Singapore, 2010.

[23] Khan F., “LTE for 4G Mobile Broadband, Air Interface Technologies and Performance,” Cambridge University Press, 2009.

[24] Korowajczuk L., “LTE, WIMAX and WLAN Network Design, Optimization and Performance Analysis,” John Wiley & Sons, 2011.

[25] Sesia S., I. Toufik, M. Baker, “LTE–The UMTS Long Term Evolution: From Theory to Practice,” John Wiley & Sons, 2nd Edition, 2011.

[26] Horlin F., A. Bourdoux “Digital Compensation for Analog Front-Ends: A New Approach to Wireless Transceiver Design,” John Wiley & Sons, 2008.

[27] Andrews J. G., Ghosh a., Muhamed R., “Fundamentals of WiMAX: Understanding Broadband Wireless Networking,” Prentice Hall, 2007.

[28] H. G. Myung, D. J. Goodman, “Single Carrier FDMA – a new air interface for long term evolution,” John Wiley and Sons, 2008.

[29] fred harris, Chris Dick, OFDM Modulation Using Square-Root Nyquist Time Domain Kernels to Obtain Reduced Peak-to-Average Power Ratio, Proceeding of the SDR 08 Technical Conference and Product Exposition. Copyright ©, 2008 SDR Forum.

[30] M. Speth, S. A. Fechtel, H. Meyr, “Optimum Receiver Design for Wireless Broad-Band Systems Using OFDM - Part I”, IEEE Transactions on Communications, vol. 47, no. 11, pp. 1668-1677, November 1999.

[31] Perez F., P. Mariño Espiñeira, “Modeling the Wireless Propagation Channel: A Simulation Approach with Matlab,” Wiley, 2008.

[32] Golomb S. W., G. Gong, “Signal Design for Good Correlation: For Wireless Communication, Cryptography, and Radar,” Cambridge University Press, 2005.

[33] Lee B. G., B. H. Kim, “Scrambling Techniques for CDMA Communications,” Kluwer Academic Publishers, 2002.

[34] Rgheff M. A. A, “Introduction to CDMA Wireless Communications,” Published by Elsevier, 2007.

[35] Mitra A., “On Pseudo–Random and Orthogonal Binary Spreading Sequences,” International Journal of Information Technology, vol. 4, No. 2. pp. 447- 454, 2007.

[36] Helleseth T., P. V. Kumar, “Mobile Communications Handbook: Pseudonoise Sequences,” CRC Press LLC, 1999.

[37] Frank R. L., S. A. Zadoff, “Phase Shifts Pulse Codes with Good Periodic Correlation Properties,” IRE Trans. Inform. Theory, pp. 381-382, Oct. 1962.

[38] Krouk E., S. Semenov (Editors), “Modulation and Coding Techniques in Wireless Communications,” John Wiley & Sons, 2011.

[39] Schmidl T., D. Cox, "Robust Frequency and Timing Synchronization for OFDM," IEEE Trans. Commun., vol. 45, no. 12, pp. 1613-1621, Dec. 1997.

[40] Minn M. H., V. K. Bhargava, and K. K. B. Letaief, "A Robust Timing and Frequency Synchronization for OFDM systems," IEEE Trans. Wireless Commun., vol. 2, no. 4, pp. 822-839, July 2003.

[41] Park B., H. Cheon, C. Kang, and D. Hong, "A Novel Timing Estimation Method for OFDM Systems," IEEE Communications Letter, vol. 7, no. 5, pp. 239-241, May. 2003.

[42] Ren G., Y. Chang. H. Zhang, H. Zhang, “Synchronization Method Based on a New Constant Envelop Preamble for OFDM Systems,” IEEE Transactions on Broadcasting, 10 April 2003, vol. 51, No. 1, pp. 139 – 143, March 2005.

[43] Benvenuto N., G. Cherubini, “Algorithms for Communications Systems and Their Applications,” John Wiley & Sons, 2002.

[44] Proakis J. G, M. Salehi, “Digital Communications,” McGraw-Hill, 5th Edition, 2008.

[45] Benedetto J. J., I. Konstantinidis, M. Rangaswamy, “Phase- Coded Waveform and Their Design: The role of the ambiguity function”, IEEE Signal Processing Magazine, vol. 26, pp. 22 – 31, Jan. 2009.

[46] Golay M. J. E., “Complementary Series,” IRE. Trans. Inform. Theory, vol. IT-7, pp. 82–87, Apr. 1961.

[47] R1-99-0205, “New RACH Preambles with Low Auto-Correlation Side-lobes and Reduced Detector Complexity”, Ericsson, pp. 22- 26, http://www.3gpp.org/, March, 1999.

[48] Shapiro H. S., “Extremal Problems for Polynomials”, M.Sc.Thesis, M.I.T., 1951.

[49] Rudin W., “Some Theorems on Fourier Coefficients,” Proceedings of the American Mathematical Society, vol. 10, pp. 855–859, 1959.

[50] Benke G., “Generalized Rudin-Shapiro Systems,” J. Fourier Anal. Appl., vol. 1, No. 1, pp. 87–101, 1994.

[51] Brillhart J., P.Morton, "A Case Study in Mathematical Research: The Golay-Rudin-Shapiro Sequence," American Mathematical Monthly, vol. 103, Part 10, pp 854-869, 1996.

[52] Benedetto J. J. and J. D. S. Moore, “Geometric Properties of Shapiro–Rudin Polynomials”, Involve, Mathematical Sciences Publishers, vol. 2, No. 4, pp. 451-470, , 2009.

[53] Cour-Harbo A. la, “The symmetric Rudin-Shapiro Transform - an Easy, Stable, and Fast Construction of Multiple Orthogonal Spread Spectrum Signals,” IEEE International Conference on Acoustics, Speech, and Signal Processing. (ICASSP '03)., vol. 6. pp. 397-400, 6-10 April 2003.

[54] Sandell, M., J. J. van de Beek, and P. Börjesson, ‘‘Timing and frequency synchronization inOFDM systems using cyclic prefix,’’ Proc. Int. Symp. Synchronization, Saalbau, Essen, Germany, pp. 16–19, December 14–15, 1995.

[55] S. H. Muller-Weinfurtner, ‘On the optimality of metric for coarse frame synchronization in OFDM: A comparison’, in Proc. IEEE Int. Symp. on Personal, Indoor, and Mobile Radio Communications, Boston, MA, pp. 533–537, Sep. 1998.

[56] Taura, K., Tsujishta, M., Takeda, M. et al. “A digital audio broadcasting(DAB) receiver”. IEEE Trans. Consumer Electronics, 42(3), 322–326, 1996.

[57] Daffara, F., and O. Adami, ‘‘A new frequency detector for orthogonal multicarrier transmission techniques,’’ Proc. IEEE Vehicular Technology Conf. (VTC’95), Chicago, Illinois, pp. 804–809, July 15–28, 1995.

[58] Moose, P.H., “A technique for orthogonal frequency division multiplexing frequency offset correction”. IEEE Trans. Commun., 42, 2908–2914, 1994.

[59] Classen, F. and Myer, H., “Frequency synchronization algorithm for OFDM systems suitable for communication over frequency selective fading channels”. IEEE VTC’94, pp. 1655–1659, June 1994.

[60] Toutier, P., R. Monnier, and P. Lopez, ‘‘Multicarrier modem for HDTV terrestrial broadcasting,’’ Signal Processing: Image Communication, vol. 5, no. 5–6, pp. 379–403, December 1993.

[61] Van de Beek, et al., ‘‘Low complex frame synchronization in OFDM systems,’’ Proc. Int. Conf. Universal Personal Commun. (ICUPC), pp. 982–986, November 6–10, 1995.

[62] Van de Beek, J.-J., M. Sandell, and P. Börjesson, ‘‘ML estimation of time and frequency offset in OFDM systems,’’ IEEE Trans. Signal Processing, vol. 45, no. 7, pp. 1800–1805, July 1997.

[63] Shi, K., and E. Serpedin, ‘‘Coarse frame and carrier synchronization of OFDM systems: A new metric and comparison,’’ IEEE Trans.Wireless Commun., vol. 3, no. 4, pp. 1271–1284, July 2004.

[64] Seung D. C., J. M. Choi, and J. H. Lee, “An Initial Timing Offset Estimation Method for OFDM Systems in Rayleigh Fading Channel”, IEEE 64th Vehicular Technology Conference, pp. 1-5, 25-28 Sept. 2006.

[65] Zhou E. X. Hou, Z. Zhang, and H. Kayama. “A Preamble Structure and Synchronization Method based on Central-Symmetric Sequence for OFDM Systems”, IEEE Vehicular Technology Conference, 2008. pp. 1478 – 1482, 11-14 May 2008.

[66] Wang H., L. Zhu, Y. Shi, T. Xing Y. Wang, “A Novel Synchronization Algorithm for OFDM Systems with Weighted CAZAC Sequence”, Journal of Computational Information Systems 8, Binary Information Press (http://www.Jofcis.com), pp. 2275-2283, March 2012.

[67] Kay M. S. “ Fundamentals of Statistical Signal Processing: Estimation Theory,” Prentice Hall, 1993.

[68] Li Y., H. Minn, J. Zeng, “An Average Cramer-Rao Bound for Frequency Offset Estimation in Frequency-Selective Fading Channels”, IEEE Transactions on Wireless Communications, Vol. 9, No 3, pp. 871-875, March 2010.

[69] Ghogho M, A. Swami, T. Durrani, “Frequency Estimation in the presence of Doppler Spread: performance analysis” IEEE Transactions Signal Processing, Vol. 49, No 4, pp. 777-789, 2001.

[70] A. Andreescu, A. Ghita, A. Enescu, C. Anghel, “Long Term Evolution Primary Synchronization Algorithms”, 9th International Symposium on Electronics and Telecommunications (ISETC), pp. 125 – 128, Jan. 2010.

[71] J. I. Mazarico, V. Capdevielle, A. Feki, V. Kumar, Detection of synchronization signals in Reuse-1 LTE networks, 2nd IFIP Wireless Days (WD), Dec. 2009.

[72] J. Kim, J. Han, H. Roh H. Choi, SSS detection method for initial cell search in 3GPP LTE FDD/TDD dual mode receiver, International Symposium on Communications and Information Technology, ISCIT 2009. 9th, pp. 199 – 203, Sept. 2009.

[73] Wassal Amr G., Elsherif Ahmed R., Efficient Implementation of Secondary Synchronization Symbol Detection in 3GPP LTE, IEEE International Symposium on Circuits and Systems (ISCAS) 2011, pp. 1680 – 1683, May 2011.

[74] Bartis M., Mocanu V., Enescu A.A., Anghel C., Achieving Secondary Synchronization for Downlink in the Long Term Evolution Standard, International Symposium on Electronics and Telecommunications (ISETC), 2010, pp. 129 – 132, Nov. 2010

RESUMEN EN EXTENSO EN ESPAÑOL

La caracterización del sistema de Multiplexación por división ortogonal de frecuencia (OFDM) basado en la transformada discreta de Fourier (DFT) se proporciona en el capítulo dos. El sistema OFDM es una modulación multiportadora que permite el uso eficiente del ancho de banda disponible mediante la transmisión de subportadoras ortogonales en el período de un símbolo. La ortogonalidad entre subportadoras en la que se basa el sistema se logra mediante la aplicación de la transformada de Fourier discreta inversa (IDFT) en el transmisor, y la transformada discreta de Fourier en el receptor. Para grandes valores relativos de subportadoras en un símbolo OFDM, una alta PAPR se produce y el amplificador de potencia del transmisor requeriría un gran rango dinámico. La relación de potencia de pico a promedio (PAPR) consiste de la superposición de muchas corrientes de baja tasa moduladas a diferentes frecuencias. Una parte importante del símbolo transmitido es el uso eficiente del espectro, por lo cual, símbolos adyacentes transmitidos evitan la interferencia entre ellos por medio de aplicar una función de ventana (*window*). Así mismo, este tipo de sistema hace uso de un prefijo cíclico (CP) para reducir las afectaciones originadas por el canal de propagación por trayectos múltiples.

Sistemas de comunicaciones digitales inalámbricas modernas, han adoptado como mecanismo de modulación al sistema OFDM para su capa física (PHY) ó acceso aéreo. El formato de transmisión de una PHY estándar es un *frame*, que consiste en una parte de preámbulo y una de datos. El *frame* tiene el objetivo de demodulación correctamente en el receptor, donde los siguientes procesos se implementan en el (PHY) de capa física; detección del *burst*, el control automático de ganancia (*AGC*), la adquisición del tiempo del símbolo, la adquisición del desfase de la frecuencia (*CFO*), estimación de canal y ecualización.

Para una PHY WLAN OFDM, un *frame* comienza con una ráfaga de transmisión, que se emplea para el control automático de ganancia y la estimación de canal, así como la sincronización de frecuencia y temporización del *frame*. La ráfaga de transmisión consiste de un preámbulo, que se divide en dos partes de igual longitud.

El estándar IEEE 802.16e define la red de banda ancha inalámbrica de área metropolitana (WMAN), la cual especifica su interfaz de aire con tres modos PHY básicos. Una red WiMAX TDD requiere la sincronización por medio de un *frame*. El *subframe* de enlace descendente sincroniza a la estación base por el sistema de posición global (GPS). La estación base (BS) controla la sincronización del símbolo mediante el *frame*, donde las señales de sincronización se extraen en el receptor. El *subframe* del enlace descendente se inicia con un preámbulo, dicho preámbulo es un patrón predefinido (secuencia de pseudo ruido PN), que permite determinar el tamaño de la DFT que define el símbolo, la estimación de canal, sincronización de tiempo, sincronización de frecuencia, identificación del segmento celular.

El sistema *long term evolution*o (LTE) es un estándar de comunicación móvil, el cual es especificado por el proyecto de la asociación de 3a generación (3GPP) , en su normativa 8. La capa física de LTE la define el sistema múltiple por división de acceso ortogonal (OFDMA) en su enlace descendente, y el sistema expandido mediante la transformada de Fourier discreta (DFT-S-OFDMA) en su enlace ascendente. La sincronización del símbolo en el sistema de comunicación 3GPP LTE es una tarea difícil, debido a que el UE en el enlace ascendente se encuentra en diferentes posicione, por lo cual cada UE debe adquirir y compensar sus desplazamientos de tiempo y frecuencia relativa antes de que la comunicación se efectué. Este proceso se logra por lo general en dos pasos; el procedimiento de búsqueda de células (*cell search*) y el acceso aleatorio (*random access*). El objetivo principal de la búsqueda de células es permitir la adquisición de la temporización recibida (la temporización de la señal de sincronización) y la frecuencia de la señal del enlace descendente.

El capítulo tres presenta la sincronización del tiempo y de la frecuencia del sistema OFDM, los desfases del tiempo y frecuencia se deben a la acción provocada por la respuesta impulso de un canal (CIR) inalámbrico sobre la señal transmitida. El CIR afecta la ortogonalidad entre las subportadoras de cada símbolo transmitido, donde la propagación multitrayecto origina las los desfases más considerables de la señal OFDM.

Una de las principales desventajas de OFDM es su sensibilidad a los errores de sincronización, que se caracteriza principalmente por los desplazamientos de frecuencia y tiempo. El desplazamiento de frecuencia causa una reducción de la amplitud de la señal deseada y se introduce la interferencia entre portadoras (ICI), lo cual origina la pérdida de ortogonalidad entre subportadoras. El desfase de tiempo del símbolo rota la constelación de los símbolos recibidos, grandes desfases de tiempo resultan en interferencia entre símbolos adyacentes (ISI) y la interferencia entre portadoras (ICI).

Los efectos del desfase en los símbolos dependen de la ubicación del punto de partida de cada símbolo OFDM, lo cual resulta en múltiples casos. Una correcta estimación del desfase del símbolo permite definir correctamente el principio de cada uno, evitando así el ISI e ICI. De la misma manera, la estimación del desfase de frecuencia requiere determinar una parte entera y fraccionaria, debido a que la parte entera está relacionada a una estimación burda ó múltiple del período del símbolo, mientras que la parte fraccionaria se relaciona con la separación entre subportadoras que componen el símbolo.

El capítulo cuatro se centra en la descripción de los diferentes métodos de sincronización con datos asistidos ó auxiliares. Los métodos de datos asistidos se basan en secuencias bien diseñadas, las cuales se configuran en un patrón llamado preámbulo. La sincronización del tiempo y la frecuencia del sistema OFDM se basa en datos de métodos asistidos, los cuales utilizan una secuencia de entrenamiento o símbolo piloto para la estimación. Este tipo de método detecta el inicio del *frame*, define la estimación de los símbolos, y lleva a cabo la estimación del offset de frecuencia de la portadora.

En un esquema de sincronización del tiempo, la estimación burda se evalúa sobre una amplia gama de muestras en función del método de estimación. En el caso de la sincronización de frecuencia, la sincronización burda aproxima la estimación de la subportadora inicial y la adquisición de frecuencia fina estima la parte fraccionaria, a partir de las subportadoras recibidas de cada símbolo.

El diseño del preámbulo se clasifica en corto y largo. El preámbulo corto se aplica para hacer estimación el offset de frecuencia de la portadora gruesa, y los preámbulos largos se utilizan para la estimación del tiempo, el offset fraccionario de frecuencia, y la estimación de canal.

La funcionalidad de los preámbulos depende de las secuencias elegidas, las cuales deben tener buenas propiedades de autocorrelación y correlación cruzada. Así mismo deben presentar un PAPR reducido, con el objeto de evitar la degradación no lineal durante la sincronización. Las secuencias más importantes que se utilizan para diseñar preámbulos son; secuencias *m*, *Gold*, *CAZAC* y secuencias Golay.

Los sistemas basados en el preámbulo se aplican para sincronizar los sistemas OFDM, como por ejemplo, IEEE 802.11a, WiMAX y LTE. Los preámbulos de sincronización están diseñadas con secuencias m, Gold, CAZAC y Golay. El sincronizador de OFDM para el estándar WLAN IEEE 802.11a utiliza dos símbolos para la detección de inicio del paquete de datos (*packet*), el desfase del tiempo y la frecuencia.

El preámbulo diseñado para OFDMA (WiMAX) es una versión extendida de preámbulo que se aplica para sistemas OFDM (WLAN). La asignación del preámbulo de sincronización se encuentra en la subtrama (*subframe*) del enlace descendente. El objetivo principal del preámbulo se lleva a cabo cuando una estación móvil se enciende o se entra en una nueva área celular, explorando la disposición de una estación base WiMAX. El primer paso en el proceso de sincronización es detectar el preámbulo y estimar la temporización burda del símbolo, y en segundo lugar se calcula el offset (CFO) de la frecuencia portadora.

El procedimiento de búsqueda de células en LTE inicia con un proceso de sincronización, haciendo uso de dos preámbulos especialmente diseñados, los cuales se transmiten en cada *frame*. El objetivo principal del procedimiento de búsqueda de células es permitir la adquisición de la sincronización del tiempo y la frecuencia de la señal de enlace descendente. En el primer paso de la sincronización del enlace descendente la estación mobil (MS) utiliza la secuencia primaria de sincronización (PSS) con un período de 5 ms, la cual se ha transmitido dos veces en un *frame*, para estimar la temporización de símbolos y CFO.

La estimación del tiempo y la frecuencia se puede implementar en el dominio del tiempo o de frecuencia, donde las estimaciones se pueden definir independiente o conjuntamente. La estimación conjunta del tiempo y la frecuencia se lleva a cabo por métodos de correlación, que se pueden dividir en métodos de auto-correlación y correlación cruzada. Estos métodos están diseñados para maximizar una métrica de correlación. El sistema OFDM utiliza un método de datos asistido aplicando una métrica de temporización (*timing metric*) para lograr la sincronización. El estado del arte de los algoritmos de sincronización mediante métricas se presenta el capítulo cinco.

Un estudio comparativo del estado del arte de las métricas de tiempo es una parte importante de esta tesis, dicho estudio ha proporcionado la teoría necesaria para el procesamiento, el análisis y la comparación de los diseño existentes. La revisión del estado del arte comienza con el análisis de la Schmidl y Cox métrica y sus preámbulos aplicados. La métrica de Schmidl y Cox se basa en dos símbolos, el primero se utiliza para la estimación del tiempo, así como la estimación de la desviación de frecuencia gruesa. El segundo preámbulo se aplica para la estimación de frecuencia fina.

La métrica de Schmidl y Cox es la base de métricas más precisas que se desarrollaron posteriormente, estos métodos adoptan un preámbulo en una configuración de preámbulo corto o largo. Las métricas de sincronización existentes varían las siguientes características de diseño; utilizar una secuencia diferente, modificar la estructura de preámbulo, aumentar el número de muestras evaluadas en la correlación, o codifica el preámbulo transmitido.

Minn et al., propuso una métrica basada en un preámbulo con segmentos idénticos y polaridades variables, mejorando el “plateau” existente en la métrica de Schmidl y Cox. Parks et al., desarrollo un método mejorado, esto en comparación con el método de Minn. El preámbulo de Park está diseñado con secuencias de valores conjugados, lo cual aumenta la diferencia entre los dos valores adyacentes, maximizando la correlación de los diferentes pares de productos comparados dentro de un preambulo. Otro método similar es la métrica de Shi-Serpedin, el cual fue diseñado, aplicando todas las combinaciones posibles de correlaciones, esto entre las diversas partes disponibles de un preámbulo corto.

Ren et, al., propusieron un método en el cual la métrica de sincronización detecta un preámbulo de envolvente constante, que es una secuencia CAZAC ponderada por una secuencia PN. Una versión modificada del método de Park fue propuesta por Seung, donde se aplica un preámbulo largo. Una métrica diseñada considerando una correlación simétrica y retrasada entre las partes de un breve preámbulo fue propuesta por Zhou. Finalmente, H.

Wang aplica una métrica de temporización, y emplea una secuencia ponderada parcial, mediante este diseño se mejora la estimación del tiempo y la frecuencia.

Una vez que las métricas de sincronización existentes han sido analizadas, es posible definir las mejores características de cada una. En el capitulo seis se presenta la evaluación del desempeño de las métricas, lo cual es necesario para corroborar cada métrica de temporización, comparando su funcionalidad por medio de simulaciones en MATLAB. Cada estimador se evalúa con el error cuadrado medio (MSE), que es un criterio importante de comparación, reflejando la tendencia (bias) y la varianza del estimador analizado.

Después de efectuar la estimación del tiempo y la frecuencia, es necesario aplicar la estimación de canal, con la finalidad de reducir las afectaciones originadas por el canal de trayectorias múltiples. El rendimiento del sistema OFDM se consigue por medio de la evaluación de la tasa de error de bit (BER). Comparando el mejor rendimiento entre las métricas revisadas es posible obtener la métrica de temporización que es más precisa.

Las métricas de Zhou y de Seung se caracterizan por emplear correlaciones múltiples entre las diversas partes del preámbulo transmitido, donde las correlaciones adicionales aumentan el proceso de tiempo para obtener la estimación. Las métricas ponderadas propuestas por Ren et al., Y H. Wang presentan los mejores resultados de la estimación de los métodos comparados, este tipo de métricas definen el momento y la frecuencia de desplazamiento aplicando un preámbulo ponderado. Los resultados de desempeño han demostrado que la mejor estimación corresponde a las métricas de tiempo desarrolladas más recientemente.

Tomando en consideración el análisis de las métricas de tiempo existentes, la presente tesis propone el diseño de sistemas de medición más precisos, la mejora de los algoritmos de métricas de tiempo existentes, los funcionan en configuraciones de preámbulo corto y largo. Donde el diseño se basa en un proceso de codificación definido por una secuencia de Golay. Así mismo el rendimiento de las métricas propuestas se evalúa mediante el MSE y BER, y se comparan con las métricas existentes en la literatura.

La primera contribución de esta tesis es la propuesta de un preámbulo modificado ponderado, que se basa en una secuencia CAZAC ponderado por una secuencia de Golay Rudin Shapiro (GRS). La segunda contribución consiste en la propuesta de un algoritmo de sincronización, basado en la idea propuesta por Ren et al., donde el algoritmo de sincronización se basa en un preámbulo largo propuesto. Técnicamente, el proceso para diseñar el preámbulo es de la siguiente manera; primero, una secuencia CAZAC con una longitud $L = N_c / 2$ se codifica con una secuencia de GRS de la misma longitud, y a continuación, la secuencia resultante es *up-sampled* al doble, para obtener una secuencia simétrica. En seguida, cada componente del preámbulo se transforma en frecuencia mediante la aplicación de la transformada discreta de Fourier (DFT), después el preámbulo resultante se multiplica por las secuencias de GRS de par complementario, donde la secuencia de GRS tiene longitud $L = N_c$, y un par complementario de secuencias de longitud $L = N_c / 2$.

La métrica de tiempo propuesta que detecta el preámbulo diseñado, se realiza de la siguiente manera. Una métrica de tiempo similar es aplicada por Ren, sin embargo, en el diseño propuesto se utiliza una secuencia de Golay Rudin-Shapiro para recuperar la señal recibida en el proceso de correlación (esta es la misma secuencia aleatoria utilizada para la secuencia de CAZAC en el preámbulo transmitido).

La tercera contribución consiste en el preámbulo corto modificado y su correspondiente métrica de temporización, el cual es basado en la idea propuesta por H. Wang et al. La métrica de temporización propuesta se basa en el preámbulo ponderada propuesta de longitud $L = N_c$. Sin embargo, solo partes seleccionadas del preámbulo están codificados con la secuencia de Golay Rudin-Shapiro, con una longitud de $L = N_c/4$, esta particularidad, al dividir en más secciones mejora la precisión en la estimación de la frecuencia.

Una evaluación completa de los preámbulos con diferentes longitudes en el sistema OFDM se consigue por medio de la medición de la tasa de error de bit. Los datos transmitidos son símbolos QPSK. El proceso de evaluar el rendimiento se desarrolla de la siguiente manera: En la primera etapa, las muestras recibidas se evalúan para definir el punto de partida del preámbulo transmitido, teniendo en cuenta el pico máximo detectado. El siguiente paso consiste en multiplicar el símbolo recibido por el valor negativo de la frecuencia estimada de desplazamiento. Además se aplica una estimación de canal para suprimir los efectos del canal.

El BER resultante obtenido de comparar las métricas ponderadas se muestra en el capítulo seis, donde es notable una considerable mejora se logra con la aplicación de la métrica de tiempo ponderado propuesto, teniendo en consideración una serie de desfases en tiempo y frecuencia.

Una contribución especial de la presente tesis consiste en evaluar mediante simulación el límite de Cramer-Rao de los preámbulos existentes y propuestos, la evaluación se realiza empleando la métrica de Schmidl y Cox, la cual permite corroborar las propiedades de correlación de cada secuencia. De los resultados obtenidos, se observa que la mejor estimación del desfase de frecuencia se obtiene con el diseño propuesto.

Al final del capítulo seis se presenta la sincronización del sistema *long term evolution* (LTE), la cual se basa en el proceso de búsqueda de células (*cell search*), y se logra con la ayuda de secuencias diseñadas especialmente. Una contribución especial de esta tesis se refirió al proceso de búsqueda de células, la cual consiste en la propuesta de una detección normalizada, donde el objetivo es conseguir una señal de sincronización primaria más precisa. Las secuencias utilizadas en la sincronización de LTE permiten estimar la sincronización del tiempo y de la frecuencia, así mismo, se utilizan para identificar la estación móvil (MS) o equipo de usuario (UE) con la estación de base (BS).

El procedimiento de búsqueda de células en LTE consiste en una serie de etapas de sincronización por el que el UE determina los parámetros de tiempo y frecuencia, las cuales son necesarias para demodular el enlace descendente y transmitir las señales de enlace ascendente con la sincronización correcta. También se utiliza para la adquisición de la frecuencia del receptor de los canales de enlace descendente. Por lo tanto, la detección de células está relacionada con la secuencia de sincronización primaria (PSS), y la secuencia de sincronización secundaria (SSS).La sincronización es un proceso continuo y periódico, que debe estar siempre activo (es decir, no sólo cuando el equipo esté encendido). Se tiene que buscar y estimar la calidad del enlace con las células vecinas, con el fin de ser capaz de ofrecer movilidad a los usuarios.

La secuencia PSS detecta la identidad de célula en la capa física ($N_{ID}^{(2)}$ en el rango de 0-2), mientras que la secuencia de SSS proporciona el grupo de identidad de la célula ($N_{ID}^{(1)}$ en el rango de 0 a 167), de tres identidades posibles, las que definen 504 identidades únicas para células en sistemas LTE. Esto significa que el procedimiento de búsqueda de células completo consta de dos pasos para identificar la identidad de la célula, una vez detectadas las secuencias de sincronización. El PSS se elige entre una clase de las secuencias polifásicas Zadoff-Chu (ZC), que ha sido seleccionado para obtener buenas propiedades de autocorrelación y correlación cruzada. En particular, estas secuencias tienen una baja sensibilidad a la frecuencia Doppler-offset.

El UE debe detectar el PSS sin ningún conocimiento a priori del canal, de manera que se requiere una correlación no coherente para la detección de temporización de PSS. Un estimador que maximiza la probabilidad es aplicado y las secuencias seleccionadas se pueden detectar con un único *correlador*, permitiendo así una reducida complejidad.

Las señales transmitidas se ven afectadas por ruido blanco aditivo Gaussiano (AWGN), un canal de propagación por trayectos múltiples, desfase en tiempo y frecuencia. La señal modificada posiblemente afecta a la detección correcta llevado a cabo por el PSS, la cual se utiliza para detectar el inicio del símbolo transmitido. Con el fin de evitar una detección confusa del máximo pico de señal, en la presente tesis se ha propuesto un sistema de detección normalizada del PSS, y que se evalúa mediante simulación en MATLAB.

La detección de la secuencia secundaria de sincronización (SSS) se realiza una vez detectada la PSS, El SSS obtiene la sincronización del *frame* de radio y de la identidad del grupo de las células. El proceso de diseño de la SSS se inicia con la generación de una secuencia básica de pseudo-ruido a partir de la cual se producen dos secuencias. A partir de ser mezcladas con los parámetros relacionados $N_{ID}^{(2)}$ y $N_{ID}^{(1)}$.

Después de ello, las secuencias se intercalan en una secuencia de 62 muestras de longitud, conformando la secuencia SSS. La combinación de las dos secuencias de longitud 31 que definen el SSS, se diferencian al ser colocadas entre la ranura 0 y la ranura 10 de la trama transmitida. La posición de las secuencias de SSS en el *frame* recibido es desconocida. Donde sólo existe el conocimiento de que el primer símbolo siempre está codificado con la secuencia C_0. Tomando en cuenta el parámetro obtenido en la detección de PSS es posible detectar las secuencias de SSS. El bloque decodificador de secuencia para detectar la SSS en el receptor contiene los siguientes bloques; des entrelazado, la descodificación y el proceso de extracción. El procedimiento de búsqueda de células se logra una vez que los parámetros $N_{ID}^{(2)}$ y $N_{ID}^{(1)}$ se obtuvieron, y así el UE es capaz de acceder a la célula en un eNodoB.